PREPARATION AND CHARACTERIZATION OF SELF ASSEMBLED MONOLAYERS ON SEMICONDUCTING SUBSTRATES FOR MEMS APPLICATION

A THESIS SUBMITTED TO THE

UNIVERSITY OF PUNE

FOR THE DEGREE OF

DOCTOR OF PHILOSOPHY

IN

CHEMISTRY

BY

SNEHA AVINASH KULKARNI

PHYSICAL CHEMISTRY DIVISION

NATIONAL CHEMICAL LABORATORY

PUNE 411008

INDIA

Dr. K. VIJAYAMOHANAN

(RESEARCH GUIDE)

APRIL, 2007

DECLARATION

I hereby declare that the thesis entitled "**PREPARATION AND CHARACTERIZATION OF SELF ASSEMBLED MONOLAYERS ON SEMICONDUCTING SUBSTRATES FOR MEMS APPLICATION**", submitted for the degree of Doctor of Philosophy in Chemistry to the University of Pune, has been carried out by me at Physical and Materials Chemistry Division, National Chemical Laboratory, Pune-411008, India, from July, 2003 to March, 2007 under the supervision of Dr. K. Vijayamohanan. The work is original and has not been submitted in part or full for any other degree or diploma to this or any other University.

Date:
Physical Chemistry Division
National Chemical Laboratory
Pune-411008

Sneha A. Kulkarni
(Research student)

Dr. K. Vijayamohanan
Scientist

Physical and Materials
Chemistry Division
National Chemical
Laboratory
Pune – 411008
INDIA

Tel: +91-020-25902588
+91-020-25902270
Res: +91-020-25893307
Fax: +91-020-25902636
Email: vk.pillai@ncl.res.in

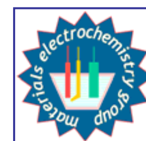

CERTIFICATE

This is to certify that the work incorporated in the thesis, "**PREPARATION AND CHARACTERIZATION OF SELF ASSEMBLED MONOLAYERS ON SEMICONDUCTING SUBSTRATES FOR MEMS APPLICATION**", submitted by **Sneha A. Kulkarni**, for the degree of **Doctor of Philosophy**, was carried out by the candidate under my supervision at Physical and Materials Chemistry Division, National Chemical Laboratory, Pune- 411008, India. All the materials obtained from other sources have been duly acknowledged in the thesis.

Date :
Place : Pune

Dr. K. Vijayamohanan
(Research Guide)

Dedicated

To My beloved Daughter

Anushka

&

My Family….

Acknowledgements

I wish to express my sincere gratitude to all my teachers, friends and colleagues, who have contributed to the development of this thesis, enabling me to have an enjoyable experience as a Ph. D student during my stay at National Chemical Laboratory.

Firstly, I would like to express my deepest sense of gratitude to Dr. K. Vijayamohanan, my research advisor, without whom this work would not have been possible. He is not only a passionate scientist with a deep vision but also, most importantly a kind person. He has introduced me to an exciting and interesting field of research. He has built my confidence through valuable discussions; he has given the freedom to think and work independently, which will definitely be useful throughout my career. His constant encouragement, support, and invaluable suggestions made this work successful. I would like to thank Dr. I. S. Mulla, for his valuable suggestions throughout my research work. I am also grateful to Prof. Satish Ogale for his kind suggestions, valuable discussions, which have boosted my confidence.

I wish to thank the Director of NCL for providing me the infrastructural facilities at this CSIR laboratory and CSIR for financial support. I am also grateful to Dr. Sourav Pal, Head of Physical and Materials Chemistry Division for allowing me to use all the available facilities in the division. I am very much thankful to Dr. S. R. Sainkar, Head of CMC for making the facilities available for material characterization. My special thanks goes to Mr. A. B. Gaikwad, Dr. A. B. Mandale, Dr. K. R. Patil, Mrs. R. Pasricha, Dr Ms. N. R. Pavaskar, Dr.Mrs. Mitra, Mrs D. Dhoble and Mr. Gholap for characterization of samples, forming the most significant part of my research work

My sincere thanks to Drs. M. G. Kulkarni, S. P. Vernekar, A. Ahmad, M. M. Bhadbhade, A. Kumar, M. Sastry, B. L. V. Prasad, P. C. Ghosh, V. Ravi, K. Shreedhar, P.A. Joy, M. Shelke, S. Mirji and S. Prasad and all others for their advice and help. I also deeply acknowledge the appreciable help from Mr. Dipak, Mr. Punekar, Mr. Patole and the entire library staff of NCL for providing excellent facilities.

I take this opportunity to thank all my senior colleagues Drs. Sushama, Varsha, Aslam, Nirmal and Jadab. My special thanks to Bhalchandra, my friend (whom I troubled a lot) for always sparing his valuable time for discussions throughout this work. I must thank Girish for his kind help and support during this work. I am also thankful to Bhaskar and Kannan for their timely help. Thanks to all my labmates, Niranjan, Mrudula, Mahima, Mukta, Meera, Dhanaraj, Praveen, Sanjay, Indulekha, Shreekuttan, Rupali, Mandar, Buddhadeb and Vivek, who created a pleasant atmosphere. I thank my dear friends, Anita, Rohini, Suvarna, Trupti, Savita and Sunita for their constant support and a special thanks to Sunita for her involvement in the 'molecular glue' formation work

I wish to thank all my fellow colleagues in my division, Sarita, Geetanjali, Shraeddha, Prerana, Shekhar, Diganta, Nagesh, Hrushikesh, Subhas, Vivek, Tushar, Manasi, Mahesh, Ravi, Sambhaji, Amit, Atul, Sanjay, Anil and Sandeep, are few among them, and all other members of Physical chemistry division for their cooperation and for providing me with an excellent working ambience during the course of this work. A special thanks to Deepti for the FTIR characterization.

I feel a deep sense of gratitude and affection to my beloved parents, Aai and Dada for their moral support and encouragement that has helped me to bring up my educational career to this stage. I would also like to thank my sister Varsha, brother Sameer, Deepak, Kaka, Kaku, Geeta and Aaji for their support. Also, at this moment I cannot forget the love of my dear Baba, whose memories and blessings have been supporting me at all times. I owe deeply to my Mama, Mami, Supriya and Milind; I never forget their valuable help in the earlier days of studies.

My heartfelt thanks to my in-laws, Aaji, Aai and Nana for their incredible understanding, support, encouragement and for boosting me and patiently waiting for this thesis to be done. I am deeply indebted to them for all their kind efforts. I am also thankful to Deepa, my sister-in-law, who made it possible for me to concentrate on my work. I find no words to express my feelings towards my lovable daughter Anushka, for her understanding, support and patience. I am also thankful to Anushka, Swarangi and Vaibhav for their cute smile, which gives me energy to work. I am also thankful to Kaku, Kaka, Manu, Sonu, Anju Tai, Maju Tai, Kiran and Hemant Jijaji, and their family, for their encouragement. My thanks to Deshapande vahini, who has always shown curiosity by inquiring about my studies.

I acknowledge an appreciation that extends beyond any words for the love and support of my husband, my best friend, Avinash. I am very thankful for his understanding, for being extremely encouraging during these years and being a source of inspiration in all my endeavors. Thank you for your enormous support in materializing this work into a reality.

- Sneha Kulkarni

List of Abbreviations

Abbreviation	Expansion
2D	Two-Dimensional
3D	Three-Dimensional
AIBN	Azobis isobutyronitrile
APTMS	3-Aminopropyltrimethoxysilane
MSMA	4-[tris (trimethylsilyloxy) silyl] propyl methacrylate
AFM	Atomic Force Microscope
ATR	Attenuated Total Reflectance
BCB	Benzocyclobutene
BE	Binding Energy
CA	Contact Angle
CCD	Charge Coupled Device
CNLS	Complex Non-Linear Least Square
CNT	Carbon Nanotube
CPE	Constant Phase Element
R_{ct}	Charge Transfer Resistance
CV	Cyclic Voltammetry
CVD	Chemical Vapor Deposition
DDS	Dodecyltrichlorosilane
DTCS	Decyltrichlorosilane
DRIFT	Diffuse Reflectance Fourier Transform Infrared
DPN	Dip Pen Nanolithography
DMSO	Dimethylsulfoxide
DSC	Differential Scanning Calorimetry
EBL	Electron Beam Lithography
EDX	Energy Dispersive Analysis of X-ray
EELS	Electron Energy Loss Spectroscopy
EGDMA	Ethylene glycol dimethacrylate
ESCA	Electron Spectroscopy for Chemical Analysis
ET	Electron Transfer

E_{fb}	Flat-Band Potential
FET	Field-Effect Transistors
FRA	Frequency Response Analyzer
FTIR	Fourier Transform Infrared
HD	Hexadecane
HOMO	Highest Occupied Molecular Orbital
HREELS	High-Resolution Electron Energy Loss Spectroscopy
LB	Langmuir Blodgett
LIGA	Lithographie, Galvanoformung and Abformung
LUMO	Lowest Unoccupied Molecular Orbital
MBE	Molecular Beam Epitaxy
MEMS/NEMS	Micro/Nano-Electromechanical Systems
MOEMS	Micro Optoelectromechanical Systems
MOSFET	Metal Oxide Semiconductor Field-Effect Transistor
MPCs	Monolayer Protected Nanoclusters
NcAFM	Non-contact Atomic Force Microscopy
NIL	Nanoimprint Lithography
OCP	Open Circuit Potential
OTCS	Octyltrichlorosilane
OTS	Octadecyltrichlorosilane
QCM	Quartz Crystal Microgravimetry
RAIRS	Reflection Absorption Infrared Spectroscopy
RE	Reference Electrode
SAM	Self-assembled Monolayer
SAXS	Small Angle X-ray Scattering
SCE	Saturated Calomel Electrode
SEM	Scanning Electron Microscope/copy
SERS	Surface Enhanced Raman Spectroscopy/Scattering
SFM	Scanning Force Microscopy
STM	Scanning Tunneling Microscopy
TEM	Transmission Electron Microscope/copy
TEOS	Tetraethyl orthosilcate
TG	Thermogravimetry

UV	Ultraviolet
VLSI	Very Large Scale Integration
WDX	Wavelength Dispersive X-ray
WE	Working Electrode
XPS	X-ray Photoelectron Spectroscopy
XRD	X-ray Diffraction

Table of Contents

Chapter I

1-56

Self-Assembled Monolayers on Semiconducting Substrates: Introduction

1.1	Introduction	2
1.1.1	Importance of SAM	4
1.2	Preparation	5
1.3	Parameters Controlling SAM Formation	6
1.3.1	Nature of the Substrate	6
1.3.2	Effect of Water Content	8
1.3.3	Effect of Solvent	9
1.3.4	Effect of Temperature	9
1.4	Structure, Kinetics and Mechanism of SAM Formation	12
1.5	Stability of SAMs	16
1.5.1	Chemical Stability	16
1.5.2	Thermal Stability	17
1.6	Characterization Techniques	17
1.6.1	Contact angle (CA) Measurements	18
1.6.2	X-ray Photoelectron Spectroscopy (XPS)	21
1.6.3	Fourier Transform Infrared Spectroscopy (FTIR)	23
1.6.4	Transmission Electron Microscopy (TEM)	24
1.6.5	Scanning Electron Microscopy (SEM)	26
1.6.6	Atomic Force Microscopy (AFM)	27
1.6.7	Thermogravimetric (TGA) Analysis	29
1.6.8	Electroanalytical Techniques	30
1.6.8.1	Cyclic Voltammetry (CV)	30
1.6.8.2	Impedance Analysis	31
1.6.9	Miscellaneous Techniques	33
1.7	Applications of SAM	33
1.7.1	Patterning of Surfaces	34
1.7.2	Molecular Electronics	34
1.7.3	Chemical Sensors and Biosensors	35
1.7.4	SAMs as an Anti-Stiction Agent in MEMS/NEMS	36
1.7.4.1	MEMS/NEMS	36
1.7.4.2	SAM for MEMS	40
1.8	Motivation, Scope and Organization of the Thesis	41
1.8.1	Objectives of the Present Study	41
1.8.2	Organization of Chapters	42
1.9	References	47

Chapter II

57-73

Preparation and Characterization of Octadecyltrichlorosilane Self-Assembled Monolayer on Si/ SiO_2 Interface: Growth Kinetics and Thermodynamic Stability

2.1	Introduction	58
2.2	Experimental Section	59
2.2.1	Materials	59
2.2.2	Monolayer Formation	60
2.2.3	Characterization	60
2.3	Results and Discussion	61
2.3.1	Contact Angle (CA) Measurements	61
2.3.2	Growth Kinetics of OTS Monolayer	62
2.3.3	Calculations of Thermodynamic Stability of OTS Monolayer	63
2.3.4	AFM and FTIR Analysis	65
2.3.5	X-ray Photoelectron Spectroscopy	68
2.3.6	Zisman Plot	69
2.4	Conclusions	70
2.5	References	71

Chapter III

74-96

Interfacial Behavior of Alkyltrichlorosilane Monolayers on Silicon: Control of Flat-Band Potential and Surface State Distribution Using Chain Length Variation

3.1	Introduction	75
3.2	Experimental Aspects	77
3.2.1	Materials	77
3.2.2	Electrode Preparation	77

3.2.3	Surface Characterization	78
3.2.4	Electrochemical Characterization	78
3.3	Results and Discussion	79
3.3.1	Contact Angle (CA) Measurements	79
3.3.1.1	Surface Wetting Properties	79
3.3.1.2	Zisman Plot and Thermal stability	79
3.3.2	FTIR Spectroscopy	81
3.3.3	Cyclic Voltammetry	82
3.3.4	Impedance Analysis	84
3.3.5	Thickness Calculations	85
3.3.6	Impedance Analysis in Presence of Ferrocene	86
3.3.7	Coverage Calculations	87
3.3.8	Analysis of Surface States	89
3.3.9	Mott-Schottky Analysis	90
3.3.10	Effect of dc Bias Potential	92
3.4	Conclusions	93
3.5	References	94

Chapter IV

97-111

Thermal Stability of Self-Assembled Octadecyltrichlorosilane Monolayer on both Planar and Curved Silica Surfaces

4.1	Introduction	98
4.2	Experimental Aspects	99
4.2.1	Materials	99
4.2.2	Silanization	100
4.2.2.1	SAM Formation on n-type Si Substrate	100
4.2.2.2	SAM Formation on Silica Particles	100
4.2.3	Characterization	101
4.3	Results and Discussion	102
4.3.1	FTIR Spectroscopy	102
4.3.2	X-ray Photoelectron Spectroscopy	103
4.3.3	Scanning Electron Microscopy	105
4.3.4	Thermogravimetric Analysis	105
4.3.5	Temperature Dependent Contact Angle (CA) Measurements	106
4.3.6	Temperature Dependent FTIR Measurements	107

4.4 Conclusions 109
4.5 References 110

Chapter V

112-131

Preparation of hydrophobic Silica by Surface Silanization

5.1 Introduction 113
5.2 Experimental Aspects 114
5.2.1 Materials 114
5.2.2 Silanization 115
5.2.2.1 Mixed Mono/ Multilayer Formation 115
5.2.2.2 Polymerization of 4-[tris (trimethylsilyloxy) silyl] propyl methacrylate (MSMA) 115
5.3 Characterization 116
5.4 Results and Discussion 117
5.4.1 FTIR Spectroscopy 117
5.4.2 Thermogravimetric Analysis 118
5.4.3 Contact Angle (CA) Measurements 119
5.4.4 Scanning Electron Microscopy (SEM) 122
5.4.5 Comparison in CA between SAM on Planar and Curved Surfaces 125
5.5 Conclusions 126
5.6 References 128

Chapter VIA

132-146

Tuning of Anisotropic Etching Rates of Silicon Using Surface Functionalization

6A.1 Introduction 134

6A.2 Experimental Aspects 135
6A.2.1 Chemicals 135
6A.2.2 Substrate Preparation 135
6A.2.3 Electrode Preparation 136
6A.3 Characterization 136
6A.4 Results and Discussion 137
6A.4.1 Contact Angle (CA) Measurements 138
6A.4.2 Cyclic Voltammetry 139
6A.4.3 Impedance and SEM Analysis 141
6A.4 Conclusions 144
6A.5 References 145

Chapter VIB

147-158

Application of Self-Assembled Mono/Multilayers as Molecular (Polymeric) Glues for Low Temperature Wafer Bonding

6B.1 Introduction 148
6B.2 Experimental 150
6B.2.1 Chemicals 150
6B.2.2 Monolayer Formation and Wafer Bonding Process 150
6B.2.3 Characterization 151
6B.3 Results and Discussion 151
6B.3.1 Monolayer Formation 151
6B.3.2 SEM Analysis 153
6B.3.3 List of Control Experiments of Wafer Bonding 153
6B.3.4 Bond Strength Measurements 155
6B.4 Conclusions 155
6B.5 References 157

Chapter VII

159-166

Conclusions and Future Prospects

7.1	Introduction	160
7.2	Major Accomplishments	160
7.3	Possible Limitations	161
7.4	Future Scope	162
7.5	References	166

List of Publications 167

CHAPTER 1

Self Assembled Monolayers on Semiconducting Substrates: Introduction

This chapter introduces the thesis giving a brief overview of the preparation, characterization and applications of alkyltrichlorosilane self assembled monolayers on semiconducting substrates with special relevance to silicon. This chapter also outlines the major objectives and the overall organization of the present investigation.

1.1 Introduction

Almost everyone agrees that the origin of nanotechnology could be easily linked to the most cited and famous talk of the great physicist and Nobel laureate Prof. Richard P. Feynman in 1959 entitled, "There's Plenty of Room at the Bottom" [1]. His vision was to build nanomachines by precise manipulation and design of matter by engineering them at the atomic or molecular level that is analogous to biological organisms. Such tiny machines, individually or assembled into designed architectures, were thought to transport medicine in the body, conduct operations in cells, move cargo around microfluidic chips, manage light beams, agitate liquids close to electrode surfaces, and search for and destroy toxic organic molecules in polluted water streams. Today, Feynman's dream is surely being realized on a grand and global scale through the nanotechnology revolution. Over the next decade, it is believed that, the size of many manufactured goods continues to decrease, resulting in ultra-small electronic devices and new hybrid technologies using Micro (and nano)-electromechanical system (MEMS/ NEMS) which integrate physical, chemical, and even biological processes in micro (nano)-and millimeter-scale technology packages through the microfabrication technology [2,3]. During this process, the substrate is normally coated with an isolation layer followed by subsequent deposition and patterning of a sacrificial spacer layer. The microstructural film is then deposited and etched selectively to create freestanding microstructures. Such MEMS / NEMS devices are used in many sectors like information technology, medicine and health, aerospace, automotive, environment, energy etc [2].

However, one of the major limitations during microfabrication is stiction where, unwanted adhesion of the underlying substrate or adjacent microstructures to the micromechanical devices, results in the breaking of these structures during their release**.** As a result, several techniques have been employed in the past few years to avoid the stiction including supercritical drying (usually with CO_2), freeze-sublimation (employing methanol), and etching with HF [4,5]. Recently, alkyltrichloro and trimethoxy silane Self-assembled monolayers have become particularly useful for MEMS to tackle the stiction problem since their mere presence provides a suitable low energy surface coating, thus eliminating the '*release stiction*' and reducing the '*in-use*' stiction [6,7].

During the early 1940's, Zisman et al., discovered that an alkanoic acid could be self-organized into a monolayer on a clean platinum surface driven by chemisorption from a solution phase [8]. Monolayer prepared by this spontaneous self organization against the entropic driving force is called Self-Assembled Monolayers (SAMs). SAMs typically are more stable than organic thin film earlier prepared by the Langmuir-Blodgett method because the molecules in a SAM are attached to the solid surfaces via chemical bonds [5, 6]. The applications of organic thin films are further extended by the preparation of trifunctional alkylsiloxane monolayers on alumina and SiO_2 surfaces by Sagiv and similar alkanethiol monolayers on gold surfaces by Nuzzo et. al., during 1980's. Both types of monolayers are very robust due to the strong bonding between head groups and substrates [6d, 9].

Molecular self-assembly, which is at the heart of many physical, chemical and biological processes, has its origin from biological systems and is one of the most fundamental processes for forming a functional and living structure. The genetic codes and sequences built in a biosystem guide and control the self-assembling process. Following nature's lead, scientists are increasingly looking into using self-assembly to make structures for a multitude of applications. Thus, designed and controlled self-assembly is a possible solution in nanotechnology for future manufacturing needs. Two major approaches currently being used for the generation of organized nano-scale assemblies are the "top-down" (engineering down) and "bottom-up" (engineering up) methods. Top down approach involves generation of patterned structures by suitable lithographic and ion implantation technique and marks the beginning of silicon-integrated chip technology [10]. However, it has been realized that the current rate of miniaturization in silicon memory technology will be affected very soon by the physical limits of device dimensions imposed by ultra-violet, electron/ion beam and soft X-ray lithographic techniques as explained in Moore's law. Therefore, the idea of building structures from the bottom-up, molecule by molecule or atom by atom, is one of the core concepts of nanotechnology, which promises to revolutionize many industries. For example, researchers in the field of molecular electronics are investigating the use of molecular self-assembly to build new types of transistors and switches that could potentially replace today's dependence on silicon electronics [1-3]. The pharmaceutical

industry is also pushing hard to find ways to use self-assembly to increase the efficiency of drug delivery processes [6]. Other industries are seeking to use SAM as protective layers to chemically functionalize a surface to control its reactivity [6,7]. The future relies on the efficient integration of nanotechnology and biotechnology with the existing technology. However, the challenge remains in integrating nanotechnology with micro/nanoelectronics since any ultra small component has to be connected using contacts with the real world. The goal should be on how to use nanotechnology to make MEMS / NEMS more efficient, multifunctional, and intelligent as well as faster and smaller capable of achieving the impossible. Thus nanotechnology comes to life, if we can accomplish the integration of nanoscale building blocks with lithographically produced structures through self-assembly. Thus self-assembly is to become a useful technology, it is important to understand the fundamental mechanisms that drive this process, both from a kinetic and structural point of view. An understanding of the driving forces involved during chemical self-assembly is imperative as scientists seek to build devices on the molecular scale.

1. 1. 1 Importance of SAM

SAMs have attracted a great deal of attention in recent years as potential candidates for isolating interfaces and improving interfacial adhesion in newly evolving integrated circuit architectures, an interest arising because of its crucial importance in modern nanotechnology [6,7]. For example, SAMs of alkyltrichlorosilane on Si / SiO_2 interface have been extensively studied due to their fundamental importance in surface modification and also for their diverse potential applications such as emerging flexible memory storage modules, nano electromechanical devices, interconnects in molecular electronics, interfacial adhesive promoters and molecular lubricants [11]. The close packing of molecules with a saturated methylene chain via coordinated interchain van der Waals interactions is expected to create a vacuum-like potential barrier at the interface that inhibits phenomena such as ionization and diffusion, making them extremely useful for interfacial isolation. In addition, the low sticking property of SAMs onto themselves is conducive for forming conformal layers whose thickness is essentially the length of the comprising molecules facilitating a remarkable control by

manipulating the chemistry of the terminal functional group. This enables us to further study complex intermolecular, substrate-molecule and molecule-solvent interactions like ordering and growth, wetting, adhesion, lubrication, and corrosion. SAMs are also structurally well defined thus making fundamental studies of chemistry and physics in two dimensions as a tangible possibility. As a result, many structure-function correlations have been reported so far using various characterization techniques [6,7]. Particularly, it is also possible to tailor both head and tail groups of constituent molecules in SAMs to suit specific applications [4]

1. 2 Preparation

The spontaneous adsorption of active surfactant molecules on many freshly cleaned substrates can be achieved by solution state methodology, molecular beam epitaxy (MBE), and chemical vapor deposition (CVD) process [12]. All these method allow SAM formation leading to a highly ordered and compact layer capable of incorporating a wide range of groups both in the alkyl chain and at the terminal position. Recently, various lithographic techniques such as microcontact printing, dip-pen lithography, and nano imprint lithography are reported for patterned SAM formation [13].

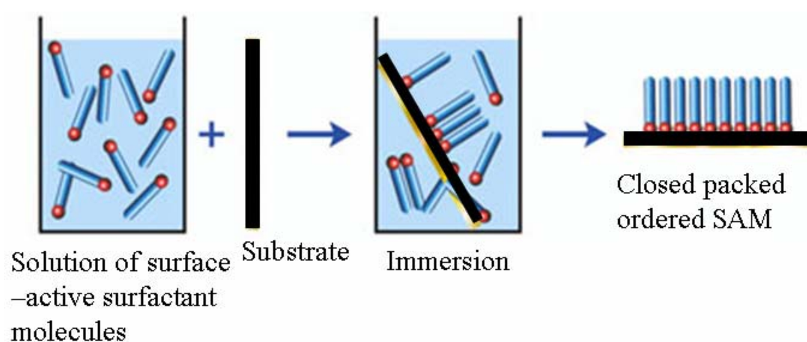

Figure 1.1: A schematic representation of the self assembled monolayer formation from a very dilute solution of the long chain organic compound from a suitable solvent on metallic or semiconducting substrate.

The solution deposition method is one of the most convenient and extensively used techniques for SAMs formation (some times called as molecular beaker epitaxy) as illustrated in Figure 1.1. In this, a freshly cleaned substrate is dipped into an appropriate organic solvent (ethanol, toluene, chloroform, and hexane etc.) containing the relevant

molecule for a certain period of time (several seconds to hours). Usually low concentration (in mM) and longer immersion time is preferred, which allow molecules to assemble in a crystalline film, also providing the possibility of desorbing the physisorbed and contaminated impurities upon extensive rinsing.

In case of trichlorosilane molecules, the reaction is carried out in nitrogen atmosphere, as it undergoes hydrolysis followed by polymerization to form cross-linked siloxane networks [6]. The substrate is subsequently removed from the solution, washed several times with the same solvent in order to remove the unbound/physisorbed molecules, dried, and annealed to get better organization. However, the reaction conditions are to be carefully controlled, to form a highly ordered organosilane SAM. Some of the key factors that affect the growth of silane SAMs on Si are discussed below.

1. 3 Parameters Controlling SAM Formation

1. 3. 1 Nature of the Substrate

The nature of the substrate plays an important role in the formation of the monolayer particularly in terms of its chemical identity, electron density and degree of crystallinity. For example, octadecyltrichlorosilane (OTS) molecules, adsorbed on coinage metal surfaces (Au, Ag, Cu etc.) behave differently than similar molecules organized on semiconducting substrates (Si, GaAs, ITO etc.) since the lattice spacing and the lattice geometry of the particular substrate determine the packing density and the surface orientation of the film [14]. A summary of such organic molecules along with the commonly employed substrates for SAM formation is given in Table 1.1 to provide a rationale for the specific interactions facilitating the process.

More specifically, SAMs of alkylchlorosilanes, alkyl-alkoxysilanes, and alkylaminosilanes require hydroxylated substrate surface for their formation. The driving force for this self-assembly is the *in situ* formation of polysiloxane, which is connected to surface silanol groups (-Si-OH) via Si-O-Si bonds. Substrates on which these monolayers have been successfully prepared include silicon oxide, aluminum oxide, quartz, glass, mica, zinc selenide, germanium oxide, and gold [15-19]. Therefore the quality of monolayer may vary with the surface density of -OH groups in all these cases [20]. Also,

this substrate-adsorbate affinity influences the adsorption rate of the silane molecules and hence the structure of the monolayer, depending on the solvent.

Table 1.1: Examples of organic molecules and the respective substrates used for SAM formation.

Sr. no.	Molecules	Substrate used for SAM
1.	Thiols, Sulfides, Disulfides , diselenides	Gold, Copper, Silver, Platinum, Mercury, Iron, Nanosized γ-Fe_2O_3 particles, InP, GaAs, CdSe, CdS and high temperature super conductor surface [21]
2.	Alkane silanols and	Gold (Au) [22]
3.	Carboxylic acids	Metal oxides like Al_2O_3 and Ag_2O [6a, 9d]
4.	Alkylchlorosilanes, Alkylalkoxysilanes, Alkylaminosilanes	Oxides surfaces, Silicon, Glass, Mica, Zinc selenide, Gold, Platinum, and Germanium [15-19]
5.	Alkyl amines	High temperature super conductor surfaces [23]
6.	Phosphine, Phosphonates.	Gold, and Phosphonate surface [24]
7.	Long chain alkanes	H-terminated Silicon [25-29]
8.	Olefins and Isonitriles	Platinum surface, Graphite [30]

A good monolayer can be prepared only if the substrate like silicon wafer has a critical density of silanol groups about 5×10^{14} Si-OH groups/cm^2 and hence for substrates lacking enough -OH groups, such as mica, a suitable chemical treatment prior to SAM formation is an essential prerequisite [31]. For example, steam treatment for mica before silanization gives an excellent coverage for SAM formation although thermal or electric field treatment for some substrates might significantly reduce the surface concentration of -OH groups, thereby suppressing the adsorption rate [14, 32]. However, the precise role of the -OH groups on the surface is not yet known. In some reports, the -OH groups are assumed to be the source of affinity, since at least some of the silane molecules are attached to the surface via reaction with the -OH groups [33]. The -OH groups may otherwise adsorb a thin layer of water, which is supposed to be important for

silanization reactions [34]. Regardless of the precise mechanism in which surface silanol groups promote the self-assembly of alkylsiloxanes, it is generally accepted that, to facilitate the self-assembly process, surface pretreatments that make the substrates clean and hydrophilic are necessary. Most of these treatments are also valid even if the same substrate is used for SAM formation in gas phase [34].

1. 3. 2 Effect of Water Content

Although, alkylsilane monolayer formation is carried out in dry nitrogen filled glove box, trace amount of water is considered to be crucial for the covalent attachment of siloxane molecules to the substrate [35]. In the absence of significant amount of water, siloxane SAM growth is extremely slow and it may require many days, whereas the critical amount of water promotes the reaction leading to the island growth at the initial stages [35-37]. It is now well established that the presence of water in the range of a few monolayers on the substrate promotes the ordering. For example, Fairbank et al., have reported that three monolayers of water are necessary for high quality surface film formation on high surface area silica gel [38]. Infrared and sum frequency generation spectroscopic measurements give clear evidence for the presence of a thin water film of molecular thickness on the substrate surface [39-41]. During the initial stages of SAM growth, silane or silanol molecules are physisorbed on this water film and subsequently get cross-linked to form a 2D network. Normally few molecules are also directly attached to the substrate during this process and get stabilized by lateral attraction with neighboring molecules [42].

The above role of water gets further experimental support from the fact that control of humidity directly influences the time needed to form a monolayer. For instance, when the monolayer is prepared by immersing the silicon wafer in a solution of alkyltrichlorosilane maintained in a dry atmosphere, a complete layer is obtained only after 5 hours although same experiment under air at 30 % relative humidity forms a complete monolayer within *approximately* 1 h. This difference in rate could be explained by the different amount of water adsorbed on the polar surface of the Si / SiO_2 substrate, which is otherwise available for Si-O-Si linkages [43].

1. 3. 3 Effect of Solvent

Solvents like, ethanol, heptane, toluene, chloroform, carbon tetrachloride, dodecane, or sometimes mixed solvents are used for the silane SAM formation. The choice of a solvent is done usually on the basis of a few criteria like, low cost, low toxicity, availability in high purity and lower tendency to get incorporated into the monolayer.

Water content of the solvent used for SAM formation has a strong effect on the quality of alkylsiloxane, since the presence of water is essentially required for the initial hydrolysis of the trichlorosilane group [44]. However, a high water content of solvent leads to the polymerization of OTS in bulk solution opposing the surface reaction of single alkylsilane molecules [45]. In contrast, low water content results in incomplete monolayers because of insufficient hydrolysis. For example, a moisture quantity of 0.15 mg/100 mL of solvent has been reported to be the optimum content for the formation of closely packed monolayers [36b, 44b, 46]. Similarly, Rozlosnik et al., reported the effect of solvent polarity and concentration on the formation of high-coverage monolayers of alkylsiloxanes on silicon oxide surfaces in heptane (intermediate water solubility), dodecane (very low water solubility) and toluene (comparatively higher equilibrium water)[47]. In case of heptane and dodecane the formation of high-quality mono/multilayers was observed although a wide variation in quality is seen as compared to toluene. Hence, much of the previously published works on the formation of monolayers of OTS have indeed used toluene as the solvent [47, 48].

1. 3. 4 Effect of Temperature

Temperature is another important variable, which can control the molecular conformations and physical properties of SAMs during the formation itself. It has been reported that certain silane molecules can undergo lateral reorganization on the surface to have 2D phase transitions [43, 49]. For example, Carraro et al., have reported that the self-assembly of octadecyltrichlorosilane (OTS) based monolayers on the oxidized Si (100) surface can be initiated by three distinct mechanisms: island growth at low temperatures ($T < 16$ °C), homogeneous growth at high temperatures ($T > 40$ °C), and a mixed regime at intermediate temperatures [50]. Accordingly, Figure 1.2 shows a

schematic phase diagram of a Langmuir film in the spreading pressure-specific area plane. The solid curves delimit the coexistence regions between liquid-condensed (LC), liquid-expanded (LE), and gas phases (G) on Si surface. The dashed lines represent two isotherms, one below and one above the triple-point temperature.

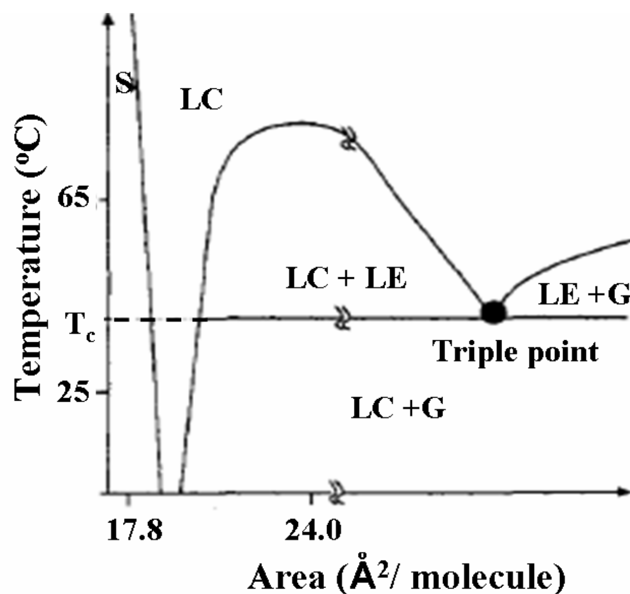

Figure 1. 2: Schematic phase diagram of a Langmuir film of OTS on Si substrate; the solid curves delimit the coexistence regions between liquid-condensed (LC), liquid-expanded (LE), and gas phases (G), the dashed line represents two isotherms, one below the triple-point temperature and one above. [Adopted from 38].

These results support the concept of a transient Langmuir film at the substrate-solution interface and the observed growth patterns are consistent with nucleation of LC domains coexisting with a two-dimensional G at low temperature, or with a LE at intermediate temperatures as shown in Figure 1. 2**.** In addition, AFM images of quenched partial OTS- SAMs on the same substrate over a range of temperatures are shown in Figure 1. 3.

At a low temperature (10 °C), dendritic islands are observed to grow and coalesce to cover the surface, while at a high temperature (40 °C) only a homogeneous uniform film is seen. At an intermediate temperature (25 °C), some dendritic islands are observed to nucleate and grow. However, before they could coalesce and cover the entire surface, the continuous phase between the islands gradually increase its thickness ending the film formation. The quenched OTS-SAM prepared on Si substrate at a temperature below ~ 30 °C contains well-ordered alkyl chains, while those at higher temperatures reveal

increasing chain disorder [43,50]. For n-octadecylsiloxane monolayers on silicon substrate, below a critical temperature (*Tc* ~30 ^{o}C) the surface energy is constant at a near-limiting value corresponding to that for a pure -CH_3 terminated surface. In this a heterogeneous structure with closely spaced islands of densely packed all-trans alkyl chains are arranged, nearly vertical to the surface. In addition it shows extremely low surface tension (γ_c = 20.5 mN/m) and low contact angle hysteresis (less than 1°).

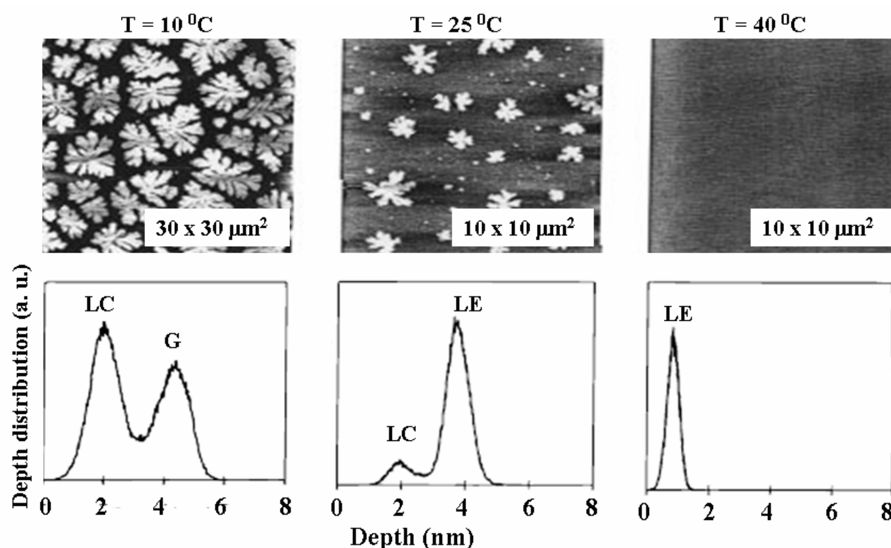

Figure 1. 3: Top: AFM images of partial SAMs of OTS on Si grown at 10, 25, and 40°C for 30 s (left to right). Bottom: Depth distribution histograms for the three images above. [Adopted from 38].

In contrast, when prepared above *Tc*, the surface energy monotonically increases, and the films exhibit monotonically diminishing coverage with increasing preparation temperature. The temperature *Tc* is an intrinsic property of the silane molecule although it depends on the chain length and perhaps insignificantly on the nature of the solvent.

Further it has also been reported that annealing improves the quality of SAM depending on the temperature. For example, Tripp and Hair, using FTIR and ^{29}Si CP/MS NMR spectroscopy, showed that no chemical attachment of OTS to the silica surface (i.e., Si_s-O-Si bond formation, where Si_s is a surface silicon atom) occurs at room temperature, although the cross-linking reaction (condensation between adjacent silanols with formation of a Si-O-Si bond) of OTS is evident at room temperature [44c, 51]. As the packing and conformational order of alkyl chains in SAMs depend on the underlying structure of the surface silanols and adsorbed water, annealing at temperatures from 120

to 200 °C, promotes further condensation reactions [52]. In case of polyoctadecylsiloxane (POS), additional cross-linking reactions in siloxane chains do occur at 170-180 °C, as reported by Tripp and Hair [44c, 51]. Further, addition of amines, such as triethylamine (TEA), is sometimes useful to improve the coverage and attachment of OTS to silica substrates [44b]. Also slow heating of OTS-monolayer to 150 °C reduces water adsorption by the OTS layers resulting into a cross-linked film with reduced number of silanols.

1. 4 Structure, Kinetics and Mechanism of SAM Formation

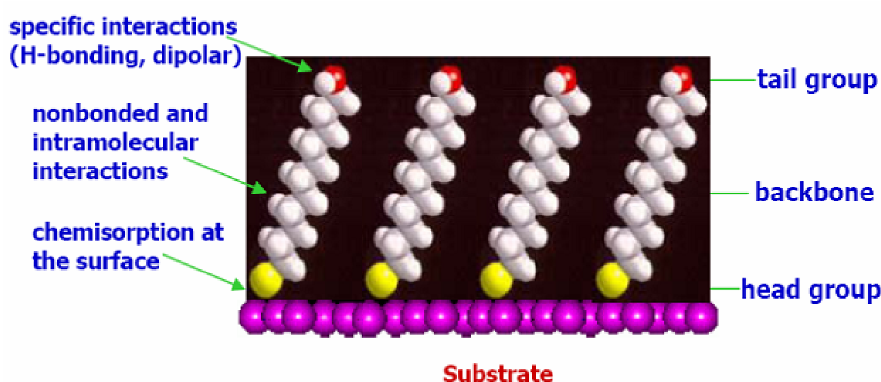

Figure 1.4: Schematic of self-assembled monolayers, including the constituents of a molecule and the driving force for the spontaneous formation of self-assembled monolayers.

Figure 1.4 depicts a schematic representation of SAMs, including the constituents of a molecule and the driving force for their spontaneous formation. These molecules selectively chemisorb on the substrate surface and from the energetic point of view should contain three parts–the active head group, hydrocarbon alkyl chain and the terminal functional group. All these parts play an important role in controlling the stability and dynamics of the monolayer. The active head group chemisorbs on the substrate by pinning the functional group to a specific site on the surface to form a chemical bond. The energy associated with this process is 40-50 kcal/mole. As the process is exothermic, molecules try to occupy every available site on the surface and the inter chain van der Waals interactions (~10 kcal/mole) play an extremely important role in controlling the stability as well as molecular alignment. The terminal functional groups in the monolayer provide hydrophobic interactions especially if they are methyl groups and the energy associated with them is less than 1 kcal/mole, which leads to a stable

monolayer. Even though the preceding scheme may appears simple, formation of a compact monolayer of alkylsiloxane in fact, remains challenging.

Although a variety of molecules such as long chain alkyl thiols, acids and amines are known to form excellent SAMs on metallic substrates, different types of organo silicon molecules like trichlorosilane or trimethoxy silanes with a long hydrocarbon chain are essential for semiconducting substrates like Si to get compact SAMs with high coverage. For example, when freshly cleaned Si substrate is dipped in millimolar OTS solution, OTS reacts with the –OH group present on the surface of the Si substrate and the trace amount of water so that a monomolecular film is adsorbed on the surface. [$RSiCl_3 + H_2O = R\ Si\ (OH)_3 + HCl$].

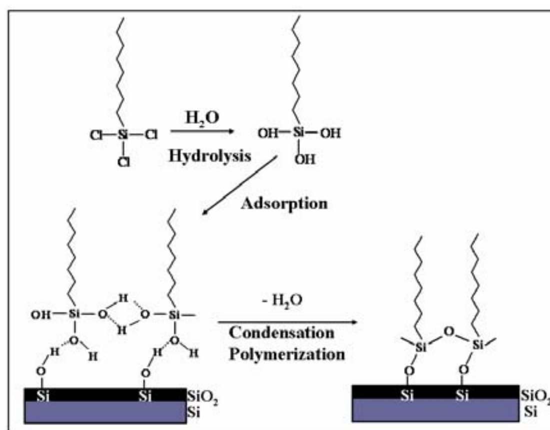

Figure 1. 5: Schematic of OTS SAM formation on Si substrate from a very dilute solution using a suitable solvent on metal or semiconducting substrate

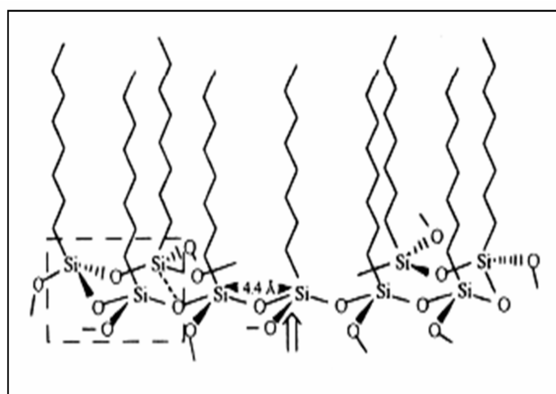

Figure 1. 6: Schematic description of a polysiloxane at the monolayer –substrate surface. The arrow points to an equatorial Si-O bond that can be connected either to another polysiloxane chain or to the surface

In some respects, the SAM could be viewed as an *in situ* formation of polysiloxane, which is connected to surface silanol groups (Si-OH) to form a network of Si-O-Si bonds

on the substrate as shown in Figure 1.5 and 1.6**.** X-ray photoelectron spectroscopy (XPS) studies confirm the complete surface reaction of the -$SiCl_3$ groups, upon the formation of a SAM [44b]. More interestingly, the Si-Si spacing between the polysiloxane chains is 4.4 Å and the chains are locked near perpendicular to the surface as shown in Figure 1. 6**.**

Most of the oligomeric units formed in solution will adsorb on the surface faster than the monomeric trichlorosilane, resulting in two different isomers, the one in which the alkyl chains are connected to the axial position and the other in which it is connected to the equatorial position with respect to the Si-O bond. This distribution indirectly affects the surface polymerization defining the free volume between the alkyl chains. The C-C distance is about 4.25- 4.35 Å (tilt angle $\leq 15^{o}$) and 4.90-5.00 Å (tilt angle $\geq 30^{o}$) for the axial and equatorial isomers respectively. For example, Tillman et. al, and others have reported that alkyl chains in the OTS monolayer tilt ca. 14° from the surface normal, which causes a reduction of ~ 0.8 Å in film thickness [16b]. However, Biernbaum et al. have reported that the OTS- SAMs are practically perpendicular to the substrate (tilt angle $0 \pm 5°$) using near-edge X-ray absorption fine structure spectroscopy (NEXAFS) and X-ray photoelectron spectroscopy (XPS) [53]. Interestingly, the adsorption mechanisms of trichlorosilane and trimethoxysilane groups are different, resulting in a higher tilt angle of the chains in octadecyltrimethoxysilane (OTMS)-SAMs ($20 \pm 5°$). Thickness of the OTS monolayer on Si is 25 ± 2 Å, which is in close agreement with the predicated value of 26.2 Å by assuming that the methylene unit (CH_2) contributes 1.26 Å to the thickness (C-C bond length of 1.54 Å and a tetrahedral angle of 109.5^{o}), the Si-C, Si-O and terminal methyl group contributes 1.52, 1.33 and 1.50 Å respectively [6, 16b, 44b].

Usually, the kinetics of monolayer formation follows a simple Langmuir isotherm, which assumes that the rate of deposition is proportional to the free space on the surface. That is, $\theta = 1-e^{(-kct)}$ where θ is the adsorbate coverage, *t* is the reaction time, c, concentration of silane and k is the rate constant, which has been frequently used to fit kinetic data for SAM growth. Although, Langmuir kinetics is solely determined by the competition between desorption, which is assumed to be proportional to the adsorbate surface coverage θ, and adsorption that is proportional to the area unoccupied by adsorbate, (1-θ). The experimental evidence, however, suggests that the self-assembly of

siloxane does not obey simple Langmuir kinetics. The adsorption and desorption depend not only on adsorbate surface coverage but also on many processes including diffusion, nucleation, lateral organization**,** hydrolysis and polymerization [54]. Peterlinz and Georgiadis, reported that the early stages of monolayer formation follow second-order Langmuir kinetics or a diffusion-limited form while a second step obeys zero-order kinetics [54a]. *In situ* IR and X-ray reflectivity studies of alkylsilane SAM growth are in reasonable agreement with Langmuir kinetics, except when the data is collected for early times or using solutions with a higher water content [55].

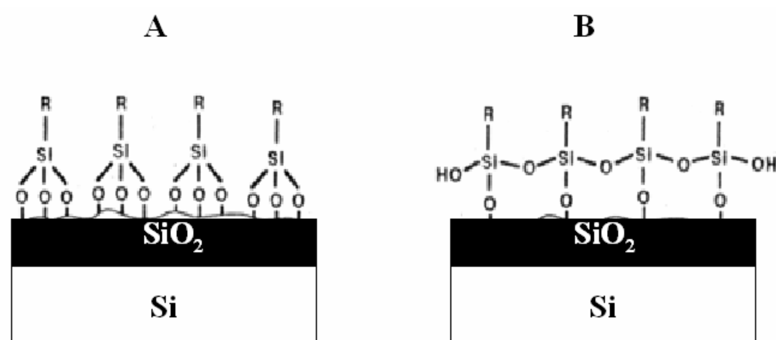

Figure 1. 7: Models for the binding of alkylsiloxane monolayers to Si/SiO_2, substrates, A) The silicon atom in the alkyltrichlorosilane, $RSiCI_3$, forms three lateral bonds to hydroxyl groups at the surface of the substrate oxide layer. The formation of this structure does not require any adsorbed water, B) the silicon atom in $RSiCI_3$, forms one or two bonds to surface hydroxyl groups. The remainder of the Si-C1 bonds is hydrolyzed, resulting in the formation of silanols (Si-OH) and Si-O-Si linkages between adjacent alkylsilanes. The Si-O-Si links can also bind within the monolayer alkylsilanes whose silicon atom has not formed any bonds to the surface.

Most often, the irreproducible nature of the siloxane SAM (due to its variable tendency to polymerize) adversely affects its applications, where well-defined and compact monolayers are required. For example, in the case of silane SAMs, horizontal polymerization (cross-linking along the surface plane) is desirable since the cross-linking of the siloxane network enhances the stability of siloxane SAMs. However, bulk polymerization is undesirable, since this could create many macroscopic islands with ill-defined morphology (shown in Figure 1.7 A and B) [44b]. Bulk polymerization is induced by the hydrolysis of trichlorosilane and is catalyzed by HCl a product of the hydrolysis. Consequently, the reaction kinetics is complex and many parameters sensitive to reaction conditions need stringent control. It has been reported that subtle variations of some experimental conditions, such as trace amounts of water, may alter the growth behavior of monolayers significantly [56].

Several laboratories report strikingly different results. For example, ODS SAMs have been reported to require reaction times ranging from a few minutes to 24 hours or even days and often the reaction is not self-limited to monolayers but to multilayers with ill-defined morphology [44b, 57-59]. Wasserman et. al., hypothesized two extreme possibilities for the structure of silane monolayers using the x-ray reflectivity as depicted in Figure 1.7 [44b].

A complete monolayer is characterized by length, *d,* and refractive index, *n.* Partial monolayers are formed by removing substrates from solutions containing alkyltrichlorosilane before complete monolayer formation and submonolayer coverages can be estimated by suitable techniques. In one possible model (uniform model) for an incomplete monolayer, the alkyl chains are uniformly distributed over the substrate in a disordered manner having a liquid like structure with a refractive index similar to that of the complete monolayer despite less thickness. In the alternate model (island model), monolayer consists of islands of alkylsiloxane groups having the thickness of a complete monolayer although the average refractive index is lower.

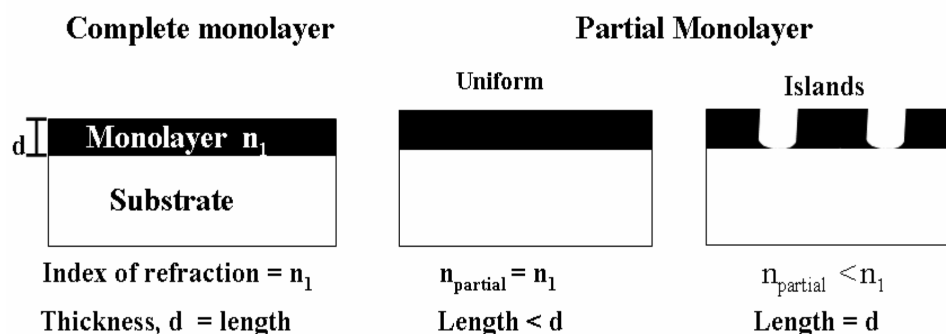

Figure 1. 8: Models for the structure of incomplete monolayers, a complete monolayer has a thickness, *d,* and an index of refraction, $n_{1,}$ in the uniform model the partial monolayer has a length less than *d* and an index of refraction approximately equal to *n,* in the island model the incomplete monolayer has a thickness, *d,* but the index of refraction is less than n_1

1. 5 Stability of SAMs

1.5.1 Chemical Stability

Stability of SAMs on different substrates been extensively studied using various characterization techniques. For example, methyl-terminated siloxanes monolayer (after being washed with ethanol to remove contaminants adsorbed from the air) after storing for 18 months in closed container in air shows contact angle and length indistinguishable

from those determined immediately after preparation. However, detailed studies reveal that more polar surfaces get contaminated more rapidly as compared to that of non-polar ones.

Rubbing the surface vigorously with a tissue or cotton swab does not change the thickness or wettability of the monolayer. Similarly, silane monolayers are chemically stable in 0.1 M HCl at room temperature and also in organic solvents like hexadecane even at 75 ^{o}C. In comparison, on exposure to aqueous alkali at room temperature, approximately 50% of the monolayer gets removed after 80 min. Although the substrate appears normal at 80 min, the surface appears visible etched after 160 min. The negative length observed in some cases at this point could be explained probably due to the attack on the native oxide, since the silicon-oxygen bond gets hydrolyzed under basic condition [56].

1.5.2 Thermal Stability

Thermal behavior of monolayer has been reported to be independent of the hydrocarbon chain length and monolayers have found to be stable in vacuum even up to 450 ^{o}C [3]. For example, OTS monolayer on Si is stable up to 350 ^{o}C in N_2 atmosphere although its stability in air is limited only up to 225 ^{o}C. Some of the monolayers are chemically stable in aqueous solutions (e.g., 0.1 M HCl at room temperature) as well as in organic solvents like hexadecane at 75 ^{o}C. This is especially significant for MEMS applications, as SAMs would be capable of sustaining different environments during various stages of micro-fabrication [5, 6].

1.6 Characterization techniques

The main emphasis of this thesis is on the preparation and characterization of the alkyltrichlorosilane monolayer on Si in order to explore their properties for selected applications. Monolayers on Si substrate as well as on silica particles have been characterized by a host of techniques such as contact angle (CA) measurements, Fourier transform infrared spectroscopy (FTIR), X-ray photoemission spectroscopy (XPS), Transmission electron microscopy (TEM), Scanning electron microscopy (SEM), X-ray diffraction (XRD), Atomic force microscopy (AFM), Thermogravimetric analysis (TGA), Cyclic voltammetry (CV) and Impedance measurements. Many other techniques

have also been used to get supporting evidence and this part of the chapter is devoted in explaining the basic principles of these techniques along with their limitations in resolving various aspects of monolayer structure and dynamics.

1.6.1 Contact Angle Measurements

CA measurement is a surface sensitive technique, which quantitatively unravels the wetting of a solid by a selected liquid like water or hexane, enabling a simple and effective method to determine the surface energies, and its relation to the structure and composition of a surface [60].

It is actually a comparative technique in which the wetting property can be studied by placing a small (2-4 μl) drop of the liquid onto a flat solid surface. Since, wetting involves the interaction of a liquid with a solid, the spreading of a liquid over a surface along with the penetration of a liquid into a porous medium, or the displacement of one liquid by another could be monitored to understand the nature of many surfaces. It also directly provides information on the interaction energy between the surface and the liquid. For example, the water CA for a smooth solid surface exposing closely packed methyl groups ($-CH_3$) is 111°-115°, while the hexadecane CA for the same surface is 45°-46° highlighting the importance of hydrophobic interactions of the terminal group [61-62].

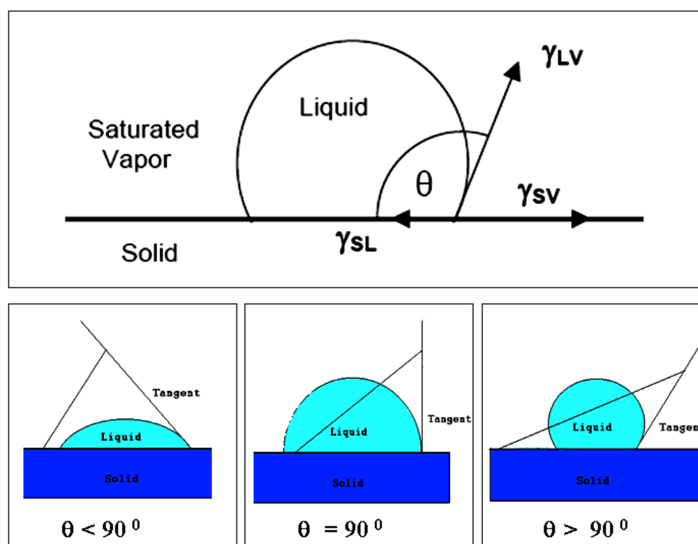

Figure 1. 9: Schematic diagram showing different possible contact angles of a liquid drops on a solid substrate

CA is defined geometrically as the angle formed by a liquid at the three phase boundary (contact line / wetting line) where a liquid, gas and solid intersect as shown in Figure 1.9. Low values of θ indicate that the liquid spreads, or wets well, while high values indicate poor wetting. If the angle θ is less than 90° the liquid is said to wet the solid (hydrophilicity) while values greater than 90° indicate non-wetting nature (hydrophobicity). On one side, a zero CA ideally represents complete wetting while 180° on the other side can reveal no interactions.

From a thermodynamic perspective, the shape of the liquid drop will be affected by the free energy of the surface, which forms an angle with the surface, known as the CA, which in turn, is a function of the surface free energy as defined by the Young – Dupre equation,

$$\gamma_{LV} \cos \theta = \gamma_{SL} - \gamma_{SV}$$

where, θ is the angle between the tangent to the droplet and the surface and $\gamma_{SV,}$ γ_{LV} and γ_{SL} are the surface tension at solid-vapor interface, liquid-vapor interface and solid-liquid interface respectively [61]. However, this relationship is valid only for a smooth surface, which is assumed to be ideal. For real i.e., rough surfaces; Wenzel modified this expression by incorporating a roughness ($r \geq 1$) as an adjustable parameter, as

$r = \cos\theta_{\text{rough surface}} / \cos\theta_{\text{smooth surface}}$, where, surface roughness is defined as a ratio of the observed CA (on rough surface) to the CA on the smooth surface. According to this equation, surface roughness should increase CA for cases greater than 90°, and decrease for cases less than 90° [63].   .

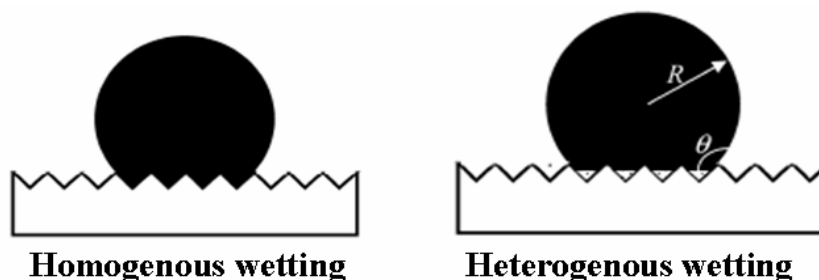

Figure 1. 10: Homogenous and Heterogeneous wetting on hydrophobic rough surfaces.

Equilibrium wetting on rough surfaces is discussed in terms of a "competition" between complete liquid penetration into the rough grooves and entrapment of air bubbles inside the grooves underneath the liquid. The former is the homogeneous wetting

regime, usually described by the Wenzel equation while the latter is the heterogeneous wetting regime that is described by the Cassie-Baxter equation (as shown in Figure 1.10) [64]. In case of heterogeneous surfaces, the Cassie equation was suggested for the interpretation of wettability results.

$$\cos\theta = f_1 \cos\theta_1 + f_2 \cos\theta_2,$$

where, θ is the CA of a liquid on the heterogeneous surface composed of a fraction f_1 of one type of chemical group and f_2 another chemical group with $f_1 + f_2 = 1$ and θ_1 and θ_2 represent CA of liquid on the pure homogenous surfaces of 1 and 2 respectively.

Some surfaces have CAs as high as 150° or even 180°, where water droplets simply rest without actually wetting to any significant extent. These surfaces are termed 'superhydrophobic' and this behavior can be seen on fluorinated surfaces (Teflon-like coatings) which have been appropriately micropatterned. These new surfaces are based on the design of lotus leaf's surface (a leaf which has little protuberances) and would be superhydrophobic even to honey. These surfaces with CA greater than 150° along with a low contact angle hysteresis (less than 5 ^{o}) usually show self cleaning properties [65].

Many methods are used for measuring CAs including sessile drop, captive drop, and the dynamic Wilhelmy and Tilting plate. The sessile drop (free standing drop) method has been extensively used in this work, since it estimates the wetting properties of a localized region on a solid surface conveniently. The method is also ideal for curved samples or where one side of the sample has different properties than the other.

Since CA depends on liquid purity, temperature, as well as the statistical errors in the actual reading of CA, reproducible studies needs accurate control of temperature, relative humidity and vapor pressure of the liquid. To minimize these errors in the reading, CA measurements should be done in a vibrationless condition, preferably using a heavy table equipped with shock absorbers also using a drop of fixed volume and an accurate syringe. This can be achieved by working in a closed, insulated compartment containing a small beaker with the liquid under study purged with water–saturated nitrogen [66].

For all our studies, we have used a sessile water drop of 1-4 μL capacity with the help of a Rame-Hart 100 goniometer and a GBX –Model 'Digidrop' contact angle meter.

1.6.2 X-ray Photoelectron Spectroscopy (XPS)

XPS is a surface technique useful to study the composition and electronic state of the surface region of a sample. Since, the technique provides a quantitative analysis of the surface composition it is sometimes known by the alternative acronym, ESCA (Electron Spectroscopy for Chemical Analysis) [67].

XPS is based on the well-known photoelectric effect (a single photon in/electron out process) first explained by Einstein in 1905. Photoelectron spectroscopy uses monochromatic sources of radiation (i.e. photons of fixed energy given by relation, E = hν, *h* - Planck constant (6.62×10^{-34} J s), ν-frequency (Hz) of the radiation) such as Al Kα (1486.6 eV), or MgKα (1253.6 eV). The photon is absorbed by an atom in a molecule or solid, leading to ionization and the emission of a core (inner shell) electron as shown in Figure 1.11. In XPS, Soft x-rays (200-2000 eV), and in Ultraviolet Photoelectron Spectroscopy (UPS), vacuum UV (10-45 eV) radiations are used to examine core levels and valance levels respectively. The kinetic energy distribution of the emitted photoelectrons (i.e. the number of emitted photoelectrons as a function of their kinetic energy) can be measured using any appropriate electron energy analyzer and a photoelectron spectrum can thus be recorded.

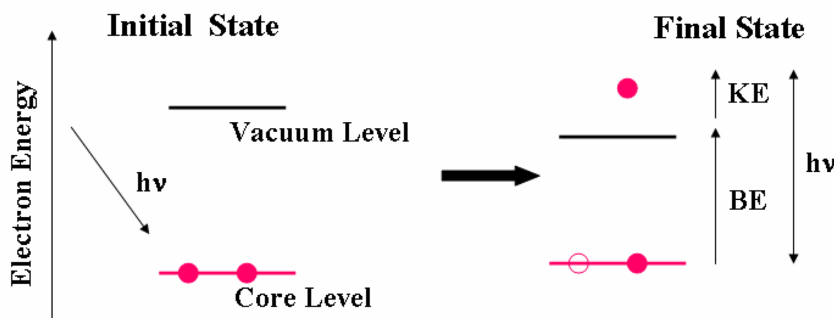

Figure 1.11: Schematic representation of the emission of a core level electron by photo-irradiation.

The overall process of photoionization is follows:

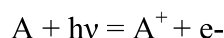

$$A + h\nu = A^{+} + e^{-}$$

According to conservation of energy,

$$E(A) + h\nu = E(A^{+}) + E(e^{-})$$

Since the electron's energy is present solely as kinetic energy (KE) this can be rearranged to give the following expression for the KE of the photoelectron:

$$KE = h\nu - (E(A^+) - E(A))$$

The final term in brackets, representing the difference in energy between the ionized and neutral atoms, is generally called the binding energy (BE) of the electron. i.e. KE = hν – BE. The BE levels in solid are conventionally measured with respect to the Fermi-level of the solid, rather than the vacuum level. This involves a small correction to the equation given above in order to account for the work function (φ) of the solid, KE = hν - BE - φ. Employing photons with fixed energy hν, it is possible to measure BE of electron in solid if kinetic energy KE and work function φ of the sample are known. Binding energies being characteristic of atoms, different elements present in the sample under investigation are identified. The soft X-rays employed in XPS penetrate a substantial distance into the sample (~ µm). Thus this method of excitation imparts no surface sensitivity at the required atomic scale. However the photoelectrons can escape from only a very short distance beneath the surface (< 100 Å). The surface sensitivity thus arises from the emission and detection of the photoemitted electrons. Sometimes, electrons traveling through a material have a relatively high probability of experiencing inelastic collisions with locally bound electrons as a result of which they suffer energy loss and contribute to the background of the spectrum rather than a specific peak. The BE of an electron depends not only upon the level from which photoemission is occurring, but also on the i) formal oxidation state and the ii) local chemical and physical environment, changes in either i) or ii) give rise to the small shift in the peak positions in the spectrum so called chemical shifts.

For insulating samples, when the photoelectrons are emitted out, a positive charge zone will establish quickly in the sample surface. As a result, the sample surface acquires a positive potential (varying typically from several volts to tens of volts) and the kinetic energies of core electrons are reduced by the same amount, C, i.e BE = hν -(KE-C). The surface charging results in the shift of the XPS peaks to higher BE. In this case, the BE has to be calibrated with an internal reference peak i.e. C 1s (BE 284.8 eV) peak from the adventitious carbon-based contaminant. In order to neutralize the surface charge during data acquisition, a low-energy electron flood gun is used to deliver the electrons to the sample surface. The electron flood gun can be tuned to provide the right current to push the XPS peaks back to the real position. Atoms of a higher positive oxidation state

exhibit a higher BE due to the extra coulombic interaction between the photo-emitted electron and the ion core. This ability to discriminate between different oxidation states and chemical environments is one of the major strengths of XPS.

The basic requirements for an XPS experiment are, X-ray source of fixed-energy radiation (usually Mg Kα with hν = 1253.6 eV or Al Kα with hν = 1486.6 eV) and a Concentric hemispherical analyser (CHA), which uses an electric field between two hemispherical surfaces to disperse the electrons according to their kinetic energy, and thereby measure the flux of emitted electrons of a particular energy and a high vacuum environment (to enable the emitted photoelectrons to be analysed without interference from gas phase collisions).

Throughout the investigations described in this thesis, XP spectra of C 1s, Si 2p, and O1s, core levels were recorded from a self assembled monolayer on Si (100) substrate on a VG Microtech ESCA 3000 instrument at a base pressure greater than 1 x 10^{-9} Torr with un-monochromatized Mg Kα radiation (1253.6 eV energy). Measurements were made in the constant analyzer energy (CAE) mode at pass energy of 50 eV and electron takeoff angle (angle between electron emission direction and surface plane) of 60° leading to an overall resolution of ~ 1 eV. Chemically distinct components in the core level spectra were resolved by a non-linear least squares fitting algorithm after background removal by the Shirley method [67].

1.6.3 Fourier Transform Infrared Spectroscopy (FTIR)

Infrared (IR) spectroscopy is a useful, nondestructive technique for the study of molecular packing and orientation in mono/multilayers. Since atoms in a molecule always vibrate about their mean position if there is a periodic alternation in the dipole moment then such mode of vibration is infrared (IR) active (100 μm–1 μm) as the vibrating molecule can absorb energy. Consequently, the appearance or non-appearance of certain vibrational frequencies gives valuable information about the structure of a particular molecule. The frequency of vibration is given by the relation:

$$\nu = \frac{1}{2\pi}\sqrt{\frac{k}{\mu}}$$

where, k is the force constant; μ is the reduced mass.

Various peaks assigned for alkyltrichlorosilane self-assembled monolayer on Si substrate are mainly in the C-H stretching region. For example, two bands at 2919 and 2850 cm^{-1} are assigned to the antisymmetric and symmetric methylene (CH_2) stretching vibrations respectively while two weak bands at about 2958 and 2875 cm^{-1} correspond to the asymmetric/degenerate and symmetric methyl (CH_3) stretching vibrations respectively. The position of the peaks and the increase in intensity of the methylene stretching vibrations relative to methyl stretching vibration with chain length indicates structural integrity of the molecule. More interestingly, actual peak values of the symmetric and antisymmetric CH_2 stretching vibrations can be used as a sensitive indicator of the ordering of the alkyl chains. The intensity and peak positions of the C-H stretching vibrational modes ($–CH_2$) of the monolayer film provide information on the monolayer formation rates and structural changes during the course of the growth process. For example specific shifts from 2928 to 2919 $cm^{–1}$ and from 2856 to 2850 $cm^{–1}$ for the methylene peaks are well known on going from a liquid to solid alkane phase and therefore the observed wavenumbers in our case are indicative of a densely packed monolayer of alkyl chains [68, 69].

Different modes are employed for analysis depending on the nature of the sample and required level of sensitivity viz., transmission (general mainly powder samples), Attenuated total reflectance (ATR) (thick samples, diffusion work), Diffuse reflectance fourier transform infrared (DRIFT)-(powders), Reflection absorption infrared spectroscopy (RAIRS)-(very thin samples) and Grazing angle infrared spectroscopy – (very thin sample)

In this work, the OTS monolayer on Si substrate was characterized by grazing angle and ATR -FTIR spectroscopy on a Perkin Elmer 1615 spectrometer. Bare silicon wafer was used as a background sample and the spectrum was recorded at a resolution of 4 cm^{-1} over 256 scans at room temperature. Similarly, OTS monolayer on silica particles was characterized by diffuse reflectance mode (DRIFT), in which, sample was made in the form of a pellet after mixing with spectroscopic grade KBr.

1.6.4 Transmission Electron Microscopy (TEM)

TEM is a powerful tool for characterizing the atomic-scale structures of materials as it not only provides a real space resolution better than 0.2 nm, but also gives

a quantitative chemical and electronic analysis from a region as small as 1 nm. In this technique, a beam of electrons accelerated by an electric field formed by a voltage difference of, typically, 200 kV is focused by condenser lenses, to a spot of 1 mm on the thin film under investigation. The transmitted electron signal is then magnified by a series of electromagnetic lenses. As the electrons travel through the specimen, they are either scattered by a variety of processes or remain unaffected by the specimen. The end result is that the non-uniform distribution of electrons emerging contains all the structural and chemical information about the specimen appearing on a fluorescent screen or layer of photographic film to be detected by a charge coupled device (CCD) camera. In *bright field imaging*, the image of a thin sample is formed by the electrons that pass the film without diffraction, while in the *dark field imaging* mode, a diffracted beam is used for imaging. Direct electron images yield information about the microstructure of the material and about its defects, while electron diffraction patterns are used to determine the crystallographic structure of the material.

Samples for electron microscopy in the form of very thin films are mounted on fine-meshed Cu grids (~ 400 μm mesh). In case near-atomic resolution is required film thickness is to be limited to a few tens of Å and hence the quality of the electron microscopy work is limited by the thinning-down procedure as structural changes may occur during the thinning. Electrons are charged particles, and because collision with charged molecules of air will absorb and deflect electrons and distort the beam, the optical system of an electron microscope must be evacuated of air. High energy electron beam is produced by heating a tungsten filament at voltages usually ranging from 6,000 to 100,00 volts. Similarly it is better to image as many areas as possible to ensure the representative nature before collecting data.

In the present study, TEM has been used for determining the size of silica nanoparticles drop coated onto a carbon-coated copper grid. TEM measurements were done on a JEOL model 1200EX instrument operated at an accelerating voltage of 120 kV. With the availability of slow-scan CCD cameras and the recent digital revolution, it is possible to treat the digital data of electron diffraction patterns and the corresponding TEM images recorded under low magnification.

1.6.5 Scanning Electron Microscopy (SEM)

SEM is a type of electron microscope capable of producing high resolution images of a sample surface. The first, true scanning electron microscope (SEM) was developed and described in 1942 by Zworykin et al., [70]. In a typical SEM, electrons are thermionically emitted from a tungsten or lanthanum hexaboride (LaB_6) cathode and are accelerated towards an anode; alternatively electrons can be emitted via field emission (FE) and this electron beam with an energy of about 100 - 50 keV, is focused by one or two condenser lenses into a beam with a very fine focal spot sized 1 - 5 nm. The beam passes through pairs of scanning coils in the objective lens, which deflect the beam in a raster fashion over a rectangular area of the sample surface. Through these scattering events, the primary electron beam effectively spreads and fills a teardrop-shaped volume, known as the interaction volume, extending from less than 100 nm to around 5 μm into the surface. Interactions in this region lead to the subsequent emission of electrons which are then detected to produce an image. X-rays, which are also produced by the interaction of electrons with the sample, may also be detected in an SEM equipped for energy-dispersive x-ray spectroscopy (EDX) or wavelength dispersive x-ray (WDX) spectroscopy.

Spatial resolution of SEM depends on the size of the electron spot which in turn depends on the magnetic electron-optical system which produces the scanning beam. The resolution is also limited by the size of the interaction volume, or the extent of material which interacts with the electron beam. Secondary electron imaging shows the topography of surface features a few nm across. Films and stains as thin as 20 nm produce adequate-contrast images. Materials are viewed at useful magnifications up to 100,000 X without the need for extensive sample preparation and ensuring no damage. Backscattered electron imaging shows the spatial distribution of elements or compounds within the top micron region of the sample and features as small as 10 nm can be resolved to determine composition variations of as little as 0.2%. In the present study, scanning electron microscopic (SEM) measurements of bare silica and silanized silica particles were carried out on a Leico stereoscan model 440 instruments equipped with Phoenix energy dispersive analysis of X-ray (EDX) attachment.

1.6.6 Atomic Force Microscopy (AFM)

AFM was invented in 1986 by G. Binnig and H. Rohrer, where one could probe the individual arrangement of the atoms to map the surface with routine single atom resolution [71]. In this technique, the surface of a sample is scanned with a stationary tip (made up of silicon nitride) mounted on a spring so that the atoms in the tip interact with those on the surface and the resulting attraction or repulsive forces could be monitored as shown in Figure 1.12. Like all other scanning probe microscopes, AFM utilizes a sharp probe rastering over the surface of a sample. The probe is a tip on the end of a cantilever, which bends in response to the force between the tip and the sample. The cantilever obeys Hooke's Law for small displacements, and the magnitude of deflection depends on the atomic forces between the surface atoms and the tip atoms, which in turn, depends on their distance of separation. The deflection can be recorded in various ways, the most common of which uses a laser focused on the top of the cantilever and reflected onto a photodetector. The photodetector signals are used to map the surface topography of samples with resolutions down to the atomic scale (i.e., fractions of an Angstrom). The lateral and vertical movements of the tip or sample (resolution of better than 0.1 nm) are controlled by piezoelectric transducers and a feedback loop that produce voltage differences proportional to movements. The image contrast can be achieved in many ways out of which, three main classes are *contact mode*, *non-contact mode* and *tapping mode*.

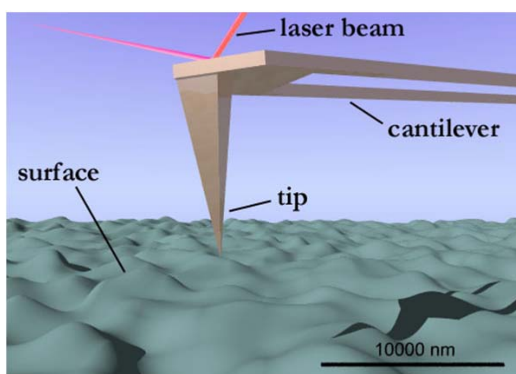

Figure 1. 12: Image of the tip of a scanning force microscope revealing the interaction between the tip and the sample.

Contact mode is the most commonly employed one and as the name suggests, the tip and the sample remain in close contact as the scanning proceeds. In this case the

force on the tip is repulsive with a mean value of 10^{-9} N. During the measurements, the contact tip deflection is used as a feedback signal. The deflection signal is boosted against noise and drift by using cantilevers with lower stiffness. But if the tip is moved too close to the substrate, where attractive forces might be quite strong, causing the tip to 'snap-in' to the surface. Therefore, it is advisable to carry out contact mode AFM always in circumstances where the overall force is repulsive. On the other hand, in non-contact mode the cantilever is oscillated above the surface of the sample at such a distance, where there is no longer repulsive interaction. However, as the tip is scanned at a constant height, it may inevitably lead to a tip crash with the substrate surface. In addition, if a thin layer of water contaminates the surface of the sample, it will invariably form a small capillary bridge between the tip and the sample causing the tip to "jump-to-contact". Therefore, non-destructive imaging is possible with these small forces. Tapping mode is the next most common mode used in AFM. When operated in air or other gases, the cantilever is oscillated at its resonant frequency (often hundreds of kHz) and positioned above the surface so that it only taps the surface for a very small fraction of its oscillation period. The tip were scanned at a constant height, there would be a risk that the tip would collide with the surface, causing damage. Tapping mode may be a far better choice than contact mode for imaging of soft samples.

AFM is a versatile technique, which can be used to study the monolayer topography and more significantly, it is possible to deposit molecules on a substrate (nanopatterning using an “inked” AFM tip) using the dip-pen nanolithography (DPN), an elegant technique recently developed by Mirkin and co-workers, where, patterned silane SAM formation has been more recently reported [23,72]. Further, time resolved atomic force microscopy could be used to study the growth mechanism of SAM formation, determination of surface roughness, grain size, and features on the nanoscale such as individual holes, defects (such as pinholes), and atomic clusters. It could be valuable to investigate a wide range of materials, including semiconductors, non-conducting surfaces, biological samples, high-resistivity materials, insulators, conducting samples, and features of microelectronic devices. AFM has several advantages over the scanning electron microscopy (SEM) since it provides a true three-dimensional surface profile especially because samples do not require any special treatments (such as metal/carbon

coatings) that would irreversibly change or damage the sample. It can be operated in ambient air or even a liquid environment. However, a major limitation is that, it can image only a maximum height on the order of micrometres and a maximum scanning area of around 150 X 150 μm^2. Another inconvenience is that, at high resolution the quality of the image is limited by the radius of curvature of the probe tip, and an incorrect choice of tip for the required resolution can lead to image artifacts. The AFM could not scan images as fast as an SEM, requiring several minutes for a typical scan, while an SEM is capable of scanning at near real-time (although at relatively low quality) after the chamber is evacuated. The relatively slow rate of scanning during AFM imaging often leads to thermal drift in the image, making the AFM microscope less suited for measuring accurate distances between artifacts on the image. However, speed has been improved in video AFM, where reasonable quality images are being obtained at a video rate - faster than that used in average SEM.

In the present work, AFM images were obtained using a Nanoscope II (Digital Instruments, Inc) operated at constant height mode with very low applied force (typically under 1 nN). All measurements were performed in ambient conditions using silicon nitride probes mounted on the micro-fabricated cantilever (force constant 0.6 N/m) in the tapping mode to avoid surface damage. The bearing ratio of the digital instrument software was used to estimate the surface coverage of the OTS monolayer.

1.6.7 Thermogravimetic Analysis (TGA)

Thermogravimetric analysis (TGA) is a widely employed technique for measuring the change in weight of a sample as a function of temperature and time in a controlled atmosphere, whereas DSC is particularly useful to understand phase transitions including the change of orientation of monolayer upon heating/cooling. Since TGA uses heat to force reactions and physical changes in materials, characteristic thermogravimetric curves of a material unravel kinetic and mechanistic information from unique sequence from physicochemical reactions occurring over specific temperature ranges and heating rates. For example, TGA is commonly employed to determine degradation temperature, absorbed moisture content of many polymeric materials, inorganic and organic components in materials, decomposition points of explosives and

solvent residues. It is also used to estimate the corrosion kinetics in the case of high temperature oxidation. However, the accuracy, precision and overall quality of thermal analysis data depends critically on the ability of the operator to optimize instrument performance and the selection of appropriate conditions for the experiment.

In the present study, thermogravimetric analysis was carried out on a Seiko thermal analyzer model No: TCA/DIA–32 of bare and surface silanized silica particles in air or nitrogen atmosphere.

1.6. 8 Electroanalytical Techniques

1. 6.8.1 Cyclic Voltammetry

Cyclic voltammetry is one of the most versatile electroanalytical techniques for the study of electroactive species. This has significant applications in the area of SAMs, as voltammetric data can provide a means to evaluate monolayer energetics and monolayer coverage (especially with respect to the barrier properties) using appropriate solvent [73, 74]. It also provides a ready means to estimate the double layer capacitance as well as the distribution of defects (like pinholes) in the monolayer. However when the monolayer is electro-inactive, an external redox couple like ferro/ferricyanide or ferrocene is employed to estimate the surface coverage, pinhole distribution etc.

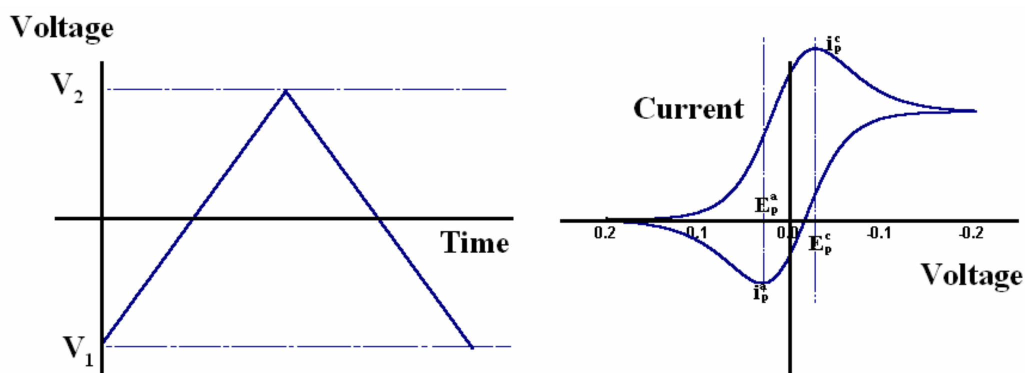

Figure 1. 13: In cyclic potential sweep, the voltage is swept between two values (initial potential) at a fixed rate, although when the voltage reaches V_2 (switching potential) the scan is reversed and the voltage is swept back to V1 (b); resulting cyclic voltammograms for a reversible case is shown on the right hand side, where E_p^a , Ep^c are anodic and cathodic peak potentials and Ip^a, Ip^c are anodic and cathodic peak currents.

The basic principle of voltammetry is the measurement of current after applying a linear potential sweep to a working electrode with respect to a reference electrode in an unstirred solution and often the potential sweep is reversed to complete one cycle. The

controlled potential applied as a triangular waveform in a linear fashion, could be considered as the signal transducing electrochemical changes at the SAM/electrolyte interface. The features of a cyclic voltammogram (a plot of current versus applied potential) like, peak potential separation and shape are extremely sensitive to the polarizability of the SAM/electrolyte interface and hence could provide valuable information about the monolayers [75]. The current-voltage curves are measured in a potentiostatic circuit using a three–electrode arrangement in order to vary the potential difference between the working electrode (WE) and the reference electrode (RE) at a predetermined rate (sweep rate).

The resultant cyclic voltammogram can provide a wealth of information for redox processes including the understanding of reaction intermediates, kinetic stability of products. For example, for a reversible redox reaction at 25 °C with n electrons peak width (ΔEp) should be 0.0592/n V or about 60 mV for one electron. In practice this value is difficult to attain because of factors such as uncompensated resistance and irreversibility arising due to a slow electron transfer rate resulting in ΔEp > 0.0592/n V, which means 70 mV for a one-electron reaction. Voltammetric techniques also have ability to unravel many adsorption processes through the appearance of pre-peaks and post-peaks in combination with an analysis using Anson plots (Q vs $t^{1/2}$). The scan rate can be varied by several orders of magnitude to suit the intrinsic rate constant of reactions and this along with the use of ultramicroelectode provides many unprecedented benefits to study coupled chemical reactions [75a]. Despite these advantages and simplicity it has many limitations such as need for charging current (nonfaradaic current) correction, dependence of voltammetric features on the nature of working electrode and supporting electrolyte, distortions due to ohmic drop, dependence on cycle number etc and hence many precautions are needed when one considers results of new systems for interpretation. In this work, cyclic voltammetric experiments of bare and monolayer derivatized Si electrodes were performed on an Autolab PGSTAT 30 (ECO CHEMIE) instrument at various scan rates.

1.6.8.2 Impedance Analysis

Electrochemical impedance is another important electroanalytical technique based on the measurements of the frequency dependent response of an electrochemical

cell after applying a small-amplitude sinusoidal signal under a potentiostatic control. When the impedance varies with frequency then real and imaginary parts come into picture. The measurement of the response of the electrochemical cell to a small amplitude alternating potential, interpreted using suitable equivalent circuit models can give valuable information about surface coverage, dielectric constant and electron-transfer behavior of the pinholes of the monolayers [75]. The reasons are often analyzed by complex impedance presentation (real versus imaginary plots) and the results are interpreted in terms of combining many passive circuit elements like capacitors, resistors and inductors. This way of equivalent circuit description of the monolayer–solution interface provides many advantages to determine the double layer structure and kinetic parameters.

For a given applied potential, $V(t) = V_0 \cos(\omega t)$, the resulting steady state current is given by $I(t) = I_0 \cos(\omega t-\theta)$, where, θ is the phase shift between the voltage and the current, which is also a function of the frequency of the input voltage. The impedance can be expressed as a complex number $Z(\omega) = V(t)/I(t) = Z_0 (\cos\theta + j\sin\theta) = Z'(\omega) + jZ''(\omega)$, where, Z' is the real component and Z" is the imaginary component of the impedance respectively. A common way to graphically present impedance data for a given system is plotting –Z" against Z' (Nyquist plot). Each point on the Nyquist plot is characteristic of the complex impedance at a given frequency although this representation does not indicate the frequency. Alternatively, in the "Bode plot" the impedance is presented against the log (frequency) and both the absolute value of the impedance ($|Z| = Z_0$) and the phase-shift are plotted on the y-axis. Unlike the Nyquist plot, the Bode plot explicitly shows frequency information [76]. The phase shift can also provide information about the cell time constants and the ideality of the SAMs capacitive behavior.

Advantages of impedance over other techniques include the use of low-amplitude sinusoidal voltage (about 5 mV) which provides only a marginal perturbation of the system from equilibrium (steady state), offers the possibility of obtaining information on important quantities such as ohmic resistance, double layer capacitance, film capacitance, as well as on other important processes such as charge transfer at the electrode/film interface and within the film in a single experiment. It is also possible to

characterize interfacial properties in the absence of a redox reaction. However, the model-dependence of the calculated parameters can sometimes mislead if an inappropriate circuit is selected. In addition, the difficulty of interpreting variations in the imaginary component is one of the major limitations [76].

In this work, electrochemical impedance measurements were carried out with Solartron 1255B frequency response analyzer (FRA) interfaced to 1287 potentiostat / galvanostat. Measurements were performed over a wide frequency range of 100 kHz-0.01 Hz with 10 mV rms amplitude and these data were analyzed using ZPLOT2 and ZVIEW2 for the frequency analysis and equivalent circuit fitting / simulation program respectively based on the complex non-linear least square (CNLS) method.

1.6.9 Miscellaneous Techniques

Apart from these techniques, several other special characterization techniques, such as Ellipsometry, X-ray reflectivity, X-ray diffraction (XRD), Scanning tunneling microscopy (STM), Surface enhanced raman spectroscopy (SERS), Sum frequency generation (SEG) spectroscopy, Energy dispersive analysis of X-ray (EDX), Electron Energy loss spectroscopy (EELS), and Quartz crystal microgravimetry (QCM) have been applied for investigation of SAMs [77-80].

1. 7 Applications of SAM

Preparation of ordered ultrathin organic films (a few nanometers to several hundred nanometers) has recently attracted considerable attention because of the possibility of controlling order and interactions at the molecular level. It can also be possible to tailor the terminal groups of SAMs for specific functionalities and molecular selectivity to suit these applications [5, 6]. Surface modification through functionalization is an essential step for many applications including sensors, microelectronics, thin film optics, water-resistant coatings, anti-corrosive coatings, adhesion enhancement, and nanoparticle synthesis. Among various surface modification techniques, SAMs have demonstrated their superiority over all others due to their simplicity and ease of formation [6]. Some of the recent applications are mentioned below.

1.7. 1 Patterning of Surfaces

Patterned monolayer formation (allows one to control the position and attachment of molecules with different functionalities) on metallic and semiconducting surfaces has become a central focus of research in recent times. These patterned monolayers have diverse potential applications in various areas such as in integrated circuits, field-effect transistors, optical memory storage devices, and electroluminescent and electrochromic displays. It has also been useful to tailor surface properties such as wetting, protein adhesion, selective etching of resists, growth of crystals, and molecular recognition along with modulation of regions for specific cell growth or protein fixation [81].

The end-group functionality of a patterned SAM can, in principle, be used to direct the assembly of functionalized nanoparticles to study specific interactions between SAM and nanoparticle interface for many interesting applications in biology (e.g., sensors), physics (e.g. photonic crystals, data storage etc.), materials science and in their many contiguous areas [82,83]. Many of these methods have been known for the patterned SAM formation, like nanoshaving and nanografting, dip pen nanolithography (DPN), e-beam lithography, soft lithography, photolithography, nanoimprint lithography (NIL) and other techniques [84-90].

1.7.2 Molecular Electronics

SAMs are promising candidates as active components in molecular electronics due to its tunable properties. Simple molecular electronic devices usually consist of organic molecules sandwiched between conducting or semiconducting electrodes (e.g., MIS junctions), leading to a, systematic variation in the electronic properties. Well known examples include molecular wires, molecular diodes, single electron transistors and even molecular motors and some of these designs use SAMs as interconnects [91, 92]. In this context electron transport through single molecule has been studied extensively by many research groups. The mechanism of charge storage and transport properties across monolayers and semiconducting substrate (i.e. across the silicon/ organic interface), are some of the key issues common to all the above applications of

molecular nanoelectronics. It is possible to make organic transistors, biosensors, and hybrid memory devices (in flash or dynamic random access memory) using many interesting types of quantum dots sandwiched with SAMs [91- 93].

The development and understanding of the electronic properties of organic insulating films with thicknesses in the few nanometer (range ~2-3 nm) are two key issues for the future of molecular nanotechnologies. SAMs of alkyltrichlorosilane molecules chemically grafted on silicon substrate can act as very efficient insulating barriers provided their fabrication and molecular architecture are well controlled. Recent theoretical and experimental studies established the energy offsets between a silicon conduction band and the lowest unoccupied molecular orbitals to be between 4.1 and 4.3 eV respectively. In addition, that of between the silicon valence band and the highest occupied molecular orbital of the alkyl chains to be between 4.1 and 4.5 eV respectively in siloxane SAM, irrespective of the alkyl chain length (between C_{12} and C_{18}). These results validated the concept of using SAMs as ultrathin insulators because of a good alignment between the carbon sp^3 and the silicon sp^3 orbitals to achieve the charge neutrality and assuming that the band structures of the carbon and silicon are almost centered on their respective sp^3 level [94].

1.7.3 Chemical Sensors and Biosensors

One of the most frequent applications of SAMs in electroanalytical chemistry is in the development of chemical sensors to monitor a variety of analytes like pH, inorganic species and organic molecules both for chemical and biological recognition. For such applications many ‘integrated molecular systems’ (i.e., integration of multiple functionality within a monolayer) have been recently developed. This approach has been more recently illustrated using voltammetric pH measurements with the help of two redox species, *viz* quinone (pH sensitive) and ferrocene (pH insensitive reference electrode), co-immobilized onto SAM. Oxidation and reduction peaks of quinone shifts linearly with pH making it possible to accurately measure the pH between 1-11. Also, in some of the SAM based inorganic sensors, it is possible to detect simultaneously both redox active and redox inactive species [95].

In addition, integrated biosensing systems (lab-on-a–chip) have attracted much attention for the detection and analysis of many analytes and in case of biomolecules; monolayer-modified electrode acts as a template for their immobilization. For example, Tetsuya Osaka et.al., have reported the fabrication of functionalized organic monolayers modified Field effect transistors (FETs) for on-chip ion and biosensing as shown in Figure 1.14 [95].

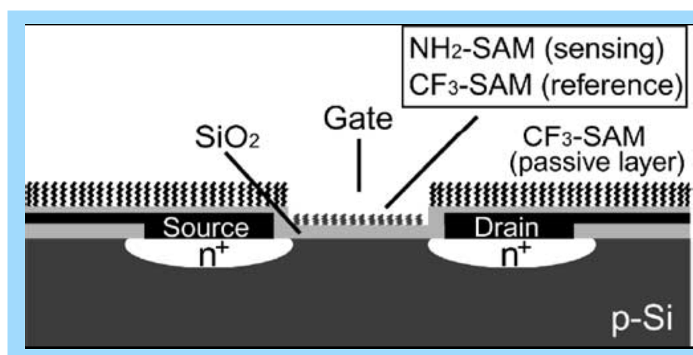

Figure 1. 14: Schematic representation of organic monolayer-modified SiO_2 gate FET devices. [Adopted from 95].

In this FET, the sensing electrode is the amino functionalized monolayer as an active layer, which is suitable for immobilization of DNA, enzyme, antibody etc. The reference electrode is a passive layer such as an alkyl, or perfluoro-alkyl functionalized monolayer, which is effective for preventing any undesired adsorption and ionic reaction at the surface. This organic monolayer-modified SiO_2 gate FET has been found to show satisfactory stability and durability to many analytes in aqueous solution.

1.7.4 SAMs as anti-stiction agents in MEMS/NEMS

1.7.4.1 MEMS/NEMS

MEMS are revolutionizing nearly every product by bringing together silicon-based microelectronics with micromachining technology, making possible the realization of complete systems-on-a-chip i.e. lab-on-a-chip. It is an enabling technology allowing the development of smart products, augmenting the computational ability of microelectronics with the perception and control capabilities of microsensors and microactuators and expanding the space of possible designs and applications. Few of its applications available commercially include inkjet-printer cartridges, accelerometers, miniature robots, microengines, locks, inertial sensors, microtransmissions, micromirrors

and micro actuators. Microelectronic circuits can be thought of as the "brains" of a system and MEMS augments this decision-making capability with "eyes" and "arms", to allow microsystems to sense and control the environment. Sensors gather information from the environment through measuring mechanical, thermal, biological, chemical, optical, and magnetic phenomena. The electronics then process the information derived from the sensors and through decision making capability direct the actuators to respond by moving, positioning, regulating, pumping, and filtering, thereby controlling the environment for some desired outcome or purpose [3, 4, 96]. MEMS fabrication process is compatible to "micromachining" processes, which involve selectively etching of parts of the silicon wafer (bulk micromachining) or addition of new structural layers (surface micromachining) to form the mechanical and electromechanical devices (Figure 1.15). There are three general approaches to the fabrication of MEMS: surface micromachining, bulk micromachining, and LIGA processing.

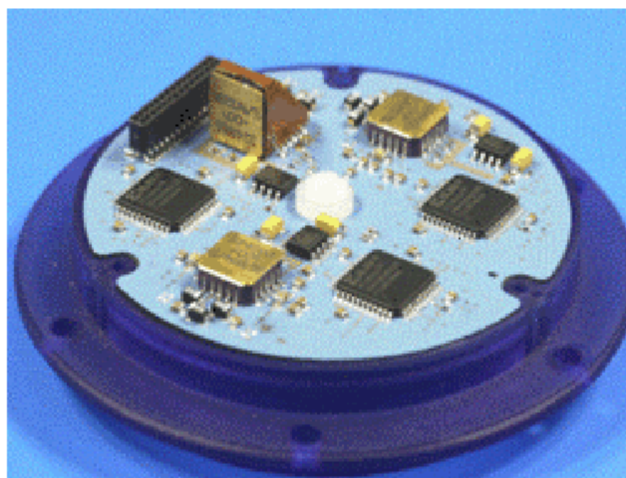

Figure 1.15: Representation of system on a chip, in which MEMS structures are assembled on a single substrate through microfabrication process; MEMS are a combination of tiny electrical and mechanical devices etched in silicon much like computer chips.

i) Bulk micromachining

In bulk micromachining, the single crystal silicon is specifically removed / etched to form three-dimensional MEMS structures (Figure 1.16). Typically, wet alkaline etchants such as potassium hydroxide (KOH) or tetramethylammonium hydroxide (TMAH) is used for the anisotropic dissolution of silicon. This method is particularly useful for fabricating, high performance pressure sensors, accelerometers, and photonic switches.

ii) Surface micromachining

Many sequences of steps are involved in the surface micromachining, *viz.*, deposition, patterning and etching of thin films on the surface of a substrate (such as silicon, glass, alumina, or metal). First, a sacrificial layer (soluble or removable) is deposited on a substrate (with a Si_3N_4 isolation layer) by chemical vapor deposition (CVD). This sacrificial layer provides temporary support for the structural layer during the subsequent fabrication, commonly used sacrificial layers being metals (Au, Al, etc.), ceramics (SiO_2 and Si_3N_4), and plastics (photoresist, polymethyl methacrylate, polyimides). A thin film of structural material (typically polysilicon) is deposited and etched to define a required structure. After etching the sacrificial layer, the patterned structure is separated from the substrate (except at the anchoring point) by removing the sacrificial layer to form a freestanding structure (Figure 1.16). This process can be repeated to form a stack of structural layers of different thicknesses with sacrificial layers sandwiched between them. This multilayer surface micromachining process can be used to create complex MEMS structures. Using this method, low cost accelerometers, cantilever beam arrays etc., are fabricated.

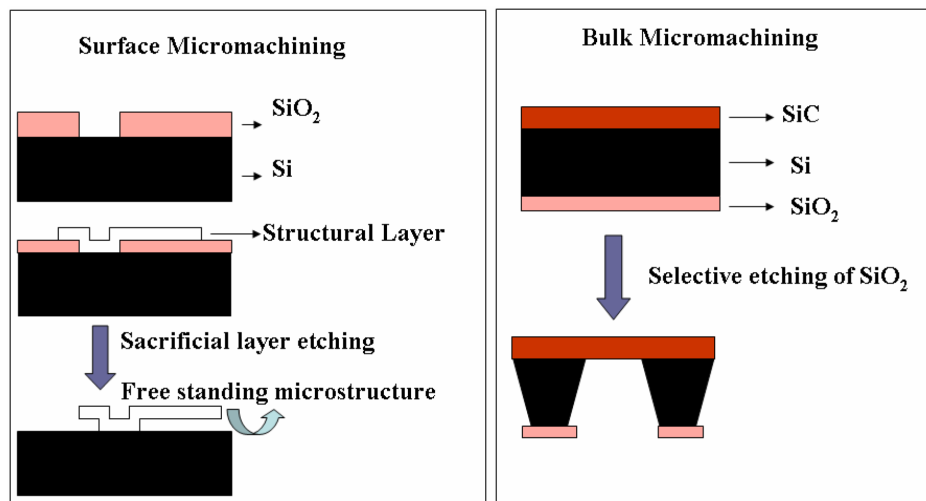

Figure 1.16: Schematic representation of surface and bulk micromachining process; where, the sacrificial layer etched to form a freestanding structure and the single crystal silicon is specifically removed to form three-dimensional MEMS structures respectively.

iii) LIGA process

LIGA (Lithographie, Galvanoformung und Abformung, German word for Lithography, Electrodeposition, and Molding) is again very similar to both wet bulk

micromachining and surface micromachining, except with a few considerable differences. In both, wet bulk and surface micromachining techniques, photoresists those are susceptible to ultraviolet (UV) radiation are used to pattern the metal layers to form devices and structures. But under the LIGA process, a different photoresist is used, which is susceptible to X-ray radiation. This difference in photoresists can allow for much taller objects to be created using LIGA, ranging anywhere from microns to centimeters high. The method is mainly used in high aspect ratio (HAR) micromachining.

Main advantages of micromachining are its extensive utility in diverse fields of applications, ability to mass produce cheaper devices, ultra small and compact nature and its versatility to offer effective solutions to many problems. However, there are also some major limitations like difficulty to fix due to their ultra-small size, operational problems in working with them and more significantly the expensive and sophisticated fabrication facility to set up at the beginning, which prevents larger commercial acceptance.

iv) Stictional Problems during the Fabrication of MEMS

One of the major factors, which limit the widespread use and reliability of MEMS is stiction (unwanted adhesion of compliant microstructure surfaces) not only during the fabrication stages, but also during their operation [97]. Stiction arises on a molecular level as a result of the dominance of surface forces such as capillary, hydrogen bonding, electrostatic, and van der Waals, over interacting at the micro-scale. When such internal restoring forces of microstructures cannot overcome all of the contributions of surface adhesive forces, these devices suffer from stiction. According to their origin and involvement of both adhesion and friction, these could be categorized into two types viz., ‘release’ and ‘in-use’ types of stiction. The former occurs while removing the sacrificial layers from the surface of micromachined structures. In this case, when the structure is released from the aqueous solution after wet etching of an underlying sacrificial layer, the liquid meniscus on hydrophilic surfaces pulls the microstructure towards the substrate and thus the stiction occurs. Although the structure is subsequently oxidized or dried after release, stiction still exists, as the high energy hydrophilic surface remains strongly adhered to the micro device, which cannot generate enough restoring force to overcome the adhesion. This type of stictional problem becomes more complicated as we reduce the

size of microstructures further since stiction dominates more for smaller microstructures. The fact is that the adhesion force decreases linearly with size, whereas gravitational force decreases with cube of size. For example, a ball bearing of 1 cm in diameter with a dirty surface would experience an adhesion force several orders of magnitude smaller than that of gravitational forces. On the other hand, a small ball bearing 1 μm diameter experiences an adhesion force a million times greater than that of gravitational force.

In comparison, the 'in-use' stiction occurs after the release stage, such as when the device is in operation, or in storage or when improperly handled. It is minimized by using suitable engineering approaches including novel processing techniques such as texturing the surfaces to reduce the contact area, avoidance of liquid–vapor interfaces altogether through the use of a supercritical fluid, freeze sublimation drying, vapor phase etching of sacrificial layers, and other dry-release methods. Other approaches include surface modification techniques such as roughening the surface of structure to reduce the contact area, controlling both the topography and the chemical composition of the contacting surfaces, supercritical drying using CO_2, and changing water meniscus shape by chemically modifying the surface. One of the recently emerging concepts is the use of SAMs to alleviate the stiction problem in the MEMS fabrication [99].

1.7.4.2 SAM for MEMS

MEMS/NEMS have experienced a rapid growth in the past decade due to its versatility and breadth of applications. The dimension of the system decreases, the surface area / volume ratio increases and this large surface area/volume ratio in MEMS/NEMS causes surface forces (i.e., adhesion and friction) to dominate over inertial forces as discussed above. Consequently, tribiological limitations, such as stiction, friction, and wear, pose many major problems that limit the efficiency, power output, steady-state motion, and reliability of MEMS/NEMS devices.

Application of sub nanometer-thick films of SAMs during microfabrication has attracted a great deal of attention to tackle the stiction problem in MEMS/NEMS because of its high hydrophobicity, low surface energies, and compact packing structures (to alleviate capillary forces). SAMs usually have low adhesion and friction, which are responsible for minimal energy losses and accordingly, exhibit stability within a wide

range of environmental conditions. More significantly, the self-assembly characteristics allow SAMs to form by itself on MEMS surfaces ensuring conformal coverage. Among various types of SAM forming molecules on Si surfaces, the best candidates for stiction perhaps, are alkylsilane and alkoxyl molecules. This is because, alkylsilane SAMs are stabilized by hydrogen bonds to the substrate, continuing one long chain hydrogen bonds within the SAM, and also covalent bonds to the substrate. Alkoxyl SAMs that are primarily covalently bonded to the SiO_2 substrate should be more stable against wear and aging [1-10].

1.8 Motivation, Scope and Organization of the Thesis

The genesis of the present thesis is inspired by several interesting issues unfolded during the foregoing critical review related to both fundamental and technological aspects of SAMs of alkyltrichloro / trimethoxysilane on semiconducting substrates. This includes the preliminary studies of several SAM forming on semiconducting substrates using various characterization techniques and their diverse potential application in the (nanotechnology and) MEMS/NEMS. Some of the details have been provided about their growth mechanism, thermal stability and about their electron transfer barrier properties on Si substrate.

The present thesis addresses few of these important issues related to the preparation, characterization, thermal stability and electrochemical properties, of self assembled alkyltrichlorosilane monolayer on Si substrate. Few selected applications have been investigated due to their importance in fabricating MEMS based device.

1.8.1 Objectives of the Present Study

The specific objectives of the present work embodied in this thesis are as follows.

(a) To study the growth kinetics and thermodynamic stability of octadecyltrichlorosilane (OTS) SAM on Si substrates;

(b) To understand the thermal stability and critical surface tension of alkyltrichlorosilane monolayer on silicon substrates by varying the chain length of the molecule;

(c) To understand the electrochemical and barrier properties by varying the chain length at Si / SiO_2 / electrolyte interface in order to correlate monolayer thickness, coverage, change in flat band potential, surface state distribution and rate constant of the redox probe;

(d) To explore the difference in the thermal stability on the planar (2D) and curved (3D) silica surfaces;

(e) To investigate the wetting behavior of the silica particles by modifying the surface using different silane molecules;

(f) To form mixed silane mono/multilayers on silica surface in order to achieve superhydrophobicity by creating the hierarchical micro-nano roughness;

(g) To control etching rate and morphology of the Si substrate through surface functionalization; and

(h) To investigate the wafer bonding process at a low temperature (less than 80 ^{0}C) for making molecular/polymeric glue using self assembled mono/multilayers of acrylate/methacrylate alkoxysilyl monomer.

1.8.2 Organization of Chapters

This thesis consists of seven chapters. **Chapter one** gives an introduction along with a brief overview of the preparation, characterization, and various properties of SAMs on semiconducting substrates. Structure, kinetics and growth mechanism of SAM formation have been discussed in relation to the nature of molecule, solvent, concentration, and temperature with special emphasis on alkyltrichlorosilane SAMs on Si substrates. This chapter also deals with the physical principles of different characterization techniques that are extensively used for the investigations of SAMs. Applications of these techniques to understand various aspects of formation of SAM on Si have been summarized. The most important function to tackle the stiction problem of MEMS by providing a suitable low energy surface coating has been discussed in more details. In the end, the specific objectives of the present study are discussed with special relevance on their growth kinetics, thermal stability, and change in surface energy, surface hydrophobicity and chain length dependent electron transfer characteristics.

Finally, further scope for research in this area with few of the major existing limitations is also discussed.

Second chapter comprises a study on the growth kinetics and thermodynamics of alkyltrichlorosilane monolayer with special emphasis on OTS monolayer on Si. More interestingly, the growth kinetics of monolayer formation on Si (100) by using time-dependent CA measurements has been elucidated, using Langmuir adsorption isotherm. Further, these monolayers have been characterized by different techniques, such as CA measurements, FTIR, XPS, and AFM.

Third chapter deals primarily with the electrochemical characterization of OTS (C_{18}), dodecyltrichlorosilane (C_{12}) and octyltrichlorosilane (C_8) SAMs on Si (100) in the presence and absence of an external redox probe like ferrocene. More specifically, the electron transfer behavior of ferrocene on Si (100) electrode is found to be drastically affected by the presence of monolayers and the reasons for such significant variation are analyzed in terms of the change in resistance, dielectric thickness and coverage of the monolayer. For example, the double layer capacitance is found to decrease systematically with increasing the chain length of the monolayer suggesting a smooth variation in the "plane of closest approach" with the thickness of the monolayer, despite the presence of a space charge layer on Si electrode. The rate constant of the ferrocene decreases by four orders of magnitude on monolayer derivatized Si electrode (in comparison with that on bare Si electrode) due to the barrier provided by various monolayers. The reasons for the observed shift in the flat-band potential (E_{fb}) and surface states distributions as a function of the monolayer chain length have also been discussed. The use of SAMs, thus to control the behavior of semiconductor-electrolyte interfaces offers several benefits to many applications like microfluidic devices, biosensors, surface engineering and surface model systems, contact printing in materials microfabrication, inhibition of corrosion and oxidation, lubrication and protein adsorption.

Understanding the structural and functional integrity of SAMs of alkyltrichlorosilane on Si/SiO_2 interface with change in temperature is critical for realizing their utility as anti-stiction coatings during the fabrication and functioning of MEMS. In the **fourth chapter**, we compare the thermal stability of two dimensional (2D) OTS monolayers on both n-type Si substrate (planar surface) and silica spheres (curved

surface). Various surface sensitive spectroscopic techniques like grazing angle FTIR spectroscopy and XPS have been used for surface characterization. Interestingly, a significant enhancement in the thermal stability is observed for the case of OTS-SAM (up to 625 K) on freshly prepared spherical silica surfaces in comparison with the stability of OTS-SAM on planar Si substrate. Despite this difference in thermal stability, the results of temperature dependent FTIR demonstrate monolayer decomposition in both cases through the involvement of both Si-C and C-C bonds leaving Si-O-Si bond intact. These results are useful to understand the mechanism by which SAM enhances the interfacial adhesion as well as the inhibition of Cu diffusion (electro-migration) into adjacent dielectric layers, which obviously improves the interconnect reliability in nanoscale electronic devices.

Various strategies to develop artificial superhydrophobic surfaces (analogous to lotus leaf) have attracted significant attention in recent time due to its fundamental relevance of molecular level manipulation of surface energy and consequent implications in commercial applications ranging from self-cleaning window glasses, paints, and fabrics to low-friction surfaces. Nature exhibits the phenomena of superhydrophobicity in 'lotus leaf effect' to harness the 'roll-off' action for self-cleaning of leaves. Several recent studies of lotus leaf reveal that its waxy surface is made up of many micron-sized bumps that in turn are covered with nanoscale hair-like tubules responsible for the 'roll-off' action of water. Since SAMs can act like nanoscale hair like structure both structurally and functionally, we show in **chapter five**, the utility of this approach to design an artificial superhydrophobic surface. More specifically, we show that the extent of the hydrophobicity of the silica nanoparticle (~ 100 nm) film can be tuned remarkably by surface functionalization using different self-assembled mono/multilayers of alkyltrichlorosilane. More specifically, the hydrophobicity of the silica surface is enhanced by a chemical modification that lowers the surface energy i.e., through the well-known method of surface silanization. Surface roughness is engineered through silanization facilitating a change in both the surface chemical composition and the geometrical microstructure to generate hierarchical structures where the CA can be anywhere between 60° to 168°. Our results indicate that these types of superhydrophobic surfaces obtained by forming mixed mono/multilayer on the silica surface could be useful

for many potential applications due to the low surface energy with enhanced thermal stability and tunable CA.

In chapter six, we present some selected applications of SAMs. In the first part of this chapter (6A) we demonstrate the role of OTS monolayer for controlling the etching rate and morphology of the Si substrate after various pretreatments, such as HF (A), *piranha* (B) and OTS (C) monolayer formation. These treatments generate a, hydrogen (-H), hydroxyl (-OH) and methyl (-CH_3) terminal functional groups respectively on the Si substrates, which assists the kinetics of silicon dissolution along with modulating the surface morphology.

In the second part of this chapter (6B), an improved process for wafer bonding at a low temperature (less than 80 ^oC) by making a molecular (polymeric) glue using self assembled mono/multilayers of acrylate/methacrylate alkoxysilyl monomer has been demonstrated, which could be used as a molecular glue for bonding silicon-silicon, silicon-glass, and glass-glass interfaces. This is mainly possible by the polymerization of terminal vinyl unsaturation of mono/multilayers on SAMs using thermal/photosensitive initiator. This type of glue will be very useful for the integration of microstructures and microelectronics involved in MEMS and Very Large Scale Integration (VLSI) packaging processes particularly under harsh thermal environment.

A summary of all the major conclusions of the present study with respect to the preparation, characterization and various properties of SAM on Si substrate is discussed in **chapter seven** with possible scope for further research in this area. The chapter also outlines some of the limitations of these materials along with possible methods to overcome them. In addition, plausible precautions and safety hazards during the preparation and processing of SAM have been elucidated.

Our experimental studies clearly show that, these SAMs can effectively be used in MEMS/ NEMS fabrication as well as in devices due to its good thermal and chemical stability, low surface energy and adhesion, tunable hydrophobic nature, and insulating properties. In addition, these SAMs would be of interest in molecular electronics ranging from biosensors to optoelectronic devices. Undoubtedly, these SAMs on Si/SiO_2 interface have a bright and long term future in both fundamental and technological interests due to its interdisciplinary nature involving areas like chemistry, physics, biology, chemical

engineering, and material science. Self-assembly as an exciting and attractive methodology found many unique applications in nanotechnology due to its flexibility and ease of selection of different types of functional groups covering a wide length scale. Similarly, SAMs of bifunctional molecules on polycrystalline substrates can be effectively used to carry out specific reactions between pendent functionalities and solution or gaseous species to produce new hybrid materials for various applications such as biosensors, surface engineering in model systems, contact printing in materials microfabrication, inhibition of corrosion and oxidation, lubrication and protein adsorption in micro-fluidic devices. Thus the results of present study are believed to be useful in all these areas of nanotechnology for understanding the fundamental advantages of using SAMs due to their tunable properties.

1.9 References

[1] (a) R. P. Feynman, *There's Plenty of Room at the Bottom: An Invitation to Enter New World of Physics. http://www.zyvex.com/nanotech/feynman.html* (accessed August) **2005.** (b) R. P. Feynman, *Engineering and Science (California Institute of Technology*) **1960**, 23, 22.

[2] (a) S. E. Lyshevski, '*MEMS and NEMS: Systems, Devices, and Structures'*, CRC Press **2002**. (b) J. Bryzek, Impact of MEMS technology on society *Sensors and Actuators A* **1996**, 56, 1. (c) M. J. Madou, 'Fundamentals of Microfabrication'Boca Raton, F L: CRC press company, **1997**.

[3] (a) R. S. Muller, R. T. Howe, S. D. Senturia, R. L. Smith, R. M. White, *Microsensors* New York: IEEE Press **1990**. (b) S. M. Sze, *Semiconductor Sensors* New York: Wiley, **1994**.

[4] (a) B. C. Bunker, R. W. Carpick, *Langmuir* **2000**, 16, 7742. (b) B. H. Kim, T. D. Chung, *J. Microelectromech. Syst.* **2001**, 10, 33. (c) P. W. Hoffmann, M. Stelzle, *Langmuir* **1997**, 13, 1877.

[5] (a) C. J. Kim, J.Y. Kim, B. Sridharan, *Sensors and Actuators A* **1998,** 64, 17. (b) H. Guckel, J. J. Sniegowski, T. R. Christenson, F. Raissi, *Sensors and Actuators A* **1990,** 21-23, 346.

[6] (a) A. Ulman, An introduction to ultra thin organic films from Langmuir Blodgett to Self-assembly, Academic Press, London **1991.** (b) A. Ulman, *Chem Rev.* **1996,** 96, 1533. (c) R. Maboudian, *Mater. Res. Soc. Bull.* **1998,** 23, 47 and references therein. (d) J. Sagiv, *J. Am. Chem. Soc.* **1980,**102, 92.

[7] (a) H.-L. Li, A.-P. Fu, D.-S. Xu, G.-L. Guo, L.-L. Gui, Y.-Q. Tang, *Langmuir* **2002,** 18, 3198. (b) U. Srinivasan, M. R. Houston, R. T. Howe, R. J. Maboudian, *J. Microelectromech. Syst.* **1998,** 2, 252.

[8] W. C. Bigelow, D. L. Pickett, W. A. Zisman, *J. Colloid Interface Sci.* **1946**, 1, 513.

[9] (a) R.G. Nuzzo, L. H. Dubois, D. L. Allara, *J. Am. Chem. Soc.* **1990,** 112, 558. (b) R. Nuzzo, D. Allara, **1983**, 105, 4481.

[10] Y. Xia, G. M. Whitesides, *Angew. Chem. Int. Ed.* **1998**, 37, 550.

[11] (a) M. J. Wirth, H. O. Fatunmbi, Anal. Chem. **1993**, 65, 822. (b) T. K. Kwei, J. Polym. Sci. Part A A3, **1965**, 3229. (c) H.-L. Li, A.-P. Fu, D.-S. Xu, G.-L. Guo, L.- L. Gui, Y.-Q. Tang, *Langmuir* **2002** 18, 3198. (d) W. A. Aue, C. R. Hastings, *J. Chromatogr.* **1969**, 42, 319.

[12] Y. X. Zhuang, O. Hansen, T. Kniling, C. Wang, P. Rombach, W. Lang, W. Benecke, M. Keilenbeck, J. Koblitz, *J. Micromech. Microeng.* **2006,** 16, 2259.

[13] (a) R. D. Piner, J. Zhu, F. Xu, S. Hong, C. A. Markin, *Science* **1999**, 283, 661. (b) Y. N. Xia, J. A. Rogers, K. E. Paul, G. M. Whitesides, *Chem. Rev.* **1999**, *99*, 1823.

[14] P. E. Laibinis, G. M. Whitesides, D. L. Allara, Y-T. Tao, A. N. Parikh, R. G. Nuzzo, *J. Am. Chem. Soc.* **1991**, 113, 7152.

[15] (a) J. Sagiv, *J. Am. Chem. Soc.* **1980**, 102, 92. (b) S. R. Wasserman, Y. -T.Tao, J. M. Whitesides, *Langmuir* **1989**, 5, 1074. (c) J. D. Le Grange, J. L. Markham, C. R. Kurjian, *Langmuir* **1993**, 9, 1749. (d) R. Maoz, J. Sagiv, *J. Colloid Interface Sci.* **1984,** 100, 465. (e) J. Gun, J. Sagiv, *J. Colloid Interface Sci.* **1986**, 112, 457.

[16] (a) J. Gun, R. Iscovici, J. Sagiv, *J. Colloid Interface Sci.* **1984**, 101,201. (b) N. Tillman, A.Ulman, J. S. Schildkraut, T. L. Penner, *J. Am. Chem. Soc.* **1988**, 110, 6136.

[17] (a) S. Brandriss, S. Margel, Langmuir **1993**, 9, 1232. (b) K. Mathauser, C. W. Frank, *Langmuir* **1993**, 9, 3002. (c) K. Mathauser, C. W. Frank, *Langmuir* **1993**, 9, 3446.

[18] (a) G. Carson, S. Granick, *J. Appl. Polym. Sci.* **1989**, 37, 2767. (b) C. R. Kessel S. Granick, *Langmuir* **1991**, 7, 532. (c) D. K. Schwartz, S. Steinberg, J. Israelachvili, Z. A. N. Zasadzinski, *Phys. Rev. Lett.* **1992**, 69, 3354.

[19] (a) H. O. Finklea, L. R. Robinson, A. Blackburn, B. Richter, D. L. Allara, T. Bright, *Langmuir* **1986**, 2, 239. (b) I. Rubinstein, E. Sabatani, R. Maoz, J. Sagiv, *Proc. Electrochem. Soc.* **1986**, 86, 175. (c) I. Rubinstein, E. Sabatani, R.Maoz, J.Sagiv, *Electroanal. Chem.* **1987**, 219, 365.

[20] (a) A.G. Lambert, D. J. Neivandt, R.A. McAloney, P. B. Davies, *Langmuir* **2000**. 16(22), 8377. (b) A. Inoue, T. Ishida, N. Choi, W. Mizutani, H. Tokumoto,

Appl .Phys. Lett. **1998,** 73 (14), 1976. (c) R. R. Rye, G. C. Nelson, M.T. Dugger, *Langmuir* **1997**. 13(11), 2965.

[21] (a) E. B. Troughton. C. D. Bain. G. M. Whitesides. D. L. Allara. M. D. Porter. *Langmuir* **1998**, 4, 365. (b)C. W. Sheen. J. –X. Shi. J. Martensson. A. N. Parikh. D. L. Allara, *J. Am. Chem. Soc.* **1992**, 114, 1514.

[22] (a) M.G. Manat. C. A. Broen. J. G. Gordon *Langmuir* **1992**, 8, 1615. (b) M. H. Dishner, J. C. Hemminger. F. J. Feher *Langmuir* **1997**, 13, 4788.

[23] K. Chen, C. A. Mirkin, R. -K. Lo, J. Zhao, J. T. McDevitt, *J. Am. Chem. Soc.* **1995**, 117, 6374.

[24] H. Lee. L. J. Kepley. H. –G. Hong. S. Akhter, T. E. Mallouk, *J. Phys. Chem.* **1988**, 92, 2597.

[25] (a) M. R. Linford, C. E. D. Chidsey, *J. Am. Chem. Soc.* **1993**, 115, 12631. (b) M. R. Linford, P. Fenter, P. M.Eisenberger, C. E. D. Chidsey, *J. Am. Chem. Soc.* **1995**, 117, 3145. (c) J. Zhao, K. Uosaki, *J. Phys. Chem. B* **2004**, 108, 17129.

[26] (a) R. Boukherrroub, S. Morin, F.Bensebaa, D. D. M. Wayner, *Langmuir* **1999**, 15, 3831. (b) R. Boukherroub, D. D. M. Wayner, *J. Am. Chem. Soc.* **1999**, 121, 11513. (c) H. Yu, S. Morin, D. M. Wayner, P. Allongue, C. H. Henry de Villeneuve, *J. Phys. Chem. B* **2000**, 104, 11157. (d) A. B. Sieval, V. Vleeming, H. Zuilhof, E. J. R. Sudholter, *Langmuir* **1999**, 15, 8288.

[27] (a) J. Terry, M. R. Linford, C. Wigren, R. Cao, P. Pianetta, C. E. D. Chidsey, *Appl. Phys. Lett.* **1997**, 71, 1056. (b) J. Cheng, D. B. Robinson, R. L. Cicero, T. Eberspacher, C. J. Barrelet, C. E. D.Chidsey, *J. Phys. Chem. B* **2001**, 105, 0900. (c) F. Effenberger, G. Gotz, B. Bidlingmaier, M.Wezstein, *Angew.Chem., Int. Ed.* **1998**, 37, 2462.

[28] (a) C. Henry de Villeneuve, J. Pinson, M. C. Bernard, P.Allongue, *J. Phys. Chem. B* **1997**, 101, 2415. (b) A. Fidelis, F. Ozanam, J. N. Chazalviel, *Surf. Sci.* **2000**, L7, 444.

[29] (a) A. Bansal, N. S. Lewis, *J. Phys. Chem. B* **1998**, 102, 1067. (b) M. R.Linford, P. Fenter, P. M. Eisenberger, C. E. D.Chidsey, *J. Am. Chem. Soc.* **1995**, 117, 3145. (c) A. Bansal, X. Li, I. Lauermann, N. S. Lewis, *J. Am. Chem. Soc.***1996**, 118, 7225. (d) A. Bansal, N. S. Lewis, *J. Phys. Chem. B* **1998**, 102, 4058.

[30] T. R. Lee, P. E. Laibinis. J. P. Folkers, G. M. Whitesides. *Pure Appl. Chem.* **1991**, 63, 821.

[31] (a) A. H. Carim, M. M. Dovek, C. F. Quate, R. Sinclair, C. Vorst, *Science* **1987**,237, 630. (b) L. T. Zhuravlev, *Langmuir* **1987**, 3, 316.

[32] (a) A. Inoue, T. Ishida, N. Choi, W. Mizutani, H. Tokumoto, *Appl. Phys. Lett* **1998**. 73(14), 1976. (b) R.R. Rye, G. C. Nelson, M.T. Dugger, *Langmuir* **1997,** 13(11), 2965.

[33] (a) H. Brunner, T. Vallant, U. Mayer, H. Hoffmann, B. Basnar, M. Vallant, G. Friedbacher, *Langmuir* **1999** 15(6),1899. (b) D. L .Angst, G. W. Simmons, *Langmuir*, **1991,** 7(10), 2236.

[34] A. N. Parikh, D. L. Allara, I. B. Azouz, F. Rondelez, *J. Physical Chemistry*, **1994,** 98(31), 7577.

[35] (a) H. Brunner, T. Vallant, U. Mayer, H. Hoffmann, B. Basnar, M. Vallant, G. Friedbacher, *Langmuir* **1999**, 15(6), 1899. (b) E. Mark McGovern, M. R. Krishna Kallury, M. Thompson, *Langmuir* **1994**,10, 3607.

[36] (a) P. Silberzan, L. Le´ger, D. Ausserre´, J. J.Benattar, *Langmuir* **1991**, *7,* 1647. (b) C. P. Tripp, M. L. Hair, *Langmuir* **1992,** 8(4),1120. (c) D. L. Angst, G.W. Simmons, *Langmuir*, **1991,** 7(10), 2236.

[37] (a) M. M. Ferris, K. L. Rowlen, *Applied Spectroscopy*, **2000,** 54(5), 664. (b) V. Zhukov, I. Popova, Jr. J.T. Yates, *J. Vac. Sci. Technol. A,* **2000**. 18(3), 992.

[38] R.W. P. Fairbank, M. J. Wirth, *J. Chromatogr.* A **1999,** 830(2), 285.

[39] (a) R. Imhof, X.Y. Xie, G. Calzaferri, **1997,** 53(7), 981. (b) D. L. Angst, G. W. Simmons, *Langmuir* **1991,** 7(10), 2236.

[40] S.E. Stein, *Infrared spectra, in NIST Chemistry WebBook, NIST Standard Reference Database Number 69 (http://webbook.nist.gov)*, P. J. Linstrom, W.G. Mallard, National Institute of Standards and Technology: Gaithersburg MD, 20899, **2003.**

[41] S. Ye, S. Nihonyanagi, K. Uosaki, **2001,** 3(16), 3463.

[42] D. H. Flinn, D. A. Guzonas, R. H. Yoon, **1994,** 87(3), 163.

[43] (a) J. B. Brzoska, N Shahidzadeh, F.Rondelez, Nature**, 1992,** 360,719. (b) A. N. Parikh D. L. Allara, I. B, Azouz, F.Rondelez, *J. Phys. Chem.* **1994,** 98, 7577. (c)

M. Goldmann, J. V. Davidovits, P. Silberzan, *Thin Solid Films***, 1998,** 329, 166.

[44] (a) M. E. McGovern, K. M. R. Kallury, M. Thompson, *Langmuir* **1994**, 10, 3607. (b) S. R. Wasserman, G. M. Whitesides, I. M.Tidswell, B. M. Ocko, P. S. Pershan, J. D. Axe, *J. Am. Chem. Soc.* **1989**, 111, 5852. (c) C. P. Tripp, M. L. Hair, *Langmuir* **1995**, 11, 149.

[45] (a) T.Vallant, J. Kattner, H. Brunner, U. Mayer, H. Hoffmann, *Langmuir* **1999,** 15(16), 5339. (b) T. Vallant, H. Brunner, U. Mayer, H. Hoffmann, T. Leitner, R. Resch, G. Friedbacher, *J. Phys. Chem. B*, **1998**. 102(37), 7190. (c) D. H. Flinn, D. A.Guzonas, R.H. Yoon, *Colloids and Surfaces a-Physicochemical and Engineering Aspects*, **1994**. 87(3), 163.

[46] M. E. McGovern, K. M. R. Kallury, M. Thompson, *Langmuir***1994**, 10, 3607.

[47] N. Rozlosnik, M. C. Gerstenberg, N. B. Larsen, *Langmuir* **2003**,19, 1182.

[48] M. E. McGovern, K.M.R. Kallury and M. Thompson, *Langmuir*. **1994**, 10, 3607.

[49] D. K. Schwartz, *Annu. Rev. Phys. Chem,* **2001,** 52, 107 and references therein.

[50] C. Carraro, O. W. Yauw, M. M. Sung, R. Maboudian, *J. Phys .Chem. B* **1998,** 102(23), 4441.

[51] (a) C. P. Tripp, M. L. Hair, *Langmuir* **1992**, 8, 1120. (b) C. P. Tripp, M. L. Hair, *J. Phys. Chem.* **1993**, 97, 5693.

[52] (a) D. L. Allara, A. N. Parikh, F. Rondelez, *Langmuir* **1995**, 11, 2357. (b) J. P. Blitz, R. S. S. Murthy, D. E. Leyden, *J. Colloid Interface Sci*. **1988**, 121, 63.

[53] K. Bierbaum, M. Kinzler, Ch. Wo¨ll, M. Grunze, G. Ha¨hner, S. Heid, F. Effecberger, *Langmuir* **1995**, *11,* 512.

[54] (a) K. A. Peterlinz, R. Georgiadis, *Langmui*r **1996** 12, 4731. (b) A.G. Richter, C. J. Yu, A. Datta J. Kmetko, P. Dutta Phys. Rev. E **2000** 61, 607. (c) S. S. Cheng, D. A. Scherson, C. N. Sukenik, **1992** *J. Am. Chem. Soc.* 1114, 5436.

[55] (a) R. Imhof, X.Y. Xie, G. Calzaferri, **1997,** 53(7), 981. (b) A. Ulman, *Chem. Rev*. **1996,** 96, 1533.

[56] F. A. Cotton, G. Wilkinson, *Advanced Inorganic Chemistry*, 6 th Ed .; John wiley **1999**.

[57] D. K. Schwartz, S. Steinberg, J. Israelachvili, J.A.N. Zasadzinski, *Phys. Rev. Lett.* **1992**, 69(23), 3354.

[58] A.G. Lambert, D. J. Neivandt, R.A. McAloney, P. B. Davies, *Langmuir*, **2000,** 16(22), 8377.

[59] (a) A. Y. Fadeev, T. J. McCarthy, *Langmuir*, **1999,**15(11), 3759. (b) A.Y. Fadeev, T. J. McCarthy, *Langmuir*, **2000,** 16(18), 7268.

[60] (a) A.W. Adamson, I. Ling, *Adv. Chem. Ser.* **1964**, 43, 57. (b) T. Young, *Miscellaneous Works; Peacock, G.; Ed.; Murray: London,* **1855**, 1, 418.

[61] (a) B. R. Ray, F. E. Bartell, *Colloid Sci.* **1953,** 8, 214. (b) N. K. Adam, G.E. P. Elliott, *J. Chem. Soc.* **1962**, 2206.

[62] H. W. Fox, W. A. Zisman, *J. Colloid Sci.* **1952**, 7, 428.

[63] (a) N. R. Wenzel, *Ind. Eng. Chem*, **1936**, 938. (b) N. R. Wenzel, *Ind. Eng. Chem.* **1936**, 28, 988**.**

[64] (a) Cassie, Baxter, *Trans. Faraday Soc*, **1944**, 40, 546. (b) Baxter and Cassie. J. Text. Inst., **1945**, 36, T67.

[65] (a) W. Barthlott, C. Neinhuis, *Planta,* **1997,** 202, 1. (b) H.C. Von Baeyer, *Science* NewYork **2000**, 40, 12. (c) R. Bossey*, Nat. Mater* **2003,** 2, 301.

[66] (a) W. A. Zisman, *Adv. Chem. Ser.* **1964**, 43, 1. (b) W. A. Zisman, *J. Chem. Phys*. **1941**, 9, 534. (c) W. A. Zisman, *J. Chem. Phys.* **1941**, 9, 729. (d) C. D. Bain, G. M. Whitesides, *Angew. Chem. Int. Ed. Engl* **1989**, 28, 506.

[67] (a) J. T. Grant, D. Briggs, *Surface Analysis by Auger and X-ray Photoelectron Spectroscopy, Ed. published by IM Publications,* **2003**, Chichester, UK. (b) J. F. Moulder, W. F. Stickle, P. E. Sobol, K .D. Bomben, *Handbook of X-ray Photoelectron Spectroscopy, published by Perkin-Elmer Corp.*, **1992**, Eden Prairie, MN, USA. (c) D. I. Ellis, R. Goodacre, *Metabolic fingerprinting in disease diagnosis: biomedical applications of infrared and Raman spectroscopy, Analyst* **2006,** 131, 875. (d) D. A. Shirley, *Phys. Rev. B* **1972**, 5, 4709.

[68] (a) M. R. Kasuri, H. Hoffmann, U. Mayer, A. Krischanitz, *Langmuir* **1995**, 11, 1304. (b) T. Vallant, J. Kattner, H. Brunner, U. Mayer, H. Hoffmann, *Langmuir* **1999**, 15, 5339.

[69] (a) Yi. Liu, K. Wolf, M.C. Messmer, *Langmuir* **2001**, 17, 4329. (b) K. Bierbaum, M. Grunze, *Langmuir* **1995**,11, 2143.

[70] V A, Zworykin, J Hillier, R. L Snyder, *A scanning electron microscope. ASTM*

Bull. **1942**, 117, 15-23.

[71] G. Binnig, H, Rohrer, *Sci, Am.* **1985,** 253, 50.

[72] (a) K.-B. Lee, S.-J. Park, C. A. Mirkin, J. C. Smith, M. Mrksich, *Science*, **2002**,295, 5560. (b) K-B. Lee, J-H. Lim, C.A. Mirkin, *J. Am. Chem. Soc.* **2003**, 125, 5588. (c) J-H. Lim, D. S. Ginger, K-B. Lee, J. Heo, J-M. Nam, C. A. Mirkin, *Angew. Chem. Int. Ed.* **2003**, 20, 2411.

[73] (a) M. D. Porter, T. B. Bright, D.L. Allara, C. E. D. Chidsey, *J. Am. Chem. Soc.* **1987**, 109, 3559. (b) H. O. Finklea, D. A. Sinder, J. Fedyk, E. Sabatini, Y. Gaini, I. Rubinstein, *Langmuir* **1993**, 9, 3660.

[74] (a) C. Amatore, M. Saveant, J. Tessier, D. *J. Electroanal. Chem.* **1983**, 147, 39. (b) E. Sabatini, I. Rubinstein, R. Maoz, J. Sagiv, *J. Electroanal. Chem.* **1987**, 219, 365.

[75] (a) A. J. Bard L. R. Faulkner *Electrochemical Method: Fundamentals and Applications, John wiley & Sons, New York*: **1980**. (b) N. Nishi, D. Hobara , M. Yamamoto, T. Kakiuchi, *Langmuir* **2003**, 19, 6187. (c) E. Sabatani, I. Rubinstein, *J. Phys. Chem.* **1987**, 91, 6663. (d) C. M. Whelan, M. R. Smyth, C. J. Barnes, *Langmuir* **1999**, 15, 116. (e) J. Kim, L. R. Faulkner, *Anal. Chem,* **1984,** 56. 874. (f) J. F. Rusling, S. L. Suib, *Adv. Mat.* **1994**, 6, 922.

[76] (a) J. R. MacDonald and W.B. Johnson, "*Fundamentals of Impedance Spectroscopy*"; Wiley, New York, **1987**. (b) E. Sabatani, J. Cohenboulakia, M. Bruening, I. Rubinstein, *Langmuir* **1993**, *9*, 2974

[77] (a) C. H. Kim, S. W. Han, T. H. Ha, K. Kim, *Langmuir* **1999**, *15*, 8399. (b) T. L. Brower, M. Cook, A. Ulman, *J. Phys. Chem. B* **2003**, *107*, 11721. (c) Y. T. Tao, C. C. Wu, J. Y. Eu, W. L. Lin, *Langmuir* **1997**,13, 4018. (d) J. M. Tour, L. Jones, D. L. Pearson, J. J. S. Lamba, T. P. Burgin, G. M. Whitesides, D. L. Allara, A. N. Parikh, S. V. Atre, *J. Am. Chem. Soc.* **1995**, 117, 9529.

[78] (a) G. Binnig, H. Rohrer, Ch. Gerber, E.Weibel, *Phys. Rev. Lett*. **1982**, 49, 57. (b) U. Demir, K. K. Balasubramanian, V. Cammarata, C. Shannon, *J. Vac. Sci. Technol., B* **1996**, *13*, 1294. (c) J. K. Schoer, F. P. Zamborini, R. M. Crooks, *J. Phys. Chem.***1996**, *100*, 11086.

[79] (a) J. Y. Huang, Y. R. Shen, H. L. Dai, W. Ho, *In Laser Spectroscopy and*

Photochemistry on Metal Surfaces, Eds.; World Scientific: Singapore, **1995**; *Adv. Ser. Phys. Chem.* Vol. 5, Chapter 1. (b) J. Y. Huang, K. J. Song, A. Lagoutchev, P. K. Yang, T. J. Chuang, *Langmuir* **1997**, 13, 58.

[80] (a) D. S. Karpovich, G. J. Blanchard, *Langmuir* **1994,** 13, 3315. (b) H. M. Schessler, D. S. Karpovich, G.J. Blanchard, *J. Am. Chem. Soc.* **1996,** 118, 9645.

[81] (a) B. Michel, A. Bernard, A. Bietsch, E. Delamaeche, M. Geissler, D. Juncker, H. Kind, J. P. Renault, H. Rothuizen, H. Schmid, P. Schmidt-Winkel, R. Stutz, H. Wolf, IBM *J. Res. Dev.***2001**, 45, 870. (b) N. Abbot, A. Kumar, G. M. Whitesides, *Chem. Mater.* **1994**, 6, 596. (c) N. J. van der Veen, S. Flink, M. A. Deij, R.J. M. Egberink, F. C. J. M. Van veggel, D.N. Reinhoudt, *J. Am. Chem. Soc.* **2000,** 122, 6112.

[82] (a) M. R. Zhou, M. A. Deshpande, Reed, *Appl. Phys. Lett* **1997**, 71, 611. (b) Y. Chen, D.A. Ohlberg, X. Li. D.R. Stewart, J. O. Jeppesen, K. A. Nielsen, J. F. Stoddart, D. L. Olynick, E. Anderson, *Appl. Phys. Lett.* **2003**, 82, 1610. (c) H. Zhu, M. Snyder, *Curr.Opin, Chem. Biol.* **2003**, 7, 55.

[83] (a) G. Kaltenpoth, M. Himmelhaus, L. Slansky, F. Caruso, M. Grunze, *Adv. Mater.* **2003**, 15, 1113. (b) I. Lee, H. Zheng, M. F. Rubner, P.T. Hammond, *Adv. Mater.* **2002**, 14, 572. (c) V. Santhanam, R. P. Andres, *Nano Lett.* **2003**, 4, 41. (d) T. Auletta, B. Dordi, A. Mulder, A. Sartori, S. Onclin, C. M. Bruinink, M. Peter, C. A. Nijhuis, H. Beijleveld, H. Schonherr, G. J. Vansco, A. Casnati, R. Ungaro, B. J. Ravoo, J. Huskens, D. N. Reinhoudt, *Angew. Chem. Int. Ed.* **2004**, 43, 369.

[84] (a) S. Xu, G.-Y. Liu, *Langmuir* **1997**, *12*, 1127. (b) G.-Y. Liu, S. Xu, Y. Qian, *Acc. Chem. Res.* **2000**, *33*, 457. (c) X. D. Xiao, G. Y. Liu, D. H. Charych, M. Salmeron, *Langmuir* **1995**, *11*, 1600. (d) W. Kiridena, V. Jain, P. K. Kuo, G. Y. Liu, *Surf. Interface Anal.* **1997**, *25*, 383.

[85] (a) Q. L.Hang, Y. L. Wang, M. Lieberman, G. H.Bernstein, *Appl. Phys. Lett.* **2002**, *80*, 4220. (b) M. E. Anderson, R. K. Smith, Z. J. Donhauser, A. Hatzor, P. A. Lewis, L. P. Tan, H. Tanaka, M. W. Horn, P. S.Weiss, *J. Vac. Sci. Technol. B* **2002**, *20*, 2739. (c) S. T. Liu, R. Maoz, G. Schmid, J. Sagiv, *Nano Lett.* **2002**, *2*, 1055. (d) S. W. Han, I. Lee, K. Kim, *Langmuir* **2002**, *18*, 182.

[86] (a) H. Zhang, Z. Li, C. A. Mirkin, *Adv. Mater.* **2002**, *14*, 1472. (c) J. H. Lim, C. A. Mirkin, *Adv. Mater.* **2002**, *14*, 2002. (d) L.M. Demers, D. S. Ginger, S. J. Park, Z. Li, S. W. Chung, C. A. Mirkin, *Science* **2002**, *296*, 1836. (e) K. B. Lee, S. J. Park, C. A. Mirkin, J. C. Smith, M. Mrksich, *Science* **2002**, *195*, 1702.

[87] (a) A. Ivanisevic, C. A. Mirkin, *J. Am. Chem. Soc.* **2001**, *123*, 7887. (b) G. Agarwal, L. A. Sowards, R. R. Naik, M. O. Stone, *J. Am. Chem. Soc.* **2003**, *125*, 580.

[88] (a) Y. N. Xia, J. A. Rogers, K. E. Paul, G. M. Whitesides, *Chem. Rev.* **1999**, *99*, 1823. (b) T. W. Odom, V. R. Thalladi, C. Love, G. M. Whitesides, *J. Am. Chem. Soc.* **2002**, *124*, 12112. (c) W. R. Childs, R. G. Nuzzo, *J. Am. Chem. Soc.* **2002**, *124*, 13583. (d) J. C. Love, D. B.Wolfe, R. Haasch, M. L. Chabinyc, K. E. Paul, G. M. Whitesides, R. G. Nuzzo, *J. Am. Chem. Soc.* **2003**, *125*, 2597. (e) Y. Harada, X. L. Li, P. W.Bohn, R. G. Nuzzo, *J. Am. Chem. Soc.* **2001**, *123*, 8709. (f) R. G. Nuzzo, *Proc. Nat.Acad. Sci.* **2001**, *98*, 4827.

[89] (a) J. A. Rogers, Z. Bao, K. Baldwin, A. Dodabalapur, B. Crone, V. R. Raju, V. Kuck, H. Katz, K. Amundson, J. Ewing, P. Drzaic, *Proc. Natl. Acad. Sci. U.S.A.* **2001**, *98*, 4835. (b) C. D. James, R. C. Davis, L. Kam, H. G. Craighead, M. Isaacson, J. N. Turner, W. Shain, *Langmuir* **1998**, *14*, 741. (c) Y. Koide, M. W. Such, R. Basu, G. Evmenenko, J. Cui, P. Dutta, M. C. Hersam, T. J. Marks, *Langmuir* **2003**, *19*, 86. (d) Y. L. Loo, J. W. P. Hsu, R. L. Willett, K. W. Baldwin, K. W. West, J. A. Rogers, *J. Vac. Sci. Technol, B* **2002**, *20*, 2853.

[90] (a) J. T. C. Wojtyk, M. Tomietto, R. Boukherroub, D. D. M.Wayner, *J. Am. Chem. Soc.* **2001**, 123, 1535. (b) L. A. Porter, H. C. Choi, J. A. Schmeltzer, J. M. Buriak, *Nano Lett.* **2002**, 2, 1369.

[91] (a) Service, R. F. *Science* **2001**, *293*, 782. (b) T. Ito, S. Okazaki, *Nature* **2000**, *406*, 1027. (c) R. M. Langford, A. K. Petford-Long, M. Rommeswinkle, S. Egelkamp, *Mater. Sci. Technol.* **2002**, *18*, 743. (d) J. T. Horstmann, K. F.Goser, *Microelectron. Eng.* **2002**, *61*, 601.

[92] (a) R. M. Nyffenegger, R. M. Penner, *Chem. Rev.* **1997**, 97, 1195. (b) G. P. Lopinski, D. D. M. Wayner, R. A. Wolkow, *Nature* **2000**, *406*, 48.

[93] (a) H. Janos Fendler *Chem. Mater.* **1996,** *8,* 1616. (b) J. H. Fendler , *Chem.*

Mater. **2001,** *13,* 3196 and references therein.

[94] (a) D. Vuillaume, C. Boulas, J. Collet, G. Allan, C. Delerue, *Phys. Rev. B: Condens. Matter* **1998**, *58*, 16491. (b) C. Boulas, J. V. Davidovits, F. Rondelez, and D. Vuillaume, *Phys. Rev. Lett.* **1997,** 76, 4797. (c) D. Vuillaume, C. Boulas, J. Collet, J. V. Davidovits, and F. Rondelez, *Appl. Phys. Lett.* **1997,** 69, 1646.

[95] (a) D. Niwa, K. Omichi, N. Motohashi, T. Homma, T. Osaka, *Sensors and Actuators B* **2005,** 108,721 and references therein. (b) D. Niwa, Y. Yamada, T. Homma, T. Osaka, *J. Phys. Chem .B* **2004,** 108, 3240. (c) N. K. Chaki, K. Vijayamohanan, *Biosensors and Bioelectronics*, **2002**, 17, 1 and references therein.

[96] J. W. Judy, *Smart Mater. Struct.* **2001**, 10, 1115 and references therein

[97] (a) R. Maboudian, *Mater. Res. Soc. Bull.* **1998,** 23, 47 and references therein. (b) H.-L. Li, A.-P. Fu, D.-S. Xu, G.-L. Guo, L.-L. Gui, Y.-Q. Tang, *Langmuir* **2002**, 18, 3198. (c) R. Maboudian, R. T. Howe, *J. Vac. Sci. Technol. B* **1997,** 15, 1.

[98] K. Kendall, *Science,* **1994,** 263,1720.

[99] (a) N. Tas, T. Sonnenberg, H. Jansen, R. Legtenberg, M. Elwenspoek, *J. Micromech. Microeng.* **1996,** 6, 385 and references therein. (b) B. Bhushan, '*Tribology and Mechanics of magnetic Storage Devices*', New York, Springer-Verlag, **1990**.

CHAPTER 2

Preparation and Characterization of Octadecyltrichlorosilane Self Assembled Monolayer on Si/ SiO_2 Interface: Growth Kinetics and Thermodynamic Stability

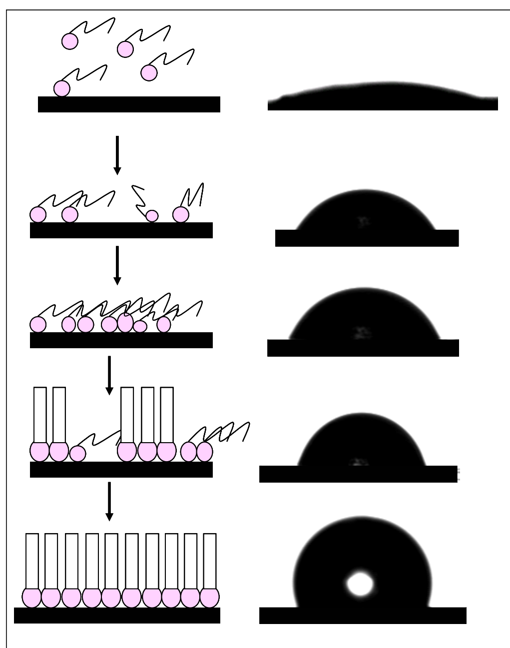

This chapter primarily deals with the kinetics of octadecyltrichlorosilane (OTS) monolayer formation on n-type Si (100) substrate. Combined evidence of SAM formation gathered from diverse techniques such as CA measurements, XPS, FTIR and AFM is used to discuss the growth kinetics and thermodynamic stability.

A part of the work reported in this chapter has been published in 'Materials Letters' **2005,** 59, 3890

2.1 Introduction

Ultra-thin organic films like self-assembled monolayers (SAMs) and Langmuir–Blodgett (LB) films are extensively studied due to their fundamental importance in surface modification and also for their diverse potential applications in nanotechnology [1–4]. The presence of a simple monomolecular film on a metallic or semiconducting surface can cause dramatic changes in its surface properties and hence these SAMs have received extensive attention during the last decade due to their ability to control wetting, adhesion, lubrication and corrosion [1–9]. For example, the presence of SAM on Si (100) surface has been shown to tackle the stiction problem of microelectromechanical systems (MEMS) by providing a suitable low energy surface coating [10–13]. These types of organic monomolecular films act as a passivation layer can, not only alleviate capillary forces and direct chemical bonding on Si–O surface, but also reduce electrostatic forces if the terminal group is tailored to possess controlled hydrophobicity. The formation of closely packed, covalently bonded monolayer with tunable chain length and hydrophobic terminal group on silicon oxide surface would eliminate the release stiction and reduce the *in-use* stiction [1-13].

Usually alkyltrichlorosilane based SAMs are used for reducing stiction during silicon micromachining and suitable candidates include octadecyltrichlorosilane (OTS), perflorodecyltrichlorosilane (FDTS) and their other structural analogs [1, 2a, 10-13]. The hydrophobic nature of these SAMs eliminates the water capillary forces responsible for the release-related stiction, in a liquid–based microfabrication process. Consequently, the growth mechanism of OTS-SAM on Si/SiO_2 substrate has been extensively studied in different solvents with a wide concentration range using various characterization tools such as FTIR-ATR spectroscopy, quartz crystal microbalance, contact angle (CA) technique, Atomic force microscopy (AFM), ellipsometry and X-ray reflectivity [15-20]. These studies demonstrate that the growth of trichlorosilane-based SAMs uniquely involve an irreversible covalent cross-linking step and the full coverage (and even in some cases multilayer coverage) is obtained within few minutes to hours depending on the experimental conditions [21]. For example, Maoz and Sagiv were the first to study the kinetics of the monolayer formation of OTS on Si using FTIR spectroscopy and CA measurements [12]. Subsequently, qualitative growth kinetics of OTS-SAM was reported

by Rozlosnik et al., and also by Wang and Lieberman illustrating the important role of solvent selection and humidity control [14, 21]. Although these and several other reports are available on the growth mechanism of SAM formation using different organic molecules by varying experimental parameters (as discussed in previous chapter), a quantitative adsorption–desorption rate constant calculation of OTS on Si is missing. This is especially significant for OTS-SAM due to its importance for both micromachining and microfabrication as explained in section 1.7.4. Consequently an accurate control of the monolayer growth kinetics is important for establishing a protocol for the construction of close packed and completely reproducible monolayer on Si surface ensuring reproducible behavior [1, 2].

In this chapter, we study the adsorption kinetics and thermodynamic stability of monolayer formation on Si (100) by using time-dependent CA measurements in accordance with Langmuir adsorption isotherm considering OTS as a typical example. The approximate rate constant and change in Gibbs free energy (ΔG) estimated within the assumption of this model are in excellent agreement with values reported by independent methods such as quartz crystal microbalance (QCM) and FTIR spectroscopy. The growth mechanism of OTS-SAM formation in toluene is also studied using AFM and FTIR spectroscopy. In addition, the critical surface tension (γ_c) for OTS monolayer on Si (100) from the Zisman plot shows the flexibility of SAMs to control the interfacial energy.

2.2 Experimental Section

2.2.1 Materials

n-Octadecyltrichlorosilane (OTS) ($CH_3(CH_2)_{17}SiCl_3$), was purchased from Aldrich, while all other chemicals were from Qualigens. Commercially available n-type, one-side polished, silicon wafers of (100) orientation with 0.001-0.007 Ω-cm resistivity were used as substrates. These substrates (1x1 cm^2) were rinsed by milliQplus (18 MΩ cm) water, sonicated in ethanol and dried under a flow of nitrogen. These wafers were soaked in 1:10 deionized HF:H_2O solution for 30 s to remove the native SiO_2 layer followed by soaking in *piranha* solution (7:3 H_2SO_4: H_2O_2) for 30 min at 90 °C to grow a fresh oxide layer, subsequently rinsed with deionized water, dried in nitrogen and used

for further experiments. (*Caution: ''piranha'' solution reacts violently with organic contaminants, one must be careful when handling*).

2.2.2 Monolayer Formation

Freshly prepared OTS in toluene (0.05, 0.1, 0.5 and 1 mM) was used for all monolayer formation experiments. Silicon wafers were dipped in this OTS solution of a particular concentration and were removed after different time intervals. CA of each sample was measured on dried surface after washing it several times with appropriate solvent used for SAM formation. These steps were carried out in nitrogen filled glove box.

2.2.3 Characterization

All CA measurements were performed using water and hexadecane (HD) sessile drops with the help of a RAME-HART NRL–Model CA goniometer and GBX-Model 'Digidrop' contact angle meter. On each sample, CA was measured at three different locations and the results were averaged.

Critical surface tension of a monolayer surface was measured by sessile drop CA measurements using various organic solvents of known surface tension (given in parenthesis, dyne/cm) including water (72.1), methanol (22.5), dimethyl sulfoxide (43.5), ethylene glycol (47.3), xylene (28.9), chloroform (26.7), and hexadecane (27.5) [22]. Monolayers were characterized by grazing angle FTIR spectroscopy as well as ATIR-FTIR spectroscopy (attenuated total internal reflection) on a Perkin Elmer 1615 spectrometer. The bare silicon wafer was used as a background sample and the spectrum was recorded at a resolution of 4 cm^{-1} over 256 scans at room temperature.

XPS measurements were carried out using VG MicroTech ESCA 3000 instrument at a pressure >1 $\times$ 10^{-9} Torr. The general scan and Si 2p and C 1s core-level spectra were recorded with unmonochromatized Mg Kα radiation (photon energy = 1253.6 eV) at pass energy of 50 eV and an electron take off angle (angle between electron emission direction and surface plane) of 60 ^{o}. The overall resolution was ~1 eV for XPS measurements and the core-level binding energy (BE) was calibrated by taking the adventitious carbon binding energy as 285 eV. AFM images were obtained using a Nanoscope II (Digital Instruments, Inc) operated at a constant height mode with a very low applied force

(typically under 1 nN). All measurements were performed in ambient conditions using silicon nitride probes mounted on the micro-fabricated cantilever (force constant 0.6 N/m) in the tapping mode to avoid any apparent surface damage. The bearing ratio of the instrument software was used to estimate the surface coverage of the OTS monolayer. The average thickness of the islands was determined from several random height profiles of the images and predefined threshold height of the monolayer (2.4 nm) was used for all coverage calculations. To avoid tip induced artifacts, each sample was imaged repeatedly in the same region for several consecutive scans.

2.3 Results and Discussion

2.3.1 Contact Angle Measurements

CA measurement is one of the important techniques to detect the hydrophobic surface properties of a monolayer, despite its poor accuracy and inability to reveal microscopic information as described well in chapter 1 (section 1.6.1). For example, the extent of hydropobicity of the monolayer derivatized Si substrates could be quantitatively assessed using CA. More significantly the change in the CA could be correlated with the variation in surface chemical composition of the substrate as well as the extent of the monolayer surface coverage using suitable physicochemical model of surfaces [23–26].

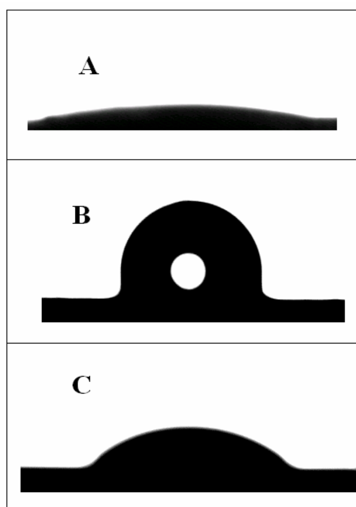

Figure 2.1: A comparison of sessile drop contact angle images on the (A) bare Si (< 15°) and monolayer derivatized OTS-Si substrate with (B) water (109 ± 2 ^{o}) and (C) hexadecane (38 ± 2 ^{o}) respectively.

A clean Si surface with native oxide (20 nm) has a water CA less than 15° (Figure 2.1A), which indicates its hydrophilic nature. In sharp contrast, the CA with water

(Figure 2.1B) and hexadecane (Figure 2.1C) obtained for OTS monolayer surface is 110 ± 1° (due to hydrophobic nature of the surface) and 38 ± 1° respectively, indicating the monolayer formation on the Si substrate. This change in CA due to SAM formation is in good agreement with the previous reports [1, 2, 18, 19].

2.3.2 Growth Kinetics of OTS Monolayer

Figure 2.2 shows the variation of CA (with a sessile water drop) as a function of dipping time for different OTS concentrations (e.g. 1 mM, 0.5 mM, 0.1 mM, and 0.05 mM). Usually a clean Si surface has a water CA less than 15°, which indicates its hydrophilic nature. Soon after the immersion of this substrate on an OTS solution in toluene, the substrate was removed and washed repeatedly with toluene and dried in a stream of nitrogen.

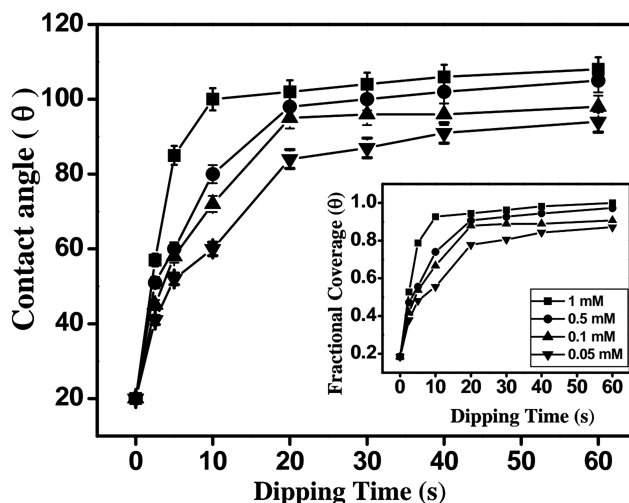

Figure 2.2: Adsorption kinetics of OTS monolayer on Si (100) substarte; CA variation and inset shows a fractional coverage as a function of dipping time for various OTS concentrations (1 mM, 0.5 mM, 0.1 mM, and 0.05 mM).

This SAM functionalized substrate shows increased CA, which is comparably higher than that of Si wafer dipped in pure toluene (without OTS). Subsequently, all samples (dipped in OTS solution for different time intervals) show rapid increase in CA values only in the initial stages of immersion and later reach a steady CA 109° corresponding to the full surface coverage [1, 2, 16, 27]. For example, in the case of 1 mM OTS solution, CA values are 57° and 100° for a soaking time of 2.5 and 10 s respectively, whereas the steady state value is ~109 ± 2° (for a soaking time of about 60 s) indicating the full surface coverage [1, 2, 16, 27]. Also, as the OTS concentration

decreases, the time required for complete monolayer formation increases. For instance, in case of dilute OTS solutions (0.5 and 0.05 mM) longer time (30 min and 16 h respectively) is required for accomplishing full monolayer coverage.

Above CA values after normalizing with respect to the steady state value are used to calculate the fractional coverage (θ), as shown in the inset of Figure 2.2. Although θ increases rapidly in the beginning, it subsequently slows down, perhaps due to the importance of adsorbate- adsorbate interactions or extensive reorganization. This trend is in complete agreement with the reported linear growth up to a surface coverage of 0.75 for 5 mM OTS and a comparatively slow saturation at higher coverage [28].

2.3.3 Calculations of Thermodynamic Stability of OTS Monolayer

Rate of adsorption / desorption can be calculated using a simple form of Langmuir isotherm, by neglecting the adsorbate-adsorbate interactions. Accordingly, we estimate the variation of coverage with time by the following equation,

$$\frac{d\theta}{dt} = k_a(1-\theta)C - k_d\theta \qquad (1)$$

where, θ is the fraction of surface covered, (1- θ) represents the available sites for adsorption and C is the OTS concentration. The values of both k_a and k_d corresponding to adsorption / desorption rate constants enable us to calculate the thermodynamic parameters.

Integration of equation (1) yields,

$$\theta(t) = K' [1- \exp(-K_{obs}t)] \qquad (2)$$

where, $K_{obs} = k_aC + k_d$ and

$$K' = \frac{C}{(C + (k_d/k_a))}$$

The values of K′ and K_{obs} are obtained by fitting the experimental data (shown as an inset of figure 1) with equation 2. Figure 2.3 shows the values of K_{obs} as a function of OTS concentration and a linear fit provides both adsorption (k_a) and desorption (k_d) rate constants. For example, the slope of this plot gives the value of $k_a = 150 \pm 30\ M^{-1}s^{-1}$ and the intercept on Y-axis gives the value of $k_d = 0.156 \pm 0.03\ s^{-1}$.

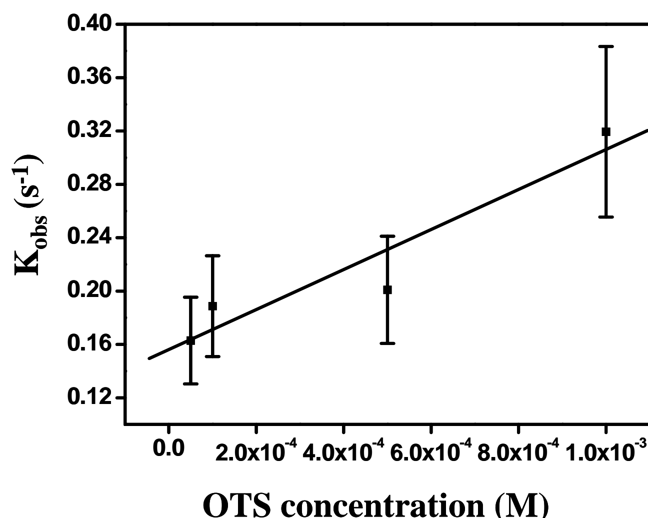

Figure 2.3: Concentration dependence of K_{obs} for OTS in Toluene. From these data the obtain best-fit values of k_a =150 ± 30 $M^{-1}s^{-1}$ and k_d = 0.156 ± 0.03 s^{-1}.

Despite large error originating due to the uncertainty in CA (± 2) values, these are useful to provide appropriate quantitative estimate of thermodynamic parameters. Since $k_d > 0$, the desorption is significant and the equilibrium constant (K_{eq}), is calculated using,

$$K_{eq} = (k_a/k_d) = (150/0.1561) = 960\ M^{-1}$$

Using this equilibrium value, the free energy of monolayer formation is calculated as,

$$\Delta G_{ads} = -RT \ln K_{eq} = -4.2\ \text{kcal / mole.}$$

This value implies thermodynamic stability of OTS monolayer on Si surface and more significantly further tuning is also possible by variation of the chain length and terminal functionality. It is interesting to compare the above free energy change with the available data for similar systems [23, 29]. The free energy of adsorption decreases by 0.16 - 0.24 kcal/mole per methylene chain and accordingly, the calculated ΔG_{ads} for OTS-SAM (C_{18}) should vary between 2.88 - 4.32 kcal / mole [23, 29]. Experimentally calculated value of free energy change for OTS-SAM is, therefore, in good agreement with this estimated value and also values of similar models [15a, 16a, and 23]. It is instructive to compare value of ΔG_{ads} for $C_{18}H_{37}SH$ and $C_7H_{17}SH$ SAM formation on gold surface as –5.5 and –4.4 kcal/mole respectively. Similarly, ΔG_{ads} for stearic acid ($C_{17}H_{35}COOH$) on glass and aluminum substrates are -7.3 ± 0.1 and –9.2 ± 0.1 kcal / mole respectively [15a, 16a, and 23] which suggest the approximate order of thermodynamic stability of these modified substrates.

2.3.4 AFM and FTIR Analysis

In order to understand the packing and orientation of OTS-monolayer, grazing angle FTIR and AFM measurements on samples of different surface coverage are very useful. Accordingly, Figure 2.4 shows AFM images (968 x 986 nm^2) and the corresponding IR spectra of partially and fully covered OTS-monolayer by exposing freshly cleaned Si substrate at various time intervals in OTS solution. For example, Image '2.4A' is taken after 2.5 s immersion, (CA of 57°, and fractional coverage ~50 %) where the OTS islands are seen to be randomly distributed on the surface. The average height of the OTS film is found to be ~0.55 nm as the molecules are randomly arranged lying flat on the surface. The height is significantly less than the theoretical length (2.4 nm) of covalently bounded OTS molecules, which is in agreement with the 'uniform' model of growth proposed by Wasserman et al., [19]. In the initial stage, OTS molecules are likely to get adsorbed in a disordered conformation, gradually aligning themselves, as the surface coverage increases and therefore the geometrical coverage is expected to be less than the saturation coverage. The inset of Figure 2.4A shows the corresponding IR spectrum of the partial monolayer. The observed methylene peaks (for sample 1) due to C-H symmetric and antisymmetric stretching at 2852 and 2924 cm^{-1} respectively indicates that the monolayer is not densely packed and oriented [30-33]. However, the intensity growth and peak positions of the C-H stretching vibrational modes ($–CH_2$) of the monolayer film provide information on the monolayer formation rates and structural changes during in the course of the growth. Images '2.4B' and '2.4C' are taken after 5 s and 10 s immersion, show CA of 85° (fractional coverage of ~ 76 %) and 100° (fractional coverage ~90 %), with an average height of the OTS monolayers as ~1.31 and 1.83 nm respectively. This indicates that the OTS monolayer still possesses disordered alkyl chains if it could follow a 'uniform' growth mechanism. The partial monolayer formed via a uniform growth mechanism has a high degree of gauche defects, which are random in nature. The monolayer coverage is about 90 % as more OTS molecules grow in the area between the primary or previously adsorbed islands, but distributed randomly on the surface indicating that the monolayer growth is not yet complete. In addition, two major peaks of methylene vibrations assigned to asymmetric and symmetric modes show red

shift with increasing surface coverage perhaps, due to conformational changes, such type of frequency shift has also been reported by Kosuri et al., [30].

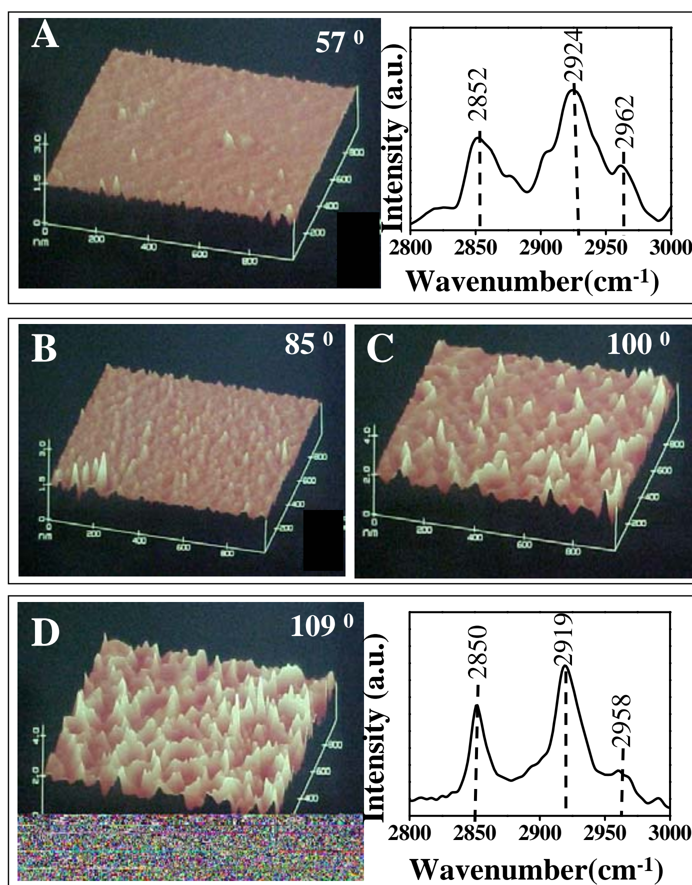

Figure 2.4: AFM images of OTS monolayer on SiO_2, A) partially grown OTS monolayer after 2.5 s soaking time and its corresponding IR spectrum, surface coverage is about 50 %; B) after 5 s, 70% surface coverage; C) 10 s, 90 % surface coverage and D) fully covered OTS monolayer after 60 s and its corresponding IR spectrum

It also suggests that the film growth follows essentially a Langmuir model of irreversible adsorption. Initially the monolayer molecules adsorb at random disordered configuration on the surface. Nevertheless, as the surface coverage increases, hydrocarbon chains gradually align themselves to stand up on the surface and their final orientation in the complete monolayer depends both on the chain length and type of terminal substitution [31-33].

Image 2.4D shows the surface morphology after 60 s dipping in OTS solution followed by rinsing and drying and the CA of 109 ± 2° corresponds to the full coverage. The uniform growth mechanism explains the filling of the remaining space among the

islands to form a compact monolayer with well-ordered alkyl chain conformation. Further, an average height of ~ 2.4 nm is consistent with an all-trans configuration of the OTS alkyl chains on the surface, which is also in good agreements with the previously reported values [16b, 34, 35]. Therefore these islands represent a near complete monolayer of OTS molecule. Interestingly for the substrate corresponding to a dipping time of 60 s (with ~ 99 % coverage) vibrational peaks observed at 2850 and 2919 cm^{-1} suggest a densely packed monolayer [22]. For example the asymmetric C-H stretching mode of terminal CH_3 appearing at 2958 cm^{-1} is a clear sign of orientated monolayer formation. Furthermore, a comparison of this IR spectrum with that of a similar long chain alkane hydrocarbon clearly suggests the presence of ordered and closely packed molecular assembly.

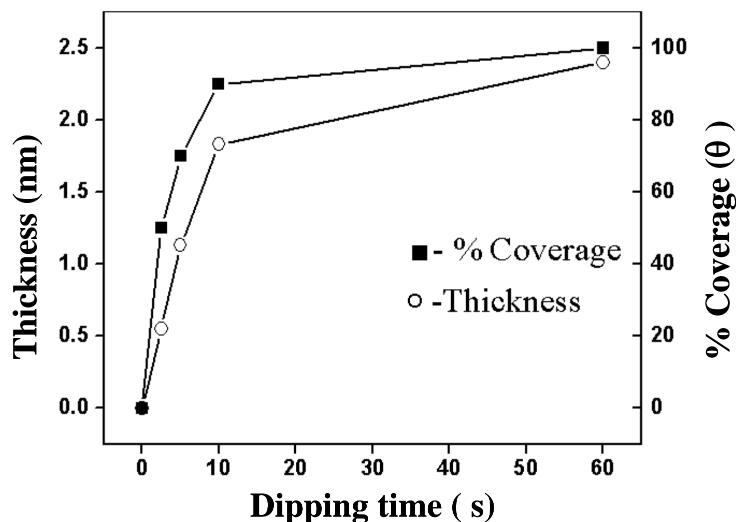

Figure 2.5: A plot of monolayer thickness and % coverage with dipping time. The thickness is calculated from the AFM measurements assuming the length of fully covered OTS-monolayer on Si substrate is 2.4 nm. The % coverage is calculated from the normalizing CA measurements assuming 109 ^{o} for full coverage.

The results obtained from the AFM and CA measurements are summarized in Figure 2.5, which give the variation of monolayer coverage with time. This also supports the 'uniform growth' mechanism of monolayer formation as discussed in details in chapter 1 (section 1.4). Thus a combined analysis of results obtained from the CA, IR and AFM measurements suggest that the adsorption rate of monolayer formation is fast in the initial stages and 90 % coverage occurs within 10 seconds, although longer time is necessary to achieve full coverage. A kinetic study of OTS monolayer formation on Si

(100) by CA technique enables the estimation of adsorption and desorption rate parameters using Langmuir adsorption isotherms as k_a=150 $M^{-1}s^{-1}$ and k_d = 0.156 s^{-1}. The Gibbs free energy (ΔG_{ads}) change amounts to –4.2 kcal/mole suggesting the thermodynamic stability of these molecules on silicon surface. The time-dependant measurements of different monolayer surface coverage by grazing angle FTIR spectroscopy and AFM show the formation of monolayer by a 'uniform' growth mechanism as proposed by Wasserman et. al, [19]. Finally, the fully covered OTS monolayer on Si substrate is characterized using XPS in order to understand its chemical composition, which supplements the results of all other studies.

2.3.5 X-ray Photoelectron Spectroscopy

XPS measurements provide useful quantitative information on the composition and chemical identity of the monolayer. XP spectra of bare (Si 2p) and OTS monolayer (for full coverage) on Si (100) are shown in Figure 2.6. In case of bare Si, (Figure 2.6 A), the Si 2p spectrum consists of two peaks at 99.08 and 103.4 eV corresponding to Si^0 (elemental Si) and Si^{IV} (Si^{IV} in SiO_2) respectively.

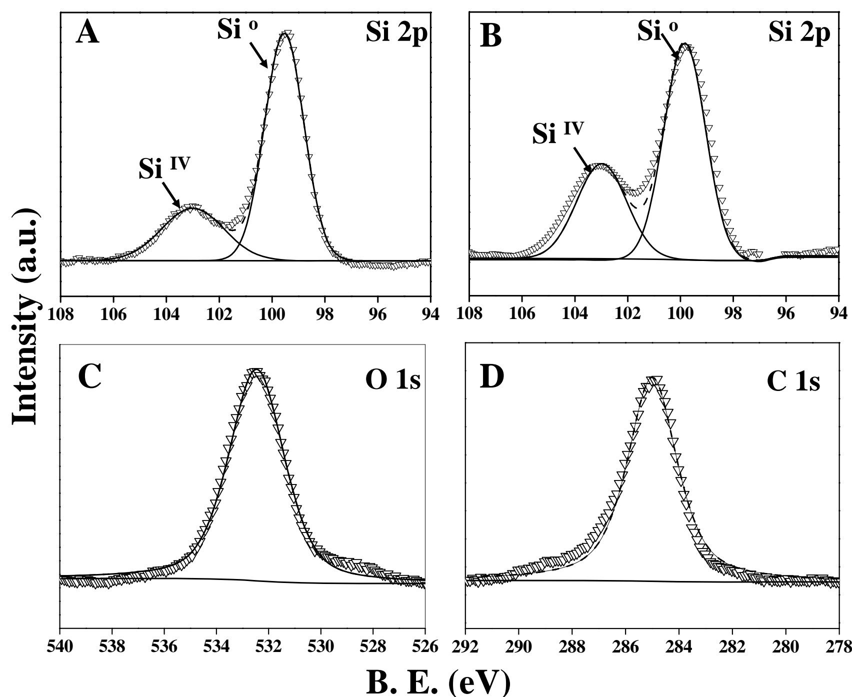

Figure 2.6: XP spectra of bare Si for A) Si 2p and OTS monolayer derivatized Si for B) Si 2p, C) O 1s and D) C 1s respectively; the triangles represent the experimental data and the solid line represents the Gaussian fits to the data.

Interestingly, the intensity ratio of Si ^{IV} to Si ^{0} peak increases (Figure 2.6B) after the monolayer formation as compared to that of bare Si substrate [21]. The increase in the peak intensity of Si^{IV} shows an additional Si^{IV} signal from OTS molecule. One can easily find evidence for the monolayer by comparing the intensity ratios of Si ^{IV} to Si ^{0} peak before and after the SAM formation. In addition, in case of OTS-Si, the C 1s peak at 285 eV (Figure 2.6 C) and O1s at 532 eV (Figure 2.6 D) correspond to alkyl chain and oxygen in the Si-O-Si linkage respectively in OTS-SAM.

2.3.6 Zisman Plot

The ability of OTS-SAM to control adhesion through surface functionalization is illustrated using Zisman plot. Accordingly, Figure 2.7 shows cosine of CA (cosθ) measured using various solvents with a wide range of surface tension on a full coverage of OTS monolayer (Zisman plot) on Si substrate.

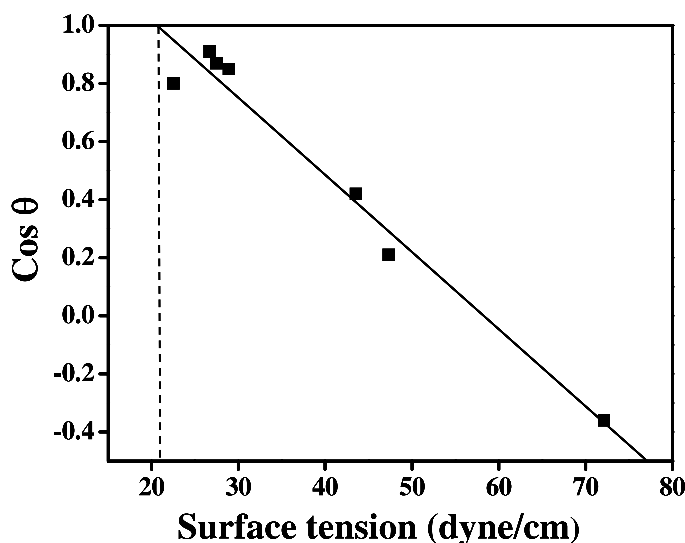

Figure 2.7: Zisman plot for a fully covered OTS monolayer on Si (100); extrapolation to cosθ = 1 gives the critical surface tension value of 20.7 dyne/cm.

As the surface tension of the solvent decreases the CA decreases and the extrapolation of this plot (cosθ = 1) gives the critical surface tension (γ_c) for wetting [36]. In this case, the obtained critical surface tension is 20.7 dyne/cm, which is in close agreement with the value reported by others (20.2 ± 1 dyne/cm) for close-packed monolayer of OTS-SAM on Si. Since the accuracy of these measurements is approximately ± 1 dyne/cm our data is in good agreement with the reported value,

although parameters like liquid purity, temperature and humidity can affect the surface tension [36].

2.4 Conclusions

A kinetic study of OTS monolayer formation on Si (100) by CA technique enables the estimation of adsorption and desorption rate parameters using Langmuir adsorption isotherms as $k_a = 150\ M^{-1}s^{-1}$ and $k_d = 0.156\ s^{-1}$ respectively. A change in the Gibbs free energy (ΔG_{ads}) of –4.2 kcal/mole suggests the thermodynamic stability of these molecules on silicon surface. Time-dependant measurements of different monolayer surface coverage by grazing angle FTIR spectroscopy and AFM indicate the formation of monolayer by a ‘uniform’ growth mechanism. The ability of OTS-SAM to control adhesion through surface functionalization is also illustrated using Zisman plot. Analysis of the interfacial adhesion properties using Zisman plot suggests a critical surface tension γ_c of 20.7 dyne/cm for OTS monolayer on Si (100).

2.5 References

[1] (a) A. Ulman, *An introduction to ultra thin organic films from Langmuir-Blodgett to Self-assembly, Academic Press, Lon*don **1991**. (b) A. Ulman*, Chem. Rev.* **1996,** 96, 1533. (c) J. Sagiv, *J. Am. Chem. Soc.* **1980,** 102, 92.

[2] (a) R. Maboudian, *Mater. Res. Soc. Bull.* **1998,** 23, 47 and references therein. (b) H.-L. Li, A.-P. Fu, D.-S. Xu, G.-L. Guo, L.-L. Gui, Y.-Q. Tang, *Langmu*ir **2002**, 18, 3198.

[3] T. Vossmeyer, S. Jia, E. Delonno, M. Diehl, R. Kim, X. Peng, A. P. Alivisatos, G.R. Heath, *J. Appl. Phys.* **1998,** 84, 3664.

[4] (a) R.G. Nuzzo, L.H. Dubois, D.L. Allara, *J. Am. Chem. Soc.* 1990, 112, 558. (b) Nuzzo, R. D. Allara, *J. Am. Chem. Soc.* **1983**, 105, 4481.

[5] (a) J. Liu, M. J. Casavant, M. Cox, D.A. Walters, P. Boul, W. Lu, A. J. Rimberg, K.A. Smith, D.T. Colbert, R.E. Smalley, *Chem. Phys. Lett.* **1999**, 303, 125. (b) M. J. Stevens, *Langmuir* **1999**, *15*, 2773. (c) M. J. Wirth, H. O. Fatunmbi, *Anal. Chem.* **1993**, *65*, 822.

[6] (a) L. S. Sander, S. A. Wise, *Anal. Chem.* **1984**, 56, 504. (b) I. Willner, A. Schlittner, A. Doron, E. Joselevich, *Langmuir* **1999**, *15*, 2766. (c) D. G. Kurth, T. Bein, *Langmuir* **1993**, *9*, 2965.

[7] (a) X. Xiao, J. Hu, D. H. Charych, M. Salmeron, *Langmuir* **1996**, *12*, 235. (b) de Gennes, P. G. *Rev. Mod. Phys.* **1985**, *57*, 827. (c) J. Andle, J. Vetelino, R. Lec, D. McAllister, *Proc. IEEE Ultrasonics Symp.* **1989,** 579. (d) P.-G. de Gennes, *Reu. Mod. Phys.* **1985**, 57, 827.

[8] (a) D. L.Angst, G. W. Simmons, *Langmuir* **1991**, *7*, 2236. (b) E. Plueddemann, Silane Coupling Agents; Plenum Press: New York, **1982**.

[9] (a) T. Komeda, K. Namba, Y. Nishioka, *J. Vac. Sci. Technol. A* **1998**, *3,* 1680. (b) N. L. Jeon, K. Finnie, K. Branshaw, R. G. Nuzzo, *Langmuir* **1997**, *13*, 3382.

[10] U. Srinivasan, M.R. Houston, R.T. Howe, R. J. Maboudian, *Microelectromech. Syst.* **1998,** 2. 252.

[11] Y. Xia, M.Mrksich, E. Kim, G.M. Whitesides, *J. Am.Chem. Soc*. **1995**, 117, 9576.

[12] W. R. Ashurst, C. Carraro, R. Maboudian, W. Frey, *Sensors and Actuators A*: *Physical* **2003,** 104, 213.

[13] P. Galambos, *Encyclopedia of materials: Science and Technology* **2001,** 5598.

[14] N. Rozlosnik, M.C. Gerstemberg, N.B, Larsen, *Langmuir* **2003,**19, 1182.

[15] (a) R. Maoz, J. Sagiv, *J. Colloid Interface Sci.* **1984,**100, 465. (b) R. Banga, J. Yarwood, A. M. Morgan, J. Kells, *Langmuir* **1995**, 11, 4393. (c) J. D. Le Grange, J. L. Markham, C. R. Kurkjian, *Langmuir* **1993**, 9, 1749. (d) J.-M. Berquier, A.-C. Fernandes, P. Chartier, H. Arribart*, SPIE Fourier Transform Spectrosc*. **1989**, 1145, 300. (e) K. Mathauer, C. W. Frank, *Langmuir* **1993**, 9, 3446. (f) K. M. R. Kallury, C. P. Tripp, M. L. Hair, *Langmuir* **1992**, 8, 947.

[16] (a) D. S. Karpovich, G. J. Blanchard, *Langmuir* **1994,** 13, 3315. (b) H. Schessler, D. S. Karpovich, G.J. Blanchard, *J. Am. Chem. Soc.* **1996,** 118, 9645.

[17] (a) D. K. Schwartz, S. Steinberg, J. Isarelachvili, J. A. N. Zasadzinski, *Phy. Rev. Lett.* **1992,** 69, 3354. (b) C. P. Tripp, M. L. Hair, *Langmuir* **1992**, 8, 1120. (c) M. E. McGovern, K. M. R. Kallury, M.Thompson, *Langmuir* **1994**, 10, 3607. (d) D. A. Offord, J. H. Griffin, *Langmuir* **1993**, 9, 3015.

[18] (a) N. Tillman, A. Ulman, J. S. Schildkraut, T. L. Penner, *J. Am. Chem. Soc.* **1988,**111, 6136. (b) I. M.Tidswell, T. A. Rabadeau, P. S. Pershan, S.D.Kosowsky, *J. Chem. Phys.* **1991**, 95, 2854. (c) I. M. Tidswell, B. M. Ocko, P. S. Pershan, *Phys. Rev. B* **1990**, 41, 1111. (d) P. Silberzan, L. Leger, J. J. Benattar, *Langmuir* **1991**, 7, 1647. (e) M. Wei, R. S. Bowman, J. L.Wilson, N. R. Morrow, *J. Colloid Interface Sci.* **1993**, 57, 154.

[19] S. R. Wasserman, G. M. Whitesides, I. M. Tidswell, B.M. Ocko, P.S. Pershan, J. D. Axe, *J. Am. Chem. Soc.* **1989,** 111, 5853.

[20] (a) A. G. Richter, Durbin, CJ. Yu, P. Dutta, *Langmuir* **1998,** 14, 5980. (b) A G. Richter, C. J. Yu, A. Dutta, J. Kmetko, P. Dutta, *Phys. Rev. E.* **2000,** 61, 607.

[21] Y. Wang, M. Lieberman, *Langmuir* **2003,** 19, 1159.

[22] A. W. Adamson, Physical Chemistry of Surfaces, John Wiley & Sons, Inc **1997,** 36.

[23] S. H. Chen, C.W. Frank, *Langmuir* **1989,** 5, 978.

[24] G. J. Sagiv, *J. Colloidal Interface Science* **1986,** 112, 457.

[25] D. L. Allara, R. G. Nuzzo, *Langmuir* **1985,** 1, 45.

[26] W. A. Zisman, in '*adhesion and cohesion'* Weiss P. Ed. Elservier New York **1962**.

[27] D. L. Angst, G. W. Simmons, *Langmuir* **1991,** 7, 2236.

[28] B. Thorsten, R. Bautista, N. Hartmann, E. Hasselbrink, *Surf. Sci*. **2003,** 532, 963.

[29] L.S. Jung, C.T. Campbell, *Phys. Rev. Lett.* **2000,** 84, 5164.

[30] M. R. Kasuri, H. Hoffmann, U. Mayer, A. Krischanitz, *Langmuir* **1995,** 11, 1304.

[31] T. Vallant, J. Kattner, H. Brunner, U. Mayer, H. Hoffmann, *Langmuir* **1999,** 15, 5339.

[32] Yi. Liu, K. Wolf, M.C. Messmer, *Langmuir* **2001,** 17, 4329.

[33] K. Bierbaum, M. Grunze, *Langmuir* **1995,**11, 2143.

[34] S. R. Wasserman, Tao, Yu – Tai. G.M. Whitesides, *Langmuir* **1989,** 5, 1074.

[35] B. Brzoska, N. Shahidazadeh, F. Rondelez, *Nature* **1992,** 360, 719.

[36] (a) W. A Zisman, *Adv. Chem. Ser.* **1964**, 43, 1. (b) W. A. Zisman, *J. Chem.Phys.* **1941**, 9, 534. (c) W. A. Zisman, *J. Chem. Phys.* **1941**, 9, 729. (d) C.D. Bain, G. M. Whitesides, *Angew. Chem. Int. Ed. Engl* **1989**, 28, 506.

CHAPTER 3

Interfacial Behavior of Alkyltrichlorosilane Monolayers on Silicon: Control of Flat-Band Potential and Surface State Distribution Using Chain Length Variation

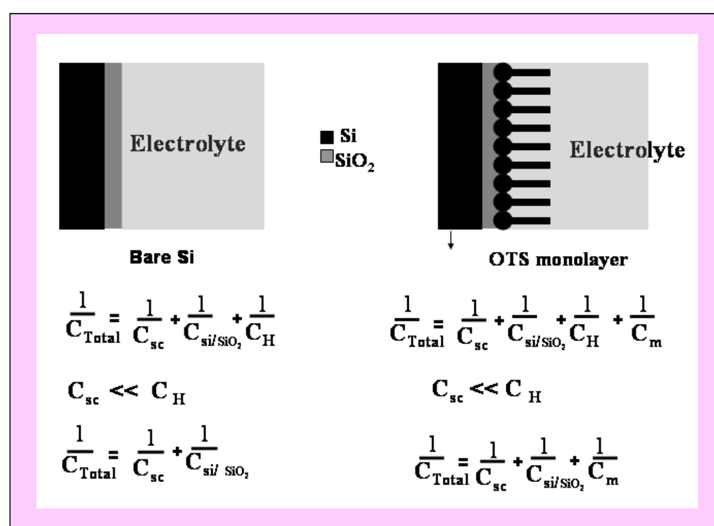

This chapter primarily deals with electrochemical properties of chain length dependent alkyltrichlorosilane (C_8, C_{12}, and C_{18}) self-assembled monolayers (SAMs) on Si (100) substrate in the presence and absence of an external redox probe like ferrocene. The electron transfer behavior of ferrocene on Si (100) electrode is found to be drastically affected by the presence of monolayer and the reasons for such significant variation are and quantitatively analyzed in terms of change in resistance, dielectric thickness and defect area.

A part of the work reported in this chapter has been published in '*J. of Colloid and Interface Science*' **2006,** 59, 3890

3.1 Introduction

Micro-Electro-Mechanical Systems (MEMS) are integrated mechanical elements like sensors, actuators and electronics on a common silicon substrate through microfabrication technology [1-5]. During this, a substrate is normally coated with an isolation layer followed by subsequent deposition and patterning of sacrificial spacer layers. The microstructural film is then deposited and etched selectively to create freestanding micromechanical structures.

One of the major limitations of microfrabrication is stiction, where either unwanted adhesion of the underlying substrate or adhesion of adjacent microstructures to the micromechanical devices, results in the failure of the device. Several strategies are known to avoid the stiction including supercritical drying usually with CO_2, freeze-sublimation employing methanol, and etching with HF [1-5]. More recently, alkyl trichloro or trimethoxy silane SAMs have become particularly useful for microelectromechanical systems (MEMS) to tackle the stiction problem since their mere presence provides a suitable low energy surface coating [6-8]. These types of organic monomolecular films acting as a passivation layer can, not only alleviate capillary forces and direct chemical bonding on Si-O surface, but also reduce electrostatic forces if the terminal group is tailored to possess controlled hydrophobicity. The formation of a close packed, covalently bonded monolayer with tunable chain length and hydrophobic terminal group on silicon oxide surface would eliminate the release stiction and reduce the in-use stiction [9-14].

In order to control these important properties of SAMs for desired applications, a molecular level investigation of the various interactions of the SAM forming molecule in relation to the substrate structure is very important. Consequently, the structure and properties of SAMs have been investigated by using various techniques including X-ray reflectivity [15], ellipsometry [16], contact angle (CA) measurements [9], FTIR spectroscopy and [9], and atomic force microscopy [17,18]. Electrochemical techniques like cyclic voltammetry and impedance methods have also been used effectively to understand the packing density and distribution of pinhole defects in the monolayer as illustrated in the first chapter [19-22]. These techniques clearly show that the dynamics of charge transfer at the electrochemical interface is strongly influenced by the nature of the

electrode surface and also by the structure of the electric double layer. For example, several investigations of the blocking efficiency of SAMs against heterogeneous electron transfer and ion penetration have recently enabled quantitative estimation of surface coverage although SAMs of long chain alkanethiols were used predominantly on gold electrodes due to their well-known chemical stability [19-24]. In comparison, only few reports are available on the characterization of SAMs on semiconductor surface [25-28], a system, which differs from that of the metal electrode due to the additional space charge layer present on the semiconductor surface. For example, organic thin films formed by the reaction of Grignard reagent with oxide free silicon surface have been examined in terms of an ideal capacitive behavior at silicon electrode/aqueous electrolyte interface [29-31]. Electric characterization of alkyl silane monolayers on Si/SiO_2 has been discussed in terms of the suppression of charge–carrier tunneling [31]. Nevertheless, a detailed electrochemical characterization of alkyltrichlorosilane SAMs on Si surface is still missing despite its importance. The presence of monolayer acting as a barrier for electron transfer, as a result, causes a significant change in the electrochemical behavior. Since controlling the chain length of SAM offers a simple method to change the barrier height and the pinhole distribution, it would be important to extend these investigations using similar molecules of various chain lengths.

In second chapter, we have discussed the growth kinetics and thermodynamic stability of OTS-SAM on Si substrate. However, in order to use these SAMs for various applications in MEMS, it is an important prerequisite to understand their electrochemical properties. In this chapter, accordingly we investigate the effect of a dielectric barrier on the redox kinetics of ferrocene using octadecyltrichlorosilane (C_{18}), dodecyltrichlorosilane (C_{12}) and octyltrichlorosilane (C_8) SAMs on Si (100). Techniques like cyclic voltammetry and impedance measurements with an external redox probe have been used to investigate the monolayer structure and ion permeation capability through it. These monolayers have also been quantitatively analyzed in terms of resistance, dielectric thickness and defect area. It has been observed that the monolayer acts as a diffusion barrier for ions in the electrolyte, resulting in a significant suppression of the charge transfer and thus demonstrating the passivation effect of the monolayers at the electrode / electrolyte interface. FTIR spectroscopy and contact angle (CA) measurements also give

an evidence of the hydrophobic monolayer formation on Si surface. These results are important since the electron-transfer mechanism and rate strongly depends on the nature of the interface between organic molecules and solid substrate [33-35]. A systematic study on the electrical properties of organic monolayers on semiconductor substrate should also extend our understanding of surface electrochemistry, semiconductor electrochemistry, and electron transfer across organic/inorganic heterojunctions. The potential applications of this type of monolayers include the reduction/elimination of stiction in micro-electromechanical systems, contact printing in materials microfabrication, and inhibition of surface degradation.

3. 2 Experimental Aspects

3.2.1 Materials

n-Octadecyltrichlorosilane ($CH_3(CH_2)_{17}SiCl_3$, C_{18}), dodecyltrichlorosilane (CH_3 $(CH_2)_{11}SiCl_3$, C_{12}), octyltrichlorosilane (CH_3 $(CH_2)_7SiCl_3$, C_8), ferrocene ($(C_5H_5)_2Fe$) and lithium perchlorate ($LiClO_4$), hexadecane ($C_{16}H_{34}$) were obtained from Aldrich, while all other chemicals were purchased from Qualigens. Commercially available n-type, one-side polished, silicon wafers of (100) orientation with 0.001-0.007 Ω-cm resistivity were used as substrates. These silicon wafers (1x1 cm^2) were cleaned as per procedure described in details in chapter 2 (section 2.2.1). For monolayer formation, freshly leaned Si wafers were immersed in 0.5 mM alkyltrichlorosilane in toluene for 30 min and subsequently were removed from solution, rinsed several times with toluene, dried and used for further characterization. All the experiments were carried out in nitrogen atmosphere.

3.2.2 Electrode Preparation

In order to obtain good electrical contact with copper wire, the Si wafer was first cleaned with HF solution for 30 s and the rear side was scratched, cleaned from the detached particles of silicon and was then rubbed with In-Ga eutectic. A copper wire was fixed using conducting silver epoxy and was finally sealed with araldite (standard epoxy adhesive) and allowed to dry it for 24 hrs.

3.2.3 Surface Characterization

CA on Si (100) substrate was measured using a water sessile drop and also a hexadecane (HD) drop on a GBX-Model 'Digidrop' instrument. All monolayer derivatized Si substrates were characterized by ATR-FTIR (attenuated total reflectance) and also by grazing angle spectroscopy on a Perkin Elmer 1615 spectrometer. A bare silicon wafer was used as a background sample and the spectrum was recorded at a resolution of 4 cm^{-1} over 256 scans at room temperature.

3. 2. 4 Electrochemical Characterization

Cyclic voltammetry and impedance measurements were carried out with a conventional three-electrode system at room temperature in nitrogen atmosphere, using a cell comprising, Si as the working electrode, a large area Pt flag as a counter electrode and Pt wire as a quasi-reference in CH_3CN using 0.1 M $LiClO_4$ as the supporting electrolyte. Cyclic voltammetry was performed on an Autolab PGSTAT 30 (ECO CHEMIE) instrument, whereas electrochemical impedance measurement was carried out with a Solartron 1255B frequency response analyzer (FRA) interfaced to 1287 potentiostat / galvanostat over a wide frequency range of 100 kHz-0.01 Hz using with a signal of 10 mV rms amplitude. The impedance data was analyzed using ZPLOT2 and ZVIEW2 for the frequency analysis and equivalent circuit fitting / simulation program based on the complex non-linear least square (CNLS) method. For this equivalent circuits consisting of simple electric elements such as resistance, capacitance, and diffusion element and in addition a constant phase element (CPE) for nonlinearity and inhomogeneity were selected. Impedance plots were interpreted using Nyquist plot (Z'' vs Z'), Bode plot (frequency (/Z/ vs f) and phase angle (φ vs f), in which symbols represent the experimental data and solid lines indicate fitting curves obtained from the CNLS data fit.

The surface state distribution of monolayer derivatized Si electrodes was studied by monitoring the variations in the capacitance versus bias potential curves in 0.1 M $LiClO_4$, CH_3CN solution in the potential range -0.8 to 0.7 V at various selected frequencies. In addition, impedance measurements in the frequency region from 10 kHz–

10 MHz at different bias potentials (0.5 to 0.5 V) were carried out to calculate the E_{fb} potential.

3.3 Results and Discussion

3.3.1 Contact Angle Measurements

3.3.1.1 Surface Wetting Properties

A clean Si surface has a water sessile drop CA less than 15°, which indicates its hydrophilic nature. In sharp contrast, the CA with water and hexadecane obtained for OTS monolayer surface is 110 ± 1° (due to hydrophobic nature of the surface) and 38 ± 1° respectively, indicating the monolayer formation on the Si substrate. This change in CA due to SAM formation is in good agreement with previous reports [1, 2, 15, 16]. Similarly CA obtained for C_8 and C_{12} monolayer are 107 ± 1° and 109 ± 1° respectively, which also indicating the hydrophobic nature of the monolayer as shown in Table 3.1. According to Fadeev and McCarthy, CA does not depend upon the chain length of the monolayer, as same surface groups are exposed to water, regardless of chain length and methylene content. However, we find that the CA slightly decreases with the alkyl chain length, as it indirectly affects the surface properties through ordering, packing and tilting of monolayers. It is known that for monolayers with same surface group possessing different hydrocarbon chain length (n), CA angle is significantly lower and for $n < 10^o$, which indicates poor ordering. Nevertheless, for $n > 20$, the CA interestingly decreases indicating disorder arising perhaps due to the mingling of longer chains [23-26].

3.3.1.2 Zisman Plot and Thermal Stability

Zisman plot is a useful method to understand the wetting behavior of surfaces, since it enables interpolative predictions using a homologues series of liquids. The empirical relation between cosine of CA and the surface tension of the liquid is used to get the value of critical surface tension. Figure 3.1A shows the zisman plot, cosine of CA as a function of surface tension of solvents, for fully covered monolayers (C_{18}, C_{12}, and C_8) [36]. Surface tension is found to be decreased with increase in the chain length of the monolayer as shown in Table 3.1. Since the accuracy of these measurements is approximately ± 1 dyne/cm, our data is in good agreement with the reported value,

although parameters like liquid purity, temperature and humidity can affect the surface tension [9, 15].

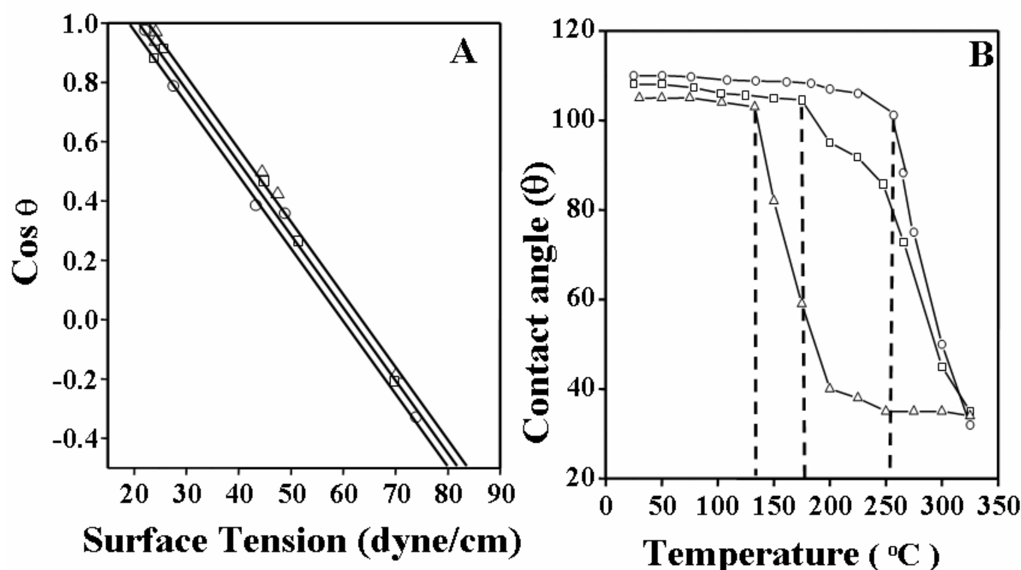

Figure 3. 1: A) Zisman plot of alkyltrichlorosilane monolayer (C_8 (∇), C_{12} (□) and C_{18} (o)) on Si substrate where extrapolation to cosθ = 1 gives the critical surface tension, and B) temperature dependent water sessile drop contact angle measurements of alkyltrichlorosilane monolayer on Si where, the measurements are carried out after heating the substrate at different temperature and subsequent cooling to room temperature.

CA measurement is also used to study the thermal stability of SAMs on Si substrate as a function of annealing temperature as shown in Figure 3.1B. For example, in case of OTS-monolayer, at room temperature the observed CA is ~ $109^o \pm 1$, remains constant up to 175 ^{o}C. It then started to decline at an annealing temperature of 350 ^{o}C up to 30 ^{o}, which is usually reported for bare Si, indicating the complete degradation of monolayer [1]. In brief, we conclude that OTS monolayer is stable up to 250 ^{o}C in the air [36]. Similarly, for C_8 and C_{12} monolayers the desorption starts at 130 ^{o}C and 170 ^{o}C and complete desorption of monolayers take place at 200 ^{o}C and 280 ^{o}C respectively. Kulth et. al., have reported that the thermal behavior of the monolayer is independent of hydrocarbon chain length and monolayers are stable in vacuum up to 450 ^{o}C [3]. We observed that the thermal stability of the monolayer decreases with decrease in the chain length, perhaps due to the more tilt angle and less packing density. As a result molecules (of a shorter chain length monolayer) are easily desorbed at lower temperature in comparison with longer chain length monolayers.

Table 3.1: Water sessile drop contact angle measurements, surface tension and thermal stability of alkyltrichlorosilane monolayer (C_8, C_{12} and C_{18}) on Si (100) substrate.

	Contact angle (^{o})			Thermal stability (^{o}C)
	HD	Water	Surface Tension (dyne/cm)	
n-type Si(100)		< 15		
C_8-Si	38 ± 1	107 ± 1	23.1	130
C_{12} Si	39 ±1	109 ± 1	22.14	170
C_{18} Si	41 ± 1	110 ± 1	20.7	225

This OTS monolayer on Si is quite stable up to 350 ^{o}C in N_2 atmosphere although the stability in air is limited only up to 250 ^{o}C. Chemical stability is also good as demonstrated in 0.1 M HCl at room temperature and these monolayers are also stable in organic solvents like hexadecane at 75 ^{o}C. The latter aspect is especially significant for MEMS applications as the SAMs are capable of sustaining different environments during various stages of the micro-fabrication [1, 2, 36].

3.3.2 FTIR Spectroscopy

In order to understand the packing and orientation of the monolayers, ATR-FTIR spectroscopy measurements were carried out on monolayer derivatized Si substrates. The superimposed FTIR spectra of monolayer derivatized Si substrate are shown in Figure 3.2. The prominent peaks at 2850 and 2919 cm^{-1} of methylene due to –C-H symmetric and asymmetric stretching respectively suggest the presence of a densely packed monolayer. The intensity and peak positions of the C-H stretching vibrational modes (–CH_2) of the monolayer film provide information on the monolayer formation rates and structural changes during the course of the growth process. For example, specific shifts from 2928 to 2919 cm^{-1} and from 2856 to 2850 cm^{-1} for the methylene peaks are well known on going from a liquid to solid alkane phase and therefore the observed wavenumbers in our case are indicative of a densely packed monolayer of alkyl chains (37). Further, the asymmetric C-H stretching mode of terminal CH_3 appearing at 2958 cm^{-1} is a clear signature of orientated monolayer formation.

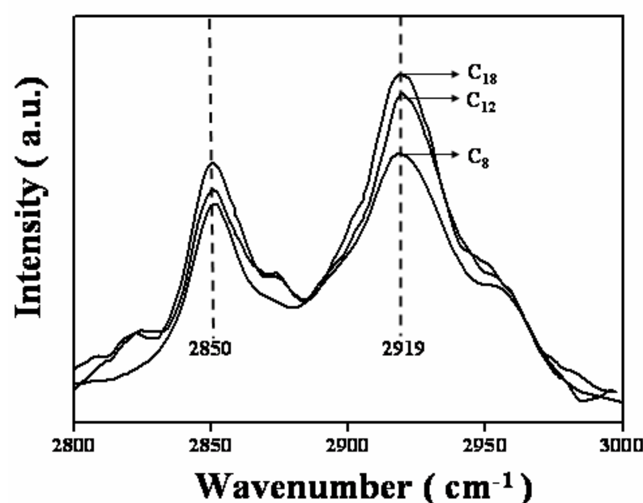

Figure 3.2: Superimposed FTIR spectra of monolayer derivatized n-type Si (100) substrate, the bare silicon wafer used as a background sample and the spectra recorded at a resolution of 4 cm^{-1} over 256 scans at room temperature.

The disappearance of a broad peak corresponding to the –OH stretching normally observed on any SiO_2 surface clearly indicates the transition from a hydrophilic to hydrophobic surface due to the presence of a monolayer. Furthermore, a comparison of this IR spectrum with that of a similar long chain alkane hydrocarbon clearly reveals the presence of ordered and closely packed molecular assembly. Similarly, peak positions of the C-H stretching vibrational modes (–CH_2) are nearly invariant for C_8 and C_{12} monolayers (Figure 3. 2) [37].

3.3.3 Cyclic Voltammetry

In order to understand the electron transfer behavior of semiconducting substrates after the monolayer formation, we have carried out electrochemical measurements on both bare and monolayer derivatized Si electrodes in presence of ferrocence as shown in Figure 3.3A and 3.3(B-D) respectively. For bare Si electrode, the oxidation and reduction peaks due to ferrocene / ferrocenium couple are observed at 0.1 V and -0.8 V respectively. After the monolayer formation on Si electrode, the shape of the voltammograms is significantly changed, the electron transfer is totally blocked clearly indicating the formation of a closely packed monolayer offering barrier for electron transfer. For all the cases the capacitance decreases by approximately an order of magnitude in comparison with that of bare Si. The capacitance is also found to decrease with an increase in the chain length of the monolayer as shown in Figure 3.3E, which

indirectly suggests that the capacitance varies inversely with the thickness of the monolayer film.

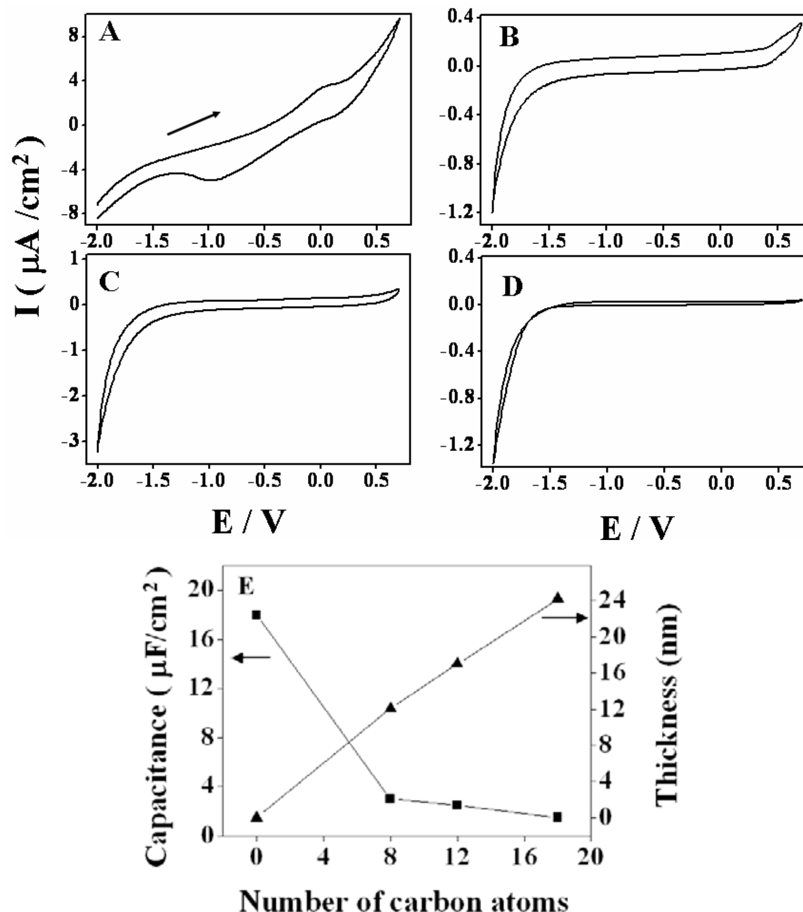

Figure 3.3: Superimposed cyclic voltammograms of A) bare Si electrode and monolayer derivatized Si electrodes ((B) C_8, (C) C_{12}, and (D) C_{18}) in presence of ferrocene performed in 0.1 M $LiClO_4$ in CH_3CN at a scan rate of 100 mV/s; E) the variation in the capacitance (calculated from cyclic voltammetry data) and the thickness with number of carbon atoms in the monolayer; arrow indicates a scan direction.

Hua-Zhong Yu et. al., have evaluated the capacitive properties of the organic thin films on silicon electode in aqueous electrolyte, where the reciprocal capacitance of the organic thin films modified silicon/aqueous electrolyte interface has been found to be proportional to the thickness of films [29]. We have carried out cyclic voltammteric measurements of monolayer derivatized Si electrode in the same electrolyte without ferrocene and the background current has been found to be negligible as compared to that from monolayer derivatized Si electrode in presence of ferrocene. It indirectly suggests that the observed electron-transfer processes and the current could be attributed solely to the electron transfer of the ferrocene probe [31].

3. 3. 4 Impedance Analysis

Figure 3.4 shows the electrochemical impedance data for bare (Figure 3.4A) and monolayer derivatized Si electrode (Figure 3.4B) in 0.1M $LiClO_4$ in CH_3CN respectively. Nyquist plot of bare Si electrode shows a well-defined semicircle. In sharp contrast, monolayer derivatized Si electrode (C_{18}, $C_{12,}$ and C_8), exhibits a nearly vertical line parallel to y-axis over the entire frequency domain (100 kHz to 0.01Hz), typical of a capacitive behavior.

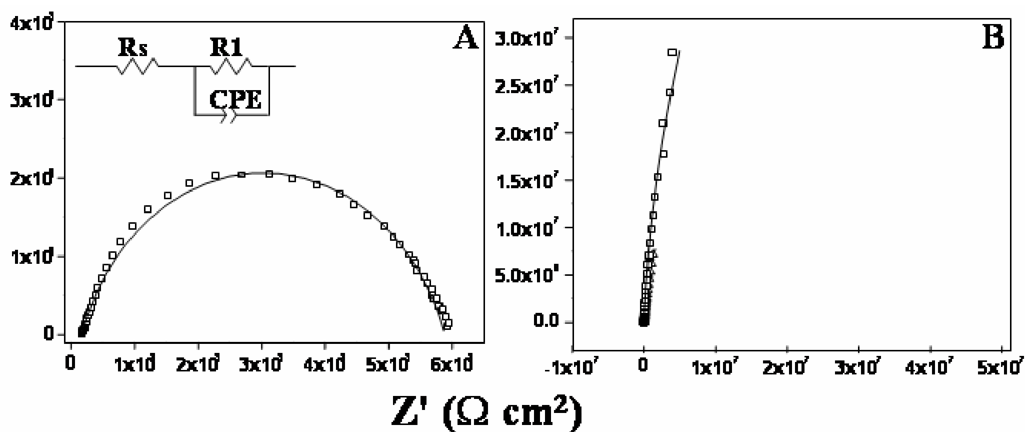

Figure 3.4: Complex plane impedance plots of A) bare Si electrode; and B) monolayer derivatized Si electrode (C_8, C_{12}, and C_{18},) in 0.1 M $LiClO_4$ in CH_3CN in the frequency range of 100 kHz to 0.01Hz with a 10 mV rms signal under open-circuit conditions; symbols represent the measured data and solid lines correspond to CNLS data fit, according to the best equivalent circuit fit shown as an inset of Figure 3.4A for the Si/SiO_2/electrolyte interface.

In addition, Figures 3.5 and 3.6 show superimposed impedance data in the form of Bode frequency and phase angle plots respectively for bare and monolayer derivatized Si electrodes. At the higher frequency region, the solution resistance dominates the impedance and thus the Bode magnitude data exhibits a slope of zero while the phase angle is near to 0°. In the intermediate frequency region for monolayer derivatized Si electrodes, the capacitance of monolayers provide a significant impedance, and log /Z/ increases linearly with decreasing log frequency (with a slope of -1) (Figure 3.5), while the phase angle is approximately 90° (Figure 3.6). As the chain length decreases from C_{18} to $C_{8,}$ a slight variation in the phase angle is observed. The slope of the Bode plot ((log /Z/ vs log frequency) for $0.1 \text{ Hz} < f < 10^4$ Hz is approximately -1 for each chain length indicating a typical capacitive behavior.

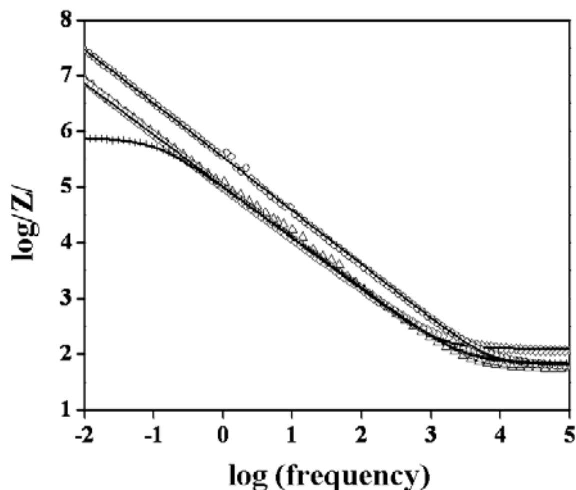

Figure 3.5: Superimposed Bode frequency plots for bare Si (+) and monolayer derivatized Si electrodes (C_{18} (o), C_{12} (□), and C_8 (∇)) in 0.1 M $LiClO_4$ in CH_3CN; the frequency range used 100 kHz to 0.01Hz with a 10 mV rms signal applied under open-circuit conditions, symbol represents the measured data, while solid lines corresponding to CNLS data fit using the equivalent circuit shown as an inset of Figure 3.4A.

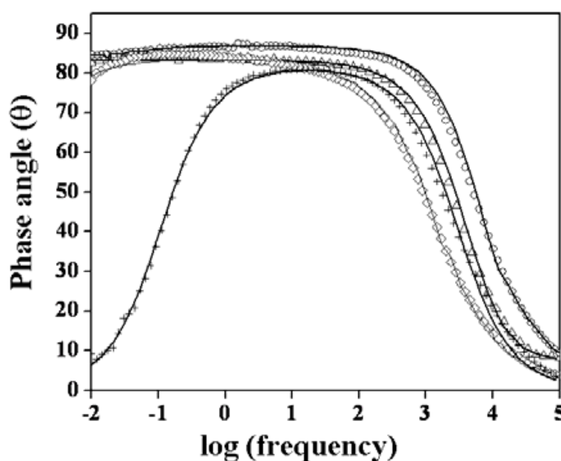

Figure 3. 6: Superimposed Bode phase angle plots for bare Si (+) and monolayer derivatized Si electrodes (C_8 (∇), C_{12} (□), and C_{18} (o)) in 0.1 M $LiClO_4$ in CH_3CN, in the frequency range is 100 kHz to 0.01Hz with a 10 mV rms signal applied under open-circuit conditions; symbol represents the measured data, while solid lines correspond to CNLS data, according to the equivalent circuit from an inset of Figure 3.4A.

Furthermore, the value of /Z/ at 10 mHz for bare Si, C_{18}, C_{12} and C_8 derivatized Si electrodes are 0.63, 6.30, 7.94, 25.1 MΩ.cm^2 respectively, revealing the insulating character of the monolayer.

3.3.5 Thickness Calculations

The impedance results are interpreted in terms of the equivalent circuit shown in the inset of Figure 3.4A involving solution resistance (R_s) in series with a constant phase

element (CPE). CPE accounts for the non-linearity and the frequency dependence of the element by expressing the electrical impedance in terms of a simple power law,

$$Z_{CPE} = Kw^{-\alpha} \quad (1)$$

For an ideal element, it is known that the frequency exponent $\alpha = 1$, $K = 1 / C$ for a capacitance and $\alpha = 0$, $K = R$ for a resistance. The deviation of the ideal behavior can be attributed to the inhomogeneties of the defects or roughness. For bare Si electrode, CPE is composed of the space charge capacitance of the semiconductor (C_{sc}) and the capacitance of the SiO_2 layer (C_{oxide}). A capacitance of 2.3 x 10^{-6} F/cm^2 has been obtained (by fitting the circuit as shown in Figure 3.4A) for Si / SiO_2/electrolyte interface under depletion conditions, which is in excellent agreement with the reported values [39].

In case of monolayer derivatized Si electrodes, the total capacitance can be determined from the series combination of the capacitances associated with the C_{sc}, C_{oxide} and C_m (monolayer capacitance) as shown in scheme 3.1. For example, a capacitance of 1.06 x 10^{-7} F / cm^2 has been obtained for the OTS-Si derivatized Si / electrolyte interface, which is approximately an order of magnitude smaller than that of bare Si electrode / electrolyte interface. The capacitance of the OTS-monolayer is 1.1 x 10^{-6} F/cm^2, which approximately yields the thickness of the monolayer of about 2.17 nm, which is in excellent agreement with the geometric length [40]. The capacitance and monolayer thickness calculated for C_{12} and C_8 monolayers are shown in Table 3.2

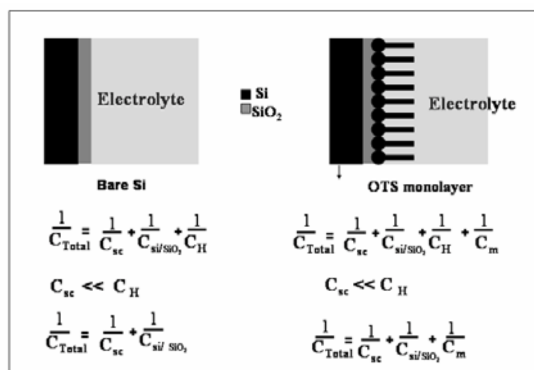

Scheme 3.1: Schematic representation of the variation in double layer capacitance at electrode/ electrolyte interfaces for bare and monolayer derivatized Si electrode.

3.3.6 Impedance Analysis in Presence of Ferrocene

A comparison of the impedance data for both the bare Si (Figure 3.7A) and monolayer derivatized Si (Figure 3.7B) electrode in presence of ferrocene is shown in

Figure 3.7. Impedance measurements were carried out after coulometry at + 0.3 V based on the voltammetric results so that a mixture of both ferrocene and ferrocenium ions were always present in the electrolyte. The response of the complex impedance plot is interpreted in terms of the equivalent circuit as shown in the inset of the Figure 3.7, where R_S indicates the solution resistance, R_1 represents monolayer resistance, CPE, the constant phase element, C_1, capacitance at semiconductor/electrolyte interface, R_{ct}, charge transfer resistance and finally Zw, the Warburg component.

For bare Si electrode, two semicircles are observed, corresponding to the space charge region and the charge transfer region respectively. While in case of the monolayer derivatized electrodes, minor deviation in the low frequency region is observed, which is attributed to the pinholes present in the monolayer, which presumably acts as a microelectrode array. Consequently, R_{ct} is expected to increase due to the inhibition of the electron transfer and from this increase the approximate monolayer coverage of the Si electrode can be calculated.

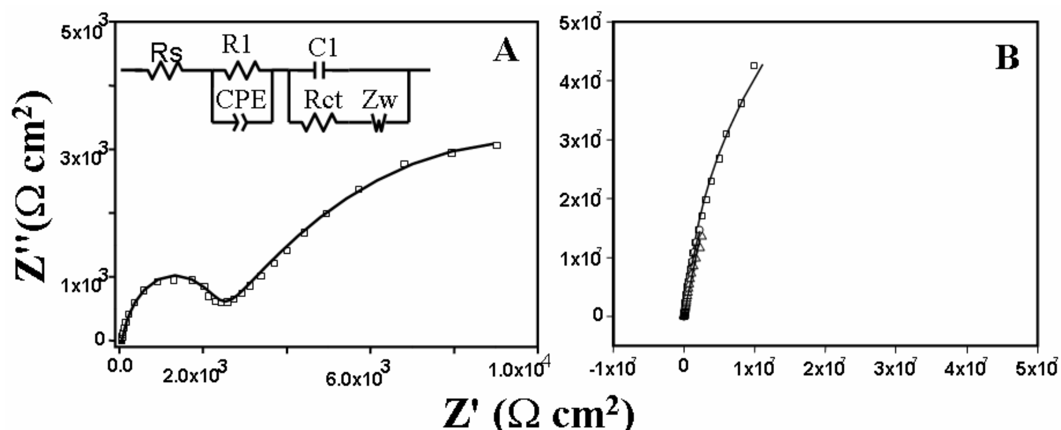

Figure 3. 7: Complex impedance plots of A) bare Si and B) monolayer derivatized Si electrode in presence of ferrocene; in the frequency range is 100 kHz to 0.01Hz with a 10 mV rms sign applied at open-circuit potential; the symbol represents the measured data, while solid lines corresponds to CNLS data fit, according to equivalent circuit shown as an inset of Figure 3.7A.

3.3.7 Coverage Calculations

For a microelectrode type of behavior, the increase in R_{ct} due to the monolayer can be related to the fraction of accessible area as

$$(1-\theta) = Rct / R'ct \qquad (2)$$

where, Rct is the charge transfer resistance at the bare Si electrode and R'ct is the charge transfer resistance of the monolayer derivatized Si electrode under the same experimental

conditions. However, this equation assumes that the electron transfer occurs only at the pinholes present in the monolayer. From the measured values of R_{ct} and R'_{ct} as 15.24 kΩ-cm^2 and 7.62 MΩ-cm^2 respectively, the corresponding monolayer coverage for C_{18} is found to be 99.8 % (as calculated from equation (2)), while for C_{12} and C_8 monolayers, it amounts to 99.4 and 98.8 respectively. Thus, the monolayer coverage increases with the chain length of the monolayer. These results are in broad agreement with the studies of Porter et. al, where the packing density of an alkanethiol monolayer on gold was found to increase according to the alkyl chain length [19].

Despite these high coverages as estimated above, there would always be possibility to develop some 'pinhole' type defects on the surface which could cause direct contact of redox active molecules with the electrode surface, as evidence by the faradaic current. Consequently, these values of the R_{ct} can also be used to estimate the rate constant of ferrocene at the monolayer–derivatized Si electrode as the monolayer provides a barrier for electron transfer leading to an expected decrease in the rate constant assuming negligible ohmic drop. Since impedance can give considerable separation in frequencies between the kinetically controlled region and the diffusion-limited low frequency region, this enables a convenient evaluation of the kinetic parameters with possible interference from the mass transport. Under these conditions, R_{ct} from the diameter of the semicircle at higher frequencies, assuming, $C_{ox} = C_{red} = C$ and a single electron first order reaction for unit geometric area, is given by,

$$R_{ct} = RT / (F^2 (1-\theta) k_0 C A)$$
$$= RT / (F^2 k_{app} C A) \qquad (3)$$

where, θ is the surface coverage of the monolayer (1- θ) corresponds to the total fraction of pinholes k_0 and k_{app} are the real and 'apparent' standard heterogeneous rate constants respectively.

The rate constant calculated for monolayer derivatized Si electrodes thus is found to be decreases with increasing chain length. For example, for bare Si and OTS – monolayer derivatized Si, rate constant for ferrocene are 4.4 x 10^{-8} cm s^{-1} and 4.85 x 10^{-12} cm s^{-1} respectively. These values are in good agreement with available reports for such charge- transfer processes as listed in Table 3.2 The thickness of monolayer is calculated

from this data and these values are compared with that of calculated from theoretical equations [41].

Table 3.2: Surface and structural characterization of alkylsilane monolayers on Si substrate as a function of chain length.

	Thickness (A^0)		Coverage (%)		C ($\mu F/cm^2$)	R_{ct} ($M\Omega$)	Rate constant 10^{-8} * (cm/s)
	Experimental Impedance	calculated [a]	Impedance	Contact angle [b]			
n-type Si(100)						0.02	4.4
C8-Si	11 ± 1	12.1	98.8	95	2.17	1.09	3.4×10^{-3}
C12 Si	17 ± 1	17	99.4	97.5	1.41	1.91	1.9×10^{-3}
C18 Si	21.7 ± 1	24.2	99.8	98.8	1.1	7.62	4.9×10^{-4}

[a] d = 1.26 x (n-1) x cos θ + (Si-O + Si-C + terminal CH_3), where, d is the thickness of the monolayer, n is the no. of carbon atoms in the alkyl chain, (the angle between the molecule axis and the surface normal. A tilt angle (~15) was used to calculate the thickness of the monolayer. IR studies suggest a much smaller angle (~20°) and an average tilt of ~ 15° for the chains [16].

[b] The surface coverage can be determined from the contact angle using Cassie equation: $\cos\theta = f_1 \cos\theta_1 + f_2 \cos\theta_2$, where, f_1 and f_2 are the fractional coverages of the first and second constituents of the surface and θ_1 and θ_2 are the angles of the pure constituents. Taking θ_1 and θ_2 114° and 15° respectively

3.3.8 Analysis of Surface states

Surface state distribution of monolayer modified Si electrodes is investigated by monitoring the variation of capacitance with dc bias potential is indicated in Figure 3.8, using a superimposed plot of C-V curves for both bare and monolayer derivatived Si electrode, in the potential range -0.8 to 0.7 V. A pronounced peak/maximum observed for bare Si, is interestingly found to decrease for monolayer derivatived Si electrodes, which is attributed to the existence of the surface states [42]. The formation of surface states at single crystalline semiconductor electrode/electrolyte interfaces is a well-known phenomenon, which could be either due to the adsorption of charged species on the surface or the abrupt ending of the periodicity of the crystalline lattice at the surface.

However in both the cases, the driving force for the formation of surface states is the presence of unsatisfied valencies of the surface atoms. On this basis, the effect of surface states is expected to vanish if the unsaturation in the surface charge is quenched by the formation of covalent bonds on the surface, like monolayer formation.

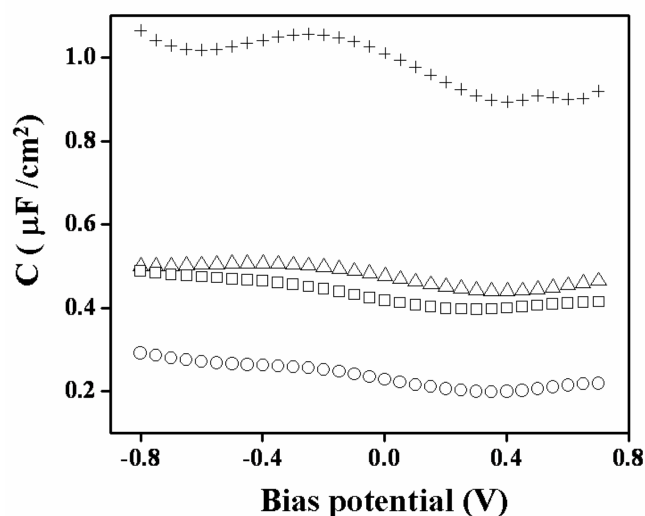

Figure 3. 8: Superimposed plot of differential capacitance as a function of bias potential for bare Si (+) and monolayer derivatized Si electrode (C_8 (∇), C_{12} (□), and C_{18}(o)) in 0.1 M $LiClO_4$ in CH_3CN.

Interestingly, in accordance with this expectation, a suppression of surface states on the Si surface by monolayer formation is noticed from the capacitance potential curves as shown in Figure 3.8. In addition, the maximum in the capacitance-potential curves decrease with increasing chain length of the monolayer, indicating an increase in passivation of the Si substrate due to Si-O-Si linkages formed by the monolayers. Thus monolayer termination provides a straightforward explanation of the low density of surface states, since all the dangling bonds at the silicon surface states are saturated with the Si-O-Si bonding, leading to electronic states far into the bands eliminating the dangling bond states from the band gap [42].

3.3.9 Mott-Schottky Analysis

The change in flat-band potentials of monolayer modified Si electrode has been studied using Mott–Schottky relation,

$$1/Csc^2 = 2\ (E-E_{fb})\ /\ q\varepsilon\varepsilon_0\ N_d\ A^2$$

where, Csc is the space charge capacitance, E represents the applied potential, E_{fb} is the flat-band potential and N_d the donor density. Thus valuable information could be obtained from the slope and intercept of the experimental 1/ Csc^2 versus E plots.

This equation is based on the assumption that the capacitance of the space charge layer is much less than that of the Helmholtz layer and at high frequency (1 kHz), the contribution of Helmholtz capacitance to the measured electrode capacitance is negligible

[43]. Thus the capacitance of the semiconductor / electrolyte interface mainly expresses the capacitance of the space charge layer of the semiconductor [44]. Based on the impedance data from Figure 3.8 separate dc bias experiments (in steps of 100 mV from -0.5 to 0.5 V) in the limited frequency region from 10 kHz–10 mHz in which the phase angle of the complex impedance is greater than 80°.

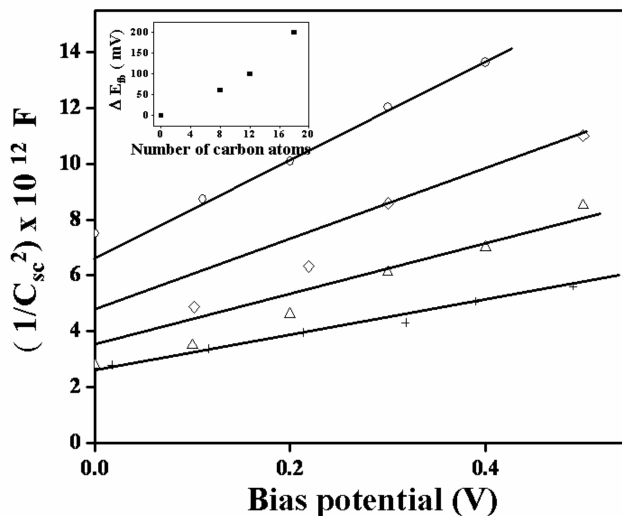

Figure 3.9: Mott-Schottky plot for bare Si (+) and monolayer derivatized (C_8 (∇), C_{12} (□), and C_{18} (o)) Si electrodes; where E_{fb} is the intercept of the extrapolated linear part of the slope with the x-axis ($1/Csc^2 = 0$); inset shows the variation in the E_{fb} vs number of carbon atoms in monolayer; ΔE_{fb} is calculated with respect to the flat band potential of bare Si.

The system behaves primarily as a capacitive circuit element provides an effective means for estimating the space charge capacitance after applying the equivalent circuits (I) for the electrode before and after the monolayer formation. Accordingly, Figure 3.9 shows the superimposed Mott-Schottky plot, suggesting the variation in E_{fb} for corresponding alkyl chains while the inset of Figure 3.9 exhibits a clear variation in the E_{fb} with respect to chain length of the monolayer. The E_{fb} potential obtained for the bare Si electrode is –460 mV, while it shows the positive shift after the monolayer formation. This positive shift in E_{fb} after the monolayer formation suggests that the surface states distribution is perhaps, altered by the covalent coupling of the silane monolayers [41]. The observed increase of slope after monolayer formation could be explained possibly due to a combination of lower charge carrier concentration (as the slope of Mott–Schottky plot is inversely proportional to N_d) and a larger space charge layer width. Since the flat-band potential of a semiconductor electrode in contact with electrolytes can be

influenced by several parameters including formation of oxide layers, pinning of the fermi level, the pH of electrolyte, and the existence of surface states, therefore it is difficulty to pin point the exact reason. However, a covalent coupling of the monolayer can significantly alter the distribution of surface states at the Si electrode [41].

3.3. 10 Effect of dc bias potential

The ionic permeability of alkyltrichlorosilane self-assembled monolayers (SAMs) on Si substrate is studied using impedance methods in the absence of redox active species. Accordingly, Figure 3.10 shows the impedance plot of the alkyltrichlorosilane monolayers at different bias potential ranging from -0.5 V to 0.5 V. At the 0 V bias potential, the phase angle is greater than 88°, revealing the capacitive behavior of the SAM. However, as the applied potential is varied from the 0 to -0.5 V, the deviation in the phase angle is prominent at lower frequency region.

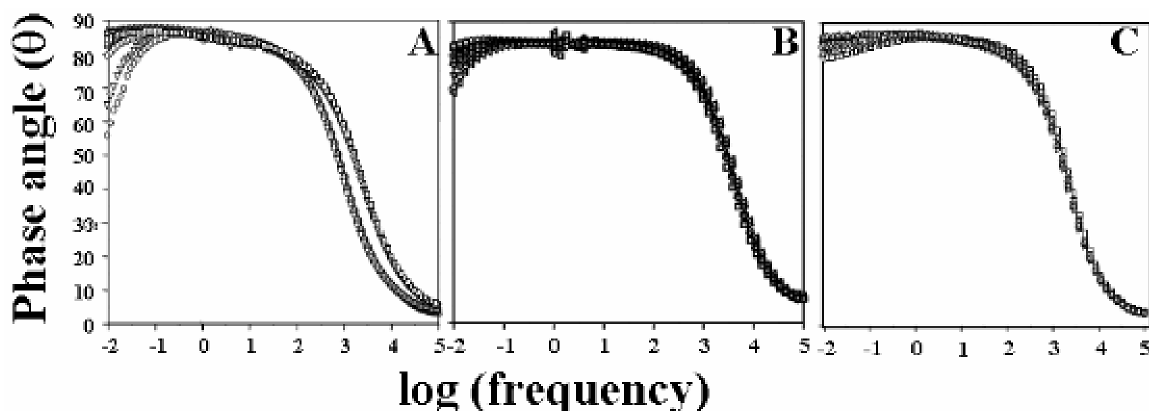

Figure 3. 10: The Bode phase angle plot at different bias potential for A) C_8 , B) C_{12} and C) C_{18} monolayer at different potential (0.5 V to -0.5 V) in the frequency range 0.1 MHz to 0.01 Hz.

A more pronounced deviation in the phase angle is observed in the case of C_8 monolayer at -0.2 V bias potential, while for C_{12} and C_{18}, it observed at -0.3 V and -0.45 V respectively. These results demonstrate that for each chain length *n*, the SAM no longer behaves as a capacitor, once a particular potential is exceeded. This experimental potential is refereed as the critical potential (*V*c) [45]. Thus confirming that SAMs do behave as ionic insulators until a critical potential, *V*c, is reached or exceeded. However, at potentials more cathodic than *V*c, SAMs are no longer behave as an ionic insulators as a significant change in the phase angle is associated with ion penetration in the low-frequency region, since *V*c is dependent on the chain length of the monolayer. It has been

reported that the changes in the electrochemical responses at Vappl ≤ *V*c are associated with molecular changes within the SAM at the SAM/electrolyte interface, or perhaps both. The range of potentials in which SAMs undergo change depends on the SAM chain length, and consequently *V*c corresponds to the onset of film perturbation [46].

3.4 Conclusions

A combined analysis of the results of contact angle measurements, FTIR spectroscopy, electrochemical impedance and cyclic voltammetry gives clear evidence for a close-packed and compact monolayer on Si substrate. The double layer capacitance decreases systematically with the chain length of the monolayers, which indirectly suggests that the change is inversely proportional to the thickness of the monolayer film. A comparison of the electrochemical properties of the SAM-derivatized Si electrodes with those of a bare Si electrode using impedance analysis shows that the apparent rate constant of ferrocene has been decreased from 4.4×10^{-8} cm s^{-1} to 4.85×10^{-12} cm s^{-1} (in case of C_{18}) due to the barrier property provided by the monolayer. Further, a positive shift of 200 mV in flat band potential suggests subtle variation in the surface state distribution due to the covalent coupling of the silane monolayers, along with plausible changes in the charge carrier concentration and larger space charge layer width. In terms of the good insulating properties of the monolayers over the entire frequency range the system somewhat resembles with that of alkanethiol monolayers on metal electrodes. These results are believed to be useful for various potential applications including the reduction/elimination of stiction in micro-electromechanical systems, contact printing in materials microfabrication, inhibition of corrosion and oxidation, and finally in the control of wetting, lubrication and protein adsorption.

3.5 References

[1] (a) A. Ulman, *An introduction to ultra thin organic films from Langmuir-Blodgett to Self-assembly, Academic Press, Lon*don **1991**.

[2] A. Ulman*, Chem. Rev.* **1996,** 96, 1533.

[3] (a) R. Maboudian, *Mater.Res.Soc.Bull.* **1998**, 23, 47-51 and references therein. (b) G. J. Kulth, M. M. Sung, R. Maboudian, *Langmuir* **1997**, 17, 3775. (c) M. M. Sung, G. J. Kulth, O. W.Yauw, R.Maboudian, *Langmuir* **1997**, 13, 6164.

[4] J.Sagiv, *J. Am. Chem. Soc.* **1980**, 102, 92.

[5] T. Vossmeyer, S. Jia, E. Delonno, M. Diehl, R. Kim, X. Peng, A. P.G. Alivisatos, R. Heath, *J. Appl. Phys.* **1998**, 84, 3664.

[6] J. Liu, M. J. Casavant, M. Cox, D. A. Walters, P. Boul, W. Lu, A.J. Rimberg, K.A. Smith, D.T. Colbert, R.E. Smalley, *Chem. Phys. Lett.* **1999**, 303, 125.

[7] I. Rubinstein, S. Steinberg, Y.Tor, A. Shanzer, J. Sagiv, *Nature* **1988,** 332, 426.

[8] C. S. Dulecy, J. H. Georger Jr, V Krauthamer, D. A Stenger, T. L. Fare, J. M. Calvert, *Science* **1991**, 252, 551.

[9] R. Maoz, J. Sagiv, *J. Colloid Interface Sci.* **1984**, 100, 465.

[10] C. R. Kessel, S.Granick, *Langmuir* **1991**, 7, 532.

[11] M. J. Wirth, H. O. Fatunmbi, *Anal. Chem.* **1993**, 65, 822.

[12] T. K. Kwei, *J. Polym. Sci., Part A* **1965**, A3, 3229.

[13] U. Srinivasan, M. R. Houston, R. T. Howe, R. J. Maboudian, *J. of Microelectromech. Syst.* **1998**, 2, 252.

[14] Y. Xia, M. Mrksich, E. Kim, G. M. Whitesides, *J. Am. Chem. Soc.* **1995**, 117, 9576.

[15] (a) S. R. Wasserman, G. M. Whitesides, I. M. Tidswell, B.M. Ocko, P.S. Pershan, J. D. Axe, *J. Am. Chem. Soc.* **1989**, 111, 5852. (b) A G. Richter, C .J. Durbin, P. Yu, Dutta, *Langmuir* **1998**,14 5980. (c) A. G. Richter, C. J. Yu, A Dutta, J. Kmetko, P. Dutta, *Phys. Rev. E.* **2000**, 61, 607.

[16] N. Tillman, A. Ulman, J. S. Schildkraut, T. L. Penner, *J. Am. Chem. Soc.* **1988**, 110, 6136.

[17] D. K. Schwartz, S. Steinberg, J. Isarelachvili, J. A. N. Zasadzinski, *Phy. Rev.*

Lett. **1992,** 69, 3354.

[18] N. Rozlosnik, M. C. Gerstemberg, N. B. Larsen, *Langmuir* **2003**, 19, 1182.

[19] M. D. Porter, T.B. Bright, D.L. Allara, C.E.D. Chidesy, *J. Am. Chem. Soc*. **1987**, 109, 3559.

[20] H. O. Finklea, D. A. Sinder, J. Fedyk, E. Sabatini, Y. Gaini, I. Rubinstein *Langmuir* **1993**, 9, 36606.

[21] C. Amatore, M. J. Saveant, D. Tessier, *J. Electroanal. Chem.* **1983**, 147, 39.

[22] E. Sabatini, I. Rubinstein, R. Maoz, J. Sagiv, *J. Electroanal. Chem*. **1987**, 219, 365.

[23] K. Bandyopadhyay, G. S. Shekhavat, R. P. Gupta, K. Vijayamohanan *J. Electroanal. Chem*. **1998**, 447, 11.

[24] O. Cailapakul, R. M. Crooks, *Langmuir* **1995**, 11, 1329.

[25] J. Cheng, D. V. Robinson, R. L. Cicero, T. Eberspacher, C. J. Barrelet, C. E. D. Chidsey, *J. Phy. Chem. B* **2001**, 105, 10900.

[26] J. Zhao, K Uosaki, *J. Phys. Chem. B* **2004**, 108, 17129 and references therein.

[27] (a) A. Bansal , N. S. Lewis, *J. Phys. Chem. B.* **1998**, 102, 1067. (b) M. R. Linford, C. E. D. Chidsey, *J. Am. Chem. Soc*. **1997**, 119, 10563.

[28] C. Gurtner, A. W. Wun, M. J. Sailor, *Angew. Chem. Int. Ed. Engl.* **1999**, 38, 1966.

[29] H.-Z. Yu, S. Morin, D. M. Danial, Wayner, A. Philippe, Catherin Henry de Villeneuve *J. Phy. Chem. B.* **2000**, 104, 11157.

[30] C. J. Barrelet, D. B. Robinson, J. Cheng, T. P. Hunt, C. F. Quate, C.E.D. Chidsey, *Langmuir* **2001**, 17, 3460.

[31] (a) M.R. Linford, P. Fenter, P. M. Eisenberger, *J. Am. Chem. Soc.* **1995**, 117, 3145. (b) A. Bansal, X. L. Li, I. Lauermann, N. S. Lewis, S. I. Yi, W. H. Weinberg, *J. Am. Chem. Soc.* **1996**, 118, 7225.

[32] S. A. Kulkarni, B. A. Kakade, I. S. Mulla, K. Vijayamohanan, *J. of Colloid and Interface Science* **2006,** 59, 3890.

[33] (a) Y. Selzer, A. Salomon, D. Cahen, *J. Am. Chem. Soc.* **2002**, 124, 2886. (b) D. J. Wold, C. D. Frisbie, *J. Am. Chem. Soc*. **2001**, 123, 5549.

[34] J. M. Beebe, V. B. Engelkes, L. L. Miller, C. D. Frisbie, *J. Am. Chem. Soc*.

2002, 124, 11268.

[35] X. D. Cui, A. Primak, X. Zarate, J. Tomfohr, O. F. Sankey, A. L. Moore, T. A. Moore, D. Gust, G. Harris, S. M. Lindsay, *Science* **2001**, 294, 571.

[36] (a) S. A. Kulkarni, S. A. Mirji, A. B Mandale, R. P. Gupta, K. Vijayamohanan, *Materials Letters* **2005**, 59, 3890. b) S. A. Kulkarni, S. A. Mirji, A. B. Mandale, K.Vijayamohanan, *Thin Solid Films* **2006**, 496, 420.

[37] (a) T. Vallant, J. Kattner, H. Brunner, U. Mayer, H. Hoffmann, *Langmuir* **1999**, 15 5339 and references therein. (b) Y-W Chang, C. D. Ukiwe, Y. Kwok, *Colloidal and Sufaces A: Physicochem. Eng. Aspects* **2005**, 260, 255. c) M. Cai, M. Ho, E. Pemberton, *Langmuir* **2000,** 16, 3446.

[38] (a) H. M. Schessler, D. S. Karpovich, G. J. Blanchard, *J. Am. Chem. Soc.* **1996**, 1189, 645. (b) S. R. Wasserman, Yu – Tai. Tao, G. M. Whitesides, *Langmuir* **1989**, 5, 1074. (c) B. Brzoska, N. Shahidazadeh, F. Rondelez, *Nature* **1992**, 360, 719.

[39] Y. Wang, M. Lieberman, *Langmuir* **2003**, 19,1159.

[40] (a) H. O. Finklea, D. D. Hanshew, *J. Am. Chem. Soc.* **1992**, 114, 3173. b) S. Sachs, S. P. Dudek, R. P. Hsung, L. R. Sita, J. F. Smalley, M. D. Newton, S. W. Feldberg, C. E. D. Chidesy, *J. Am. Chem. Soc.* **1997**, 119, 10563.

[41] H. Hillebrandt, M. Tanaka, *J. Phys. Chem. B* **2001**, 105, 4270.

[42] (a) H. Kobayashi, N. Takeda, H. Sugahara, H.Tsubomura, *J. Phys. Chem.* **1991**, 95, 813. (b) D. Vanmaekelbergh, *Electrochimica Acta*, **1997**, 42, 1121. (c) A. Belaı¨di, J.-N. Chazalviel, F. Ozanam, O. Gorochov, A. Chari, B. Fotouhi, M. Etman, *J. of Electroanalytical Chemistry* **1998**, 444, 55.

[43] A. J. Bard, L. R. Faulkner, *Electrochemical Methods, Fundamentals and Applications, second Ed.,* Wiley, New York, **2001**.

[44] (a) K. E. Polmykal, N. S. J. Lewis, *Phys. Chem. B* **1997**, 101, 2476. (b) A. M. Fajardo, N. S. Lewis, *Science* **1996**, 274, 968. (c) K. E. Polmykal, A. M. Fajardo, N. S. Lewis, *J. Phys. Chem. B* **1996**, 100, 3652.

[45] E. Boubour, R. Bruce Lennox, *J. Phys. Chem. B* **2000,** *104,* 9004.

[46] M. Cai, M. Ho, E. Pemberton, *Langmuir* **2000,**16, 3446.

CHAPTER 4

Thermal Stability of Self-Assembled Octadecyltrichlorosilane Monolayer on both Planar and Curved Silica Surfaces

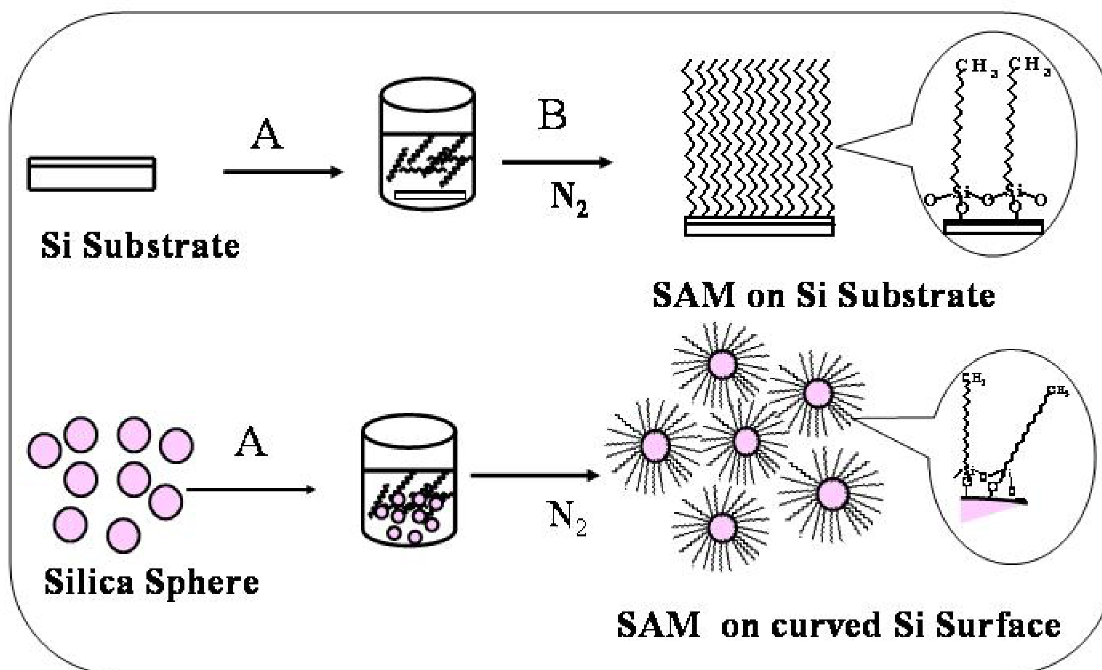

This chapter compares the (OTS) monolayer formation both on n-type Si substrate (planar surface) and silica sphere (curved surface), using various surface sensitive spectroscopic techniques. Interestingly, a relative enhancement in thermal stability is observed in case of OTS-SAM on the curved surface although the orientation of molecules is similar on both the surfaces. The implications of these are discussed using results from thermogravimetric analysis, temperature dependent IR measurements and contact angle data in terms of the importance of SAMs for MEMS and micro fluidic applications

A part of the work reported in this chapter has been published in '*Thin Solid Films*, **2006,** 496, 420.

4.1 Introduction

Self–assembled monolayers (SAMs) have attracted a great deal of attention in recent years due to their interesting properties as candidates for isolating interfaces and improving interfacial adhesion in newly evolving integrated circuit architectures, an interest arising because of its crucial importance in nanotechnology [1-4]. For example, SAMs of alkyltrichlorosilane on Si/SiO_2 interface have been extensively studied due to their fundamental importance in surface modification and also for their diverse potential applications, as emerging flexible memory storage modules, nano electromechanical devices, interconnects in molecular electronics, [5-6] interfacial adhesive promoters and molecular lubricants [7-8]. The close packing of the molecules with a saturated methylene chain via coordinated interchain van der Waals interactions is expected to create a vacuum-like potential barrier at the interface that inhibits phenomena such as ionization and diffusion, making them extremely useful for applications in a variety of fields like microelectronics and microfluidics. In addition, the low sticking property of SAMs onto themselves is conducive for forming conformal layers whose thickness is essentially the length of the comprising molecules facilitating a remarkable control by manipulating the chemistry of the terminal functional group. As a result, many structure function correlation studies have been reported so far using various characterization techniques [1-8].

Alkyl trichloro or trimethoxy silane SAMs are particularly useful for micro-electromechanical systems (MEMS) to tackle the well-known 'stiction' problem, since their mere presence provides a suitable low energy coating [9-12]. For example, the formation of close packed, covalently bounded monolayer with tunable chain length and hydrophobic terminal group on silicon oxide surface would eliminate the '*release*' stiction and reduce the '*in-use*' stiction. However, during the fabrication of MEMS, a small variation in the processing temperature may cause degradation of monolayer because most of MEMS packaging processes contains steps at elevated temperatures [13]. Therefore, the assessment and understanding of the growth and thermal stability of these monolayers is an important prerequisite for their proper utilization with respect to both microfabrication and device performance. More significantly, for these types of applications, the onset of performance degradation can be unpredictable and hence it is

important to monitor the thermal behavior, as some of the organic films can be quite unstable at these operational temperatures. For example, Yeh et.al., have reported permanent structural changes of octadecyltrichlorosilane (OTS) monolayers in air above 120 ^{o}C although this stability is extended up to 330 ^{o}C in nitrogen atmosphere depending on the heating rate and thermal history [9,14]. Similarly, Kluth et. al., have recently reported the stability of hydrocarbon chains up to 475 ^{o}C in vacuum, whereas the perfluorodecytrichlorosilane film is stable only up to 400 ^{o}C and 500 ^{o}C in air and nitrogen respectively [9]. All these studies however are for 2D SAMs on planar surfaces and it is important to compare the behavior of SAMs of same molecule on both planar and curved surfaces in order to understand the effect of curvature on thermal stability. These results are believed to be useful for selecting suitable monolayers for MEMS application. Finally OTS-SAM on silica surfaces has also attracted much attention because of their similarity to biological membranes for potential applications in BioMEMS due to its ability to control friction and wear resistance of surfaces [6-8].

In the previous chapter, we have discussed the chain length dependent electrochemical behavior and thermal stability of the alkyltrichlorosilane monolayers on the Si/SiO_2 interface (planar). In comparison, this chapter describes relative improvement in the thermal stability of OTS monolayer on curved surfaces i.e., on spherical silica surfaces in order to highlight the role of curvature on packing and stability. We demonstrate the superior thermal stability of OTS monolayer on curved silica surface by using a variety of techniques like temperature dependent Fourier transform infrared (FTIR) spectroscopy, X-ray photoelectron spectroscopy (XPS), Scanning electron microscopy (SEM), Thermogravimetric analysis (TG) and Contact angle (CA) measurements.

4. 2 Experimental Aspects

4. 2.1 Materials

n-Octadecyltrichlorosilane (OTS) (95%) and tetraethyl orthosilcate (TEOS) were obtained from Aldrich, while toluene (99.5 %), ethanol (99.5 %) and ammonia were purchased from Qualigens. Commercially available n-type, one-side polished, silicon wafers of (100) orientation with 0.001-0.007 Ω-cm resistivity were used as substrates.

These silicon wafers (1x1 cm^2) were rinsed with deionized water (18 MΩ cm), sonicated in ethanol and dried under a flow of nitrogen. These wafers were cleaned as the procedure described in the chapter 2 (section 2.2.1) soaked in 1:10 deionized HF: H_2O solution for 30 s to remove the native SiO_2 layer and treated with *piranha* (7:3 H_2SO_4: H_2O_2) solution for 30 min at 80 ^oC to grow a fresh oxide layer. Subsequently, wafers were rinsed with deionized water, dried in a stream of nitrogen and used for further experiments. Silica spheres were prepared by using the well-known Stober's method as reported elsewhere [15]. In brief, 1.3 ml TEOS was added into the 5 ml ethanol and stirred for 10 min. To this solution, 3 ml ammonia in 22.7 ml of ethanol was added drop-by-drop and stirring was continued for 2 h to get silica nanoparticles. These silica particles were washed several times and redispersed in ethanol after drying and further refluxed for 2 h to get monodispersed particles.

4. 2. 2 Silanization

4.2.2.1 SAM formation on n-type Si substrate

Freshly cleaned Si wafers were immersed in 1 mM OTS solution for 10 min. Subsequently, they were removed, rinsed several times with toluene, dried under nitrogen atmosphere and were used for further characterization [16].

4.2.2.2 SAM formation on Silica Particles

Prior to functionalisation, the silica particles were dried for 10 h at 150 ^oC under nitrogen atmosphere and were used immediately. In a typical synthesis procedure, 10 mg silica particles (400-500 nm) were dispersed in adequate amount of dry toluene with intermediate stirring for 1 h. To the above mixture 10 ml, 1 mM OTS solution was added drop wise, and the mixture was refluxed for 24 h under nitrogen atmosphere in order to ensure a complete monolayer formation of OTS on silica (scheme 4.1). This solution was then allowed to stand for few hours, filtered and washed several times with toluene and ethanol in order to remove unreacted OTS. This (OTS-silica) was subsequently dried in a vacuum oven at 70-80 ^oC for 4 h and used for further characterization.

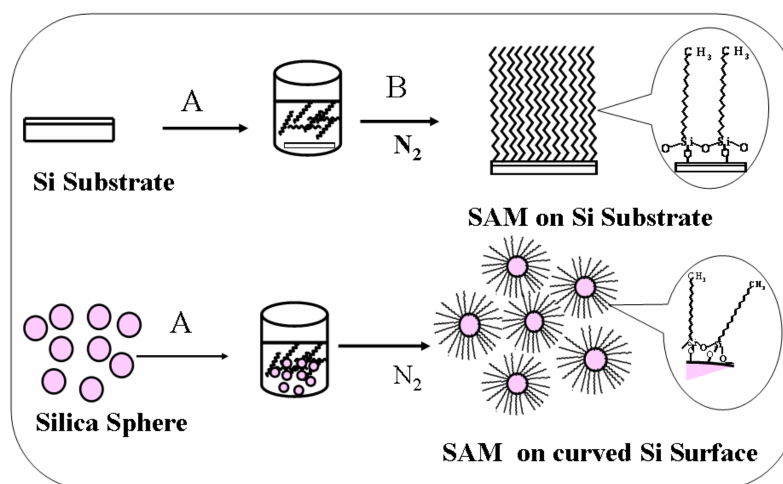

Scheme 4.1: A schematic representation of the process involved in OTS-SAM formation on Si substrate and on silica particles, A) bare Si substrate is dipped in OTS (mM) in toluene solution, while silica particles refluxed in OTS (mM) in toluene for 24 hrs under N_2 atmosphere, B) structure of OTS molecule on Si substrate and silica particles.

4. 2. 3 Characterization

Scanning electron microscopy (SEM) was carried out on a Leico stereoscan model 440 instruments equipped with Phoenix energy dispersive analysis of X-ray (EDX) attachment. The contact angle (CA) on Si (100) substrate was measured using a water sessile drop on RAME-HERT NRL–model CA goniometer and also on GBX-'Digidrop' CA meter. FTIR spectra of the OTS monolayer on Si substrate as well as on SiO_2 particles were recorded using a Perkin Elmer 1615 spectrometer in a diffuse reflectance mode (DRIFT), OTS-silica sample was made in the form of pellet after mixing with spectroscopic grade KBr. The OTS monolayer on Si substrate was characterized by grazing angle FTIR spectroscopy after recording the background spectra at a resolution of 4 cm^{-1} over 256 scans at room temperature using bare Si wafers. Thermogravimetric analysis (TGA) was carried out on a Seiko thermal analyzer model No: TCA/DIA–32. Thermal stability of OTS monolayer on Si substrate was studied by water sessile drop CA measurements after annealing the Si substrate in air for 5 minutes at different temperatures and subsequently cooling to room temperature. XPS measurements were carried out using a VG scientific ESCA-3 MK II spectrometer operated at a pressure below 1.33 x 10^{-7} Pa (electron take off angle 60°, and overall resolution ~ 1 eV) using Mg-Kα source (hν= 1253.6 eV). Alignment of the binding energy was carried out using the C 1s binding energy of 285 eV as a reference to compensate for surface-charging effects and the X-ray flux (power 70 W) was kept deliberately low in order to

reduce the beam induced damage. The core spectra were background corrected using the Shirley algorithm. The deconvolution of overlapping peaks in the final, high resolution spectra was accomplished using standard curve–fitting algorithms assuming the shape of all peaks to be Gaussian

4. 3 Results and Discussion

4.3.1 FTIR Spectroscopy

In order to understand the nature of functional groups on silica after surface modification, superimposed FTIR-DRIFT spectra of silica and OTS-silica are shown in Figure 4.1A. For simplicity, a spectrum is divided into two regions; in the low frequency region (700-1400 cm^{-1}), the fundamental Si-O bands are invariant with surface modification, while in the high frequency region (2800-4000 cm^{-1}) certain distinct changes could be seen [17]. Nevertheless, both samples show bands at 803, 1030 and 1220 cm^{-1} which could be attributed to fundamental Si-O vibrations [18-19]. The band at 980 cm^{-1} is related to the stretching modes of isolated silanols and is visible only in case of bare silica, which interestingly disappears after the thermal treatment at 300 ^{o}C. Further, the absence of this band in OTS-silica sample indirectly suggests OTS bonding on the silica surface. In case of SiO_2, bands at 1672, 1872, 1987 and 3342 cm^{-1} could be due to physically/ chemically adsorbed water [17-19]. However, these bands do disappear after thermal treatment at 700-800 ^{o}C, although these bands are absent in the case of OTS-silica, perhaps due to the hydrophobic nature of the surface. New bands at 1623, 2850 and 2917 cm^{-1} due to C-H stretching vibrational modes of $–CH_2$ in OTS strongly indicate the presence of OTS monolayer on silica surface [20-22].

Figure 4.1B shows superimposed FTIR spectra of OTS-SAMs on planar and curved surfaces respectively in the frequency range of 2800-3000 cm^{-1}. The methylene peaks (for sample 1) due to C-H symmetric and antisymmetric stretching at 2850 and 2919 cm^{-1} respectively indicate common features during the formation of OTS monolayer on both surfaces. For example, the presence of asymmetric C-H stretching mode due to terminal CH_3 at 2958 cm^{-1} is a clear sign of densely assembled monolayer [1-2]. A comparison of this spectrum with that of long chain alkane hydrocarbon clearly suggests the presence of ordered and close packed molecular assembly.

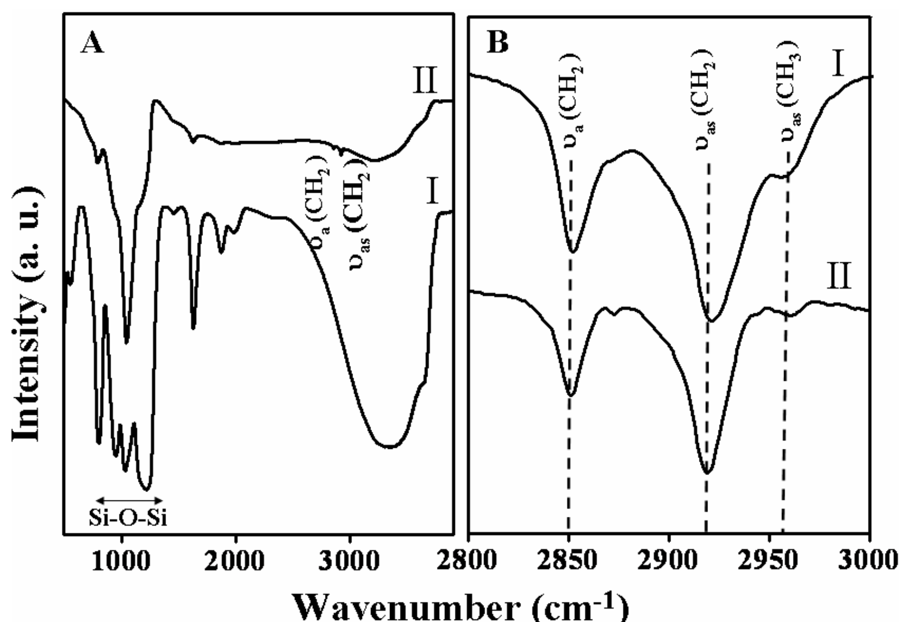

Figure 4.1: Superimposed FTIR-DRIFT spectra of A) bare (I) and OTS-silica (II) particles; B) OTS SAM on silica particles (I) and Si substrate (II) in the frequency region 2800-3000 cm^{-1} respectively.

Monolayer formation is also confirmed by the data obtained from CA measurements before and after OTS formation on Si/SiO_2 surface. For example, a clean Si surface has CA less than 15°, indicating its hydrophilic nature. In sharp contrast, CA obtained on OTS monolayer surface is 109 ± 1° (due to the hydrophobic nature of the surface) and this change in CA due to SAM formation is in good agreement with that available in the previous reports using similar molecules [23].

4.3.2 X-ray Photoelectron Spectroscopy

XPS provides useful quantitative information on the composition and chemical identity of both monolayer and the substrate. Consequently, Si 2p, C 1s and O 1s core binding energies estimated on the basis of C 1s of alkyl chains at 285 eV are summarized in Table 4.1. Accordingly, OTS-monolayer on Si substrate shows two peaks in Si 2p binding energy range, the peak at lower binding energy (i.e. 99.3 eV) corresponds to elemental Si^0 while the one at 103.4 eV corresponds to Si^{IV} in SiO_2 as well as Si^{IV} from the OTS molecule. Interestingly, the intensity ratio of Si^{IV} to Si^0 peaks increases after the monolayer formation as compared to that of bare Si substrate [24]. The increase in the peak intensity of Si^{IV} shows an additional Si^{IV} signal from the OTS molecule. In case of silica and OTS-silica samples, only the Si peak is observed at 103.4 eV that

corresponds to Si ^{IV} from SiO_2. The peak intensity of Si 2p rather increases although the position is invariant after the monolayer formation. A slight shift of 1 eV is observed for O 1s along with a decrease in peak intensity, may be due to the Si-O-Si bonding on the modified silica surface while C 1s peak at 285 eV corresponds to alkyl chain of OTS-silica. Thus XPS results confirm the structural similarity of OTS monolayer on silica with that on Si/SiO_2 interface.

Table 4.1: A comparison of binding energies of Si, C and O for OTS SAM on n-type Si substrate and on silica particles. The values given in the bracket show corresponding FWHM of fitted Gaussian peaks. The deconvolution of X-ray photoelectron spectroscopic data for SAM on overlapping peaks in the final, high resolution spectra was accomplished using standard curve–fitting algorithms, assuming the line shape of all peaks as Gaussian.

Substrates	Binding energy (eV)			
	Si 2p		C1s	O1s
	Si ^{IV}	Si ^{0}		
SiO_2 particles	103.4 (2.04)	-	285	532.8
OTS- SiO_2	103.4 (2.16)	-	285	532.8
n-type Si Substrate	103.4 (2.96)	99.3 (1.64)	285	532.8
OTS SAM on Si substrate	103.4 (1.85)	99.3 (1.38)	285	532.7

Some of the important differences between SAMs on planar and curved surfaces, like higher concentration of defects present on the curved surface, and higher radius of curvature, would naturally cause different packing density of the monolayer. For example, Murray et. al., have reported similarities and differences between thiol-SAM on planar and curved gold surfaces, and according to him latter has higher concentration of a high density of monolayer defects [25]. Despite high radius of curvature, the packing density of alkanethiolate chains bonded to the gold cluster surface has been found to be nearly twice than that found on flat Au (111) and similar reasoning is valid also for OTS SAMs. Hence the subtle effects of the SAMs on curved surfaces could be indirectly seen if we compare the morphology of silica particles prepared identically with and without OTS monolayers.

4.3.3 Scanning Electron Microscopy

Figure 4.2 demonstrates comparison of SEM images of silica and OTS-silica indicating their polydispersed nature. These silica particles (Figure 4.2A) were redispersed in ethanol and refluxed for 2 h to get monodispersed silica particles as shown in Figure 4.2 B, where they are spherical in shape with size approximately in the range 400-500 nm. Although the thickness of OTS monolayer is 2.5 nm, any distinguishable change is not observed after silanization (Figure 4.2C). The aggregation of the individual particles could be attributed to the siloxane bonds between silica particles as well as due to the polymerization of silane molecules on the silica surface [26]. However, EDX measurements show a change in the elemental composition, the ratio of Si:O being approximately 1:2 before the monolayer formation. The carbon percentage is very low (less than 3 %) although after monolayer formation, the ratio changes to 1:1.3 since carbon content increase up to 24 %. X-Ray diffraction (XRD) patterns of as prepared particles indicate their amorphous nature.

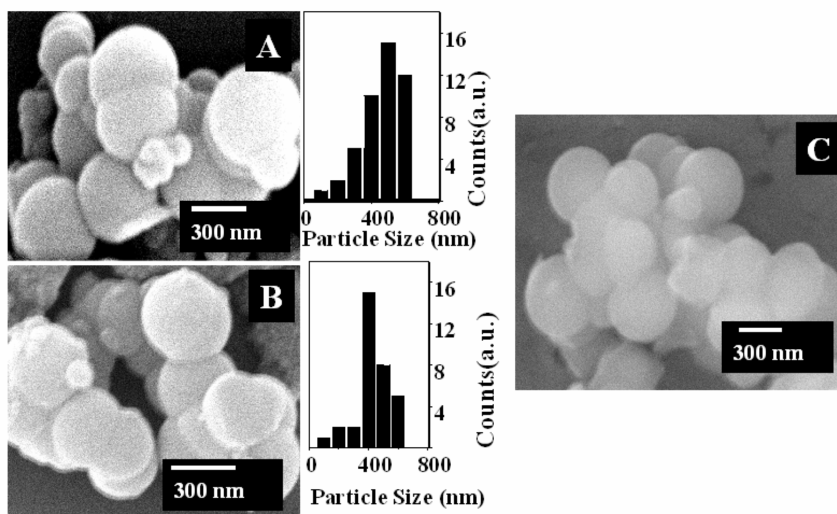

Figure 4.2: The Scanning electron microscopic images of (A) as synthesized silica particles, (B) silica particles after refluxing in ethanol for 2 h, (C) OTS-monolayer capped silica particles. Corresponding histogram showing the particle size distribution. The size distribution has been extracted from 120 particles.

4. 3. 4 Thermogravimetric Analysis

Figure 4.3 shows TG curves of both (A) silica and (B) OTS-silica samples. In case of silica, a sharp decrease in weight occurs in the temperature range 50-150 ^{o}C, which is attributed to the loss of physisorbed water. On the contrary, the TG profile of

OTS-silica shows two steps of weight loss, one below 150 °C and other in the region of 350-600 °C. The former weight loss is either due to the desorption of water or due to solvents used for monolayer formation, although the weight loss in this region is less as compared to that of silica, due to the hydrophobic nature of the monolayer. Further weight loss is attributed to the loss of OTS monolayer, which is not at a particular temperature although organic layer (OTS) decomposes slowly from the silica surface up to 873 K; after which the weight loss is similar to that of silica. TG analysis reveals pronounced weight loss for OTS-silica (1.8 %) as compared to that for pristine silica due to the decomposition of OTS monolayer [27]. TG analysis thus shows that the monolayer is stable even up to 350 °C in air. Lastly, the thermograms obtained for silica match with that of commercially available silica, as reported by many others [27].

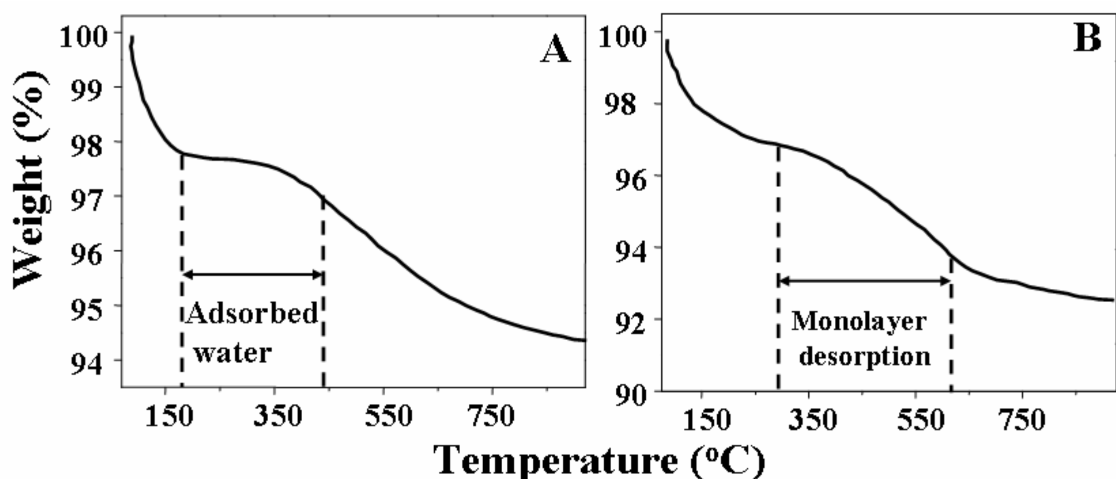

Figure 4. 3: TGA curves of A) Silica and B) OTS-Silica samples in air at a heating rate of 10 °C / min

4.3.5 Temperature Dependent Contact Angle Measurements

CA measurement is used to study the thermal stability of SAM on planar surface as a function of annealing temperature as shown in Figure 4.4. The CA of monolayer sample (at full coverage) is 109 °± 1, remaining almost constant up to the substrate annealed at temperature 150 °C, although it then starts to decline slowly from 250 °C. At an annealing temperature of 350 °C CA rapidly decreases up to 30°, which is usually reported for bare Si, indicating the complete degradation of OTS monolayer. The CA shows that the OTS monolayer degrades in air above 250 °C. This behavior is in good

agreement with previous CA measurements carried out in nitrogen atmosphere [9]. High-resolution electron loss spectroscopy results indicate that the thermal behavior of monolayers is independent of the hydrocarbon chain length and monolayers are stable in vacuum up to 475 ^{o}C [28-29]. The stability of the OTS monolayer on Si substrate is up to 250 ^{o}C in air while on silica surface it is up to 350 ^{o}C. It is well known that the 2D SAM on planar surface is more stable than that on curved surface as the curvature of surface creates more defects on SAM. The results show that the SAM is thermally more stable on silica particles, perhaps due to the particle aggregation that hinders heat-induced degradation in some SAM layers sandwiched between particles.

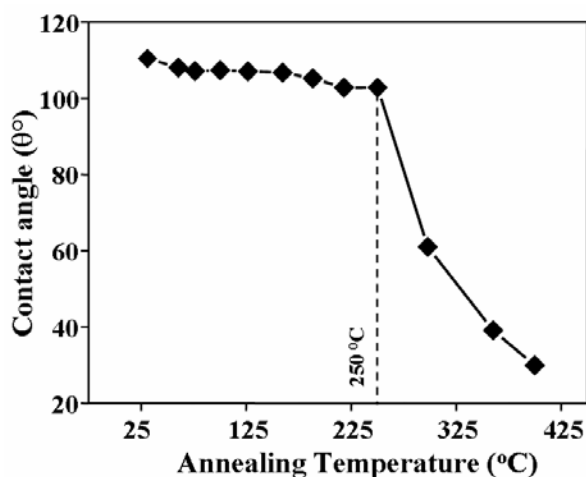

Figure 4.4: Temperature dependent water sessile drop CA measurements of OTS monolayer on n-type Si substrate. The measurements are carried out after heating the substrate at different temperature and subsequent cooling to room temperature.

4.3.6 Temperature Dependent FTIR Measurements

Further understanding of the stability difference, requires the knowledge of the nature of thermally desorbed species on the silica surface. Alkyltrichlorosilane monolayer forms through the -Cl group interaction of the silane molecule with the -OH group on the substrate, forming the Si-O-Si bond through condensation reactions between the adjacent molecules, are creating a cross-linked network at the surface [30-31]. Considering the formation mechanism, there are three possibilities in the decomposition steps including the cleavage of the Si-C, C-C and Si-O-Si bond. To understand the nature of the desorbed species, we have indeed carried out many temperature dependent IR measurements. Accordingly, Figure 4.5 shows FIIR spectra of OTS silica sample annealed at different temperatures and subsequently cooling at room temperature. The sample annealed at 150

^{o}C shows the C-H symmetric and antisymmetric stretching vibrational modes at 2850 and 2919 cm^{-1} of CH_2 respectively while small peaks at lower frequencies are assigned to C-H bending modes. The peak in the region 800-850 cm^{-1} and 1100-1200 cm^{-1} are observed due to symmetric and antisymmetric Si-O-Si stretch between the surface alkylsiloxane head group and the oxidized surface. All these observations suggest that the monolayer film is still intact. However, after heating at 350 ^{o}C, the intensity of the -C-H desorb at this temperature.

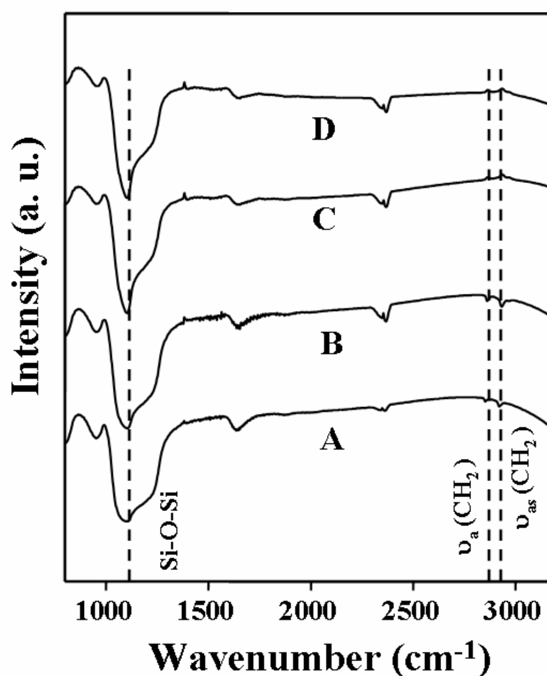

Figure 4.5: FTIR-spectra as a function of annealing temperature for OTS-silica sample at A) room temperature, B) 150 ^{o}C, C) 350 ^{0} C and D) 600° C, Spectrum was recorded after cooling the sample to room temperature.

Interestingly, annealing at 600 ^{o}C, diminishes the intensity of the C-H band, indicating the complete desorption and consequently inherent peaks at lower frequency region due to Si-O-Si bonding are observed.

All these results are in good agreements with the previously reported results of OTS-monolayer on Si surface [28]. For example, IR results show that above 600 ^{o}C bands due to C-H stretching disappear while, bands due to Si-O-Si are still intact, indicating that the monolayer decomposition takes place through the involvement of both Si-C and C-C bonds. Thermal behavior of monolayer does not depend on the Si-O–Si linkage between the adjacent chains, and hence remains intact up to 820 ^{o}C in case of OTS monolayer on silica surface.

In addition, thermal stability of OTS on silica particle has been found to decrease with decreasing particle size [32]. As the particles size decreases, surface curvature increases (disordering of the alkyl chains increases) resulting in an incomplete coverage of the alkyl chains and enhanced free volume. There is also a possibility of aggregation/agglomeration of silica particles causing a lower surface coverage.

Several effects could essentially be contributed to the enhanced stability of the alkyl silane chains (on silica particles in comparison with Si substrate) including the removal of interfacial water layers, extent of cross-linking between alkylsilane headgroups, and the formation of permanent covalent bonds between the alkylsilane hydrolyzed headgroups and surface silanols [32]. These results are believed to be useful for the applications of SAMs for lubrication and wear reduction while using MEMS devices.

4.4 Conclusions

A comparative analysis of FTIR and XPS data shows the formation of OTS monolayer on both planar as well as curved surfaces despite sharing more similarities than differences. Thermogravimetric analysis shows the stability of SAM on curved surface up to 350 ^{o}C in air although a complete decomposition of monolayer takes place around 600 ^{o}C. In comparison, 2D SAM on planar surface is found to be stable up to 225 ^{o}C despite complete decomposition around 400 ^{o}C. FTIR results show that the monolayer decomposition takes place through the involvement of both Si-C and C-C bonds. Thermal behavior of the monolayer does not depend on the Si-O–Si linkage between the adjacent chains, and is intact up to 820 ^{o}C.

4. 5 References

[1] A. Ulman, *An introduction to ultra thin organic films from Langmuir-Blodgett to Self-assembly*, Academic Press, London **1991**

[2] A. Ulman, *Chem. Rev.* **1996,** 96, 1533.

[3] R. Maboudian, *Mater. Res. Soc. Bull.* **1998,** 23, 47 and references therein.

[4] J. Sagiv, *J. Am. Chem. Soc.* **1980,** 102, 92.

[5] H.-L. Li, A.-P. Fu, D.-S. Xu, G.-L. Guo, L.-L. Gui, Y.-Q. Tang, *Langmuir* **2002,**18, 3198.

[6] W. A. Aue, C. R. Hastings, *J. Chromatogr.* **1969,** 42, 319

[7] M. J. Wirth, H. O. Fatunmbi, *Anal. Chem.* **1993,** 65, 822.

[8] T. K. Kwei, *J. Polym. Sci. Part A A3* **1965,** 3229.

[9] U. Srinivasan, M. R. Houston, R. T. Howe, R. J. Maboudian, *J. of Microelectromech. Syst.* **1998,** 2, 252.

[10] Y. Xia, M. Mrksich, E. Kim, G. M. Whitesides, *J. Am. Chem. Soc.* **1995,** 117, 9576.

[11] W. R. Ashurst, C. Carraro, R. Maboudian, W. Frey, *Sensors and Actuators A: Physical* **2003,**104, 213.

[12] P. Galambos, *Encyclopedia of materials: Science and Technolog*y **2001** 5598.

[13] R. Maboudian, R. T. Howe, *J. Vac. Sci. Technol. B* **1997,** 15, 1.

[14] M. Calistri-Yeh, E. J. Kramer, R. Sharma, W. Zhao, M. H. Rafailovich, J. Sokolov, J. D. Brock, *Langmuir*, **1996,** 12**,** 2747.

[15] W. Stober, A. Fink, E. Bohn, *J. Colloid Interface Sci.* **1968,** 26, 62.

[16] J. B. Brzoska, I. Ben Azouz, F. Rondelez, *Langmuir* **1994,** 10, 4367.

[17] A. G. S. Prado, C. Airoldi, *J. Colloid Interface Sci.* **2001,** 236, 161.

[18] N. B. Colthup, L. H. Daly, S. E. Wiberly *Introduction to Infrared and Raman Spectra, Academic Press*, **1990**.

[19] L. J. Bellamy ‘*Advances in Infrared Group Frequencies’*, Chapman and Hall, London, **1968**.

[20] K. Bierbaum, M. Grunze, A. A. Baski, L.F. Chi, W. Schrepp, H. Fuchs, *Langmuir* **1995,**11, 2143.

[21] Y. Liu, L. K. Wolf, M. C. Messmer, *Langmuir* **2001,**17, 4329.

[22] T. Vallant, J. Kattner, H. Brunner, U. Mayer, H. Hoffmann, *Langmuir* **1999,**15, 5339.

[23] N. Tillman, A. Ulman, J. S. Schildkraut, T. L. Penner, *J. Am. Chem. Soc.* **1988,** 111, 6136.

[24] Y. Wang, M. Lieberman, *Langmuir* **2003,** 19, 1159.

[25] M. J. Hostetler, J. J. Stokes, R. W. Murray, *Langmuir* **1996,**12, 3604.

[26] H.-L. Li, N. Perkas, Q.-L. Li, Y. Gofer, Y. Koltypin, A. Gedanken, *Langmuir* **2003,** 19, 10409.

[27] (a) R. Wang, G. Baran, S. L. Wunder, *Langmuir* **2000,** 16*,* 6298. (b) M. Calistri-Yeh, E. J. Kramer, R. Sharma, W. Zhao, M. H. Rafailovich, J. Sokolov, J. D. Brock, *Langmuir* **1996,** 12, 2747. (c) R. K. Ilier, 'The chemistry of silica' New York: Wiley **1979**.

[28] G. J. Kulth, M. M. Sung, R. Maboudian, *Langmuir* **1997,** 17, 3775 and references therein.

[29] M. M. Sung, G. J. Kulth, O. W. Yauw, R. Maboudian, *Langmuir* **1997,** 13, 6164.

[30] S. R. Wasserman, Y. T. Tao, G. M. Whitesides, *Langmuir* **1989,** 5, 1074.

[31] P. Silberzan, L. Leger, D. Ausserre, J. J. Benattar, *Langmuir* **1991**, 7, 1647.

[32] R. Wang, S. L. Wunder *J. Phys. Chem. B* **2001,** *105,* 173.

CHAPTER 5

Preparation of hydrophobic Silica by surface Silanization

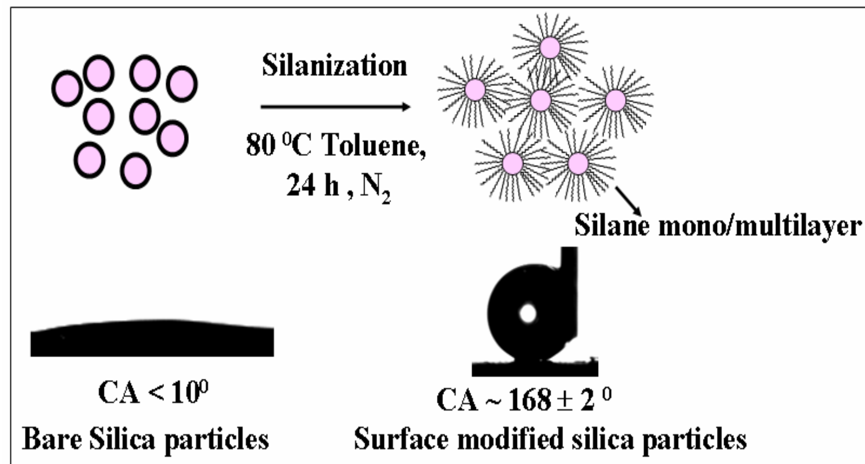

This chapter describes a novel method of preparing hydrophobic silica particles (100-150 nm) by surface functionalization using different alkyltrichlorosilanes. During their preparation interestingly, surface roughness has been engineered through silanization facilitating a change in both the surface chemical composition and the geometrical microstructure to generate hierarchical structures which gives water contact angle ranging from 60° to 168°. The enhancement in the water contact angle on 3D (curved) SAMs in comparison to that on 2D (planar) surface is discussed using the Cassie-Baxter equation. These silica particles can be utilized for many potential applications including selective adsorbents and catalysts, chromatographic supports, self cleaning coating and separators in microfluidic devices.

5.1 Introduction

In recent years, the use of self-assembled monolayers (SAMs) to impart desired function to a surface has received extensive attention due to its ease of manipulation of surface energy, and thereby also of such properties like adhesion, lubrication, corrosion and anti-stiction [1]. It is well-known that the water contact angle (CA) (θ), $\theta < 90^{o}$ and $\theta > 90^{o}$ can indicate surface 'hydrophilicity' or 'hydrophobicity' respectively and when it is above 150°, the word 'superhydrophobic' is sometimes used. Nature exhibits this phenomenon in 'lotus leaf' to harness the roll-off action for self-cleaning of leaves which has been attributed to a combined micro and nanoscale morphology of its surface [2]. More specifically, the surface of the lotus leaf is textured with micron-sized hills and valleys (bumps) that are decorated with nanometer sized particles of a hydrophobic wax like material, which prevents the penetration of the water into valleys [3-10]. As a result, water cannot wet the surface and therefore forms nearly spherical water droplets, leading to superhydrophobicity. Achieving superhydrophobicity is of great current interest in view of its diverse applications such as self-cleaning window glasses, paints, fabrics and low-friction surfaces [3, 4].

Artificial superhydrophobic surfaces have been prepared using various strategies including the generation of rough surfaces first and then modification with low surface energy molecules or roughening the surface of hydrophobic materials by creating well-ordered structures using micromachining and etching [5-10]. Using this concept, various methods have recently been proposed to create superhydrophobic surfaces, including electrochemical deposition, plasma fluorination, sol-gel, and UV irradiation etc [11-17]. It is well known that, the wetting property of a solid surface is governed by both its chemical composition and geometric microstructure [1-24]. In addition, few methods have been reported to make the superhydrophobic coating on silica particles by forming polyelectrolyte multilayer films by layer–by–layer process, or by forming the film of silica particles on substrate by Langmuir-Blodgett (LB) technique and subsequent formation of a alkylsilane SAM for fabricating hydrophobic surfaces [18-20]. However, these methods are tedious, complicated, time consuming and difficult to control accurately and hence better strategies are desired to improve stability of these superhydrophobic films.

In earlier chapters, we have demostrated the usefulness of OTS monolayers on both curved (silica particles) and planar (Si substrate) surface to tune surface properties. For example, in the second chapter OTS molecule has been found to link with the terminal methyl group causing the surface to be hydrophobic as demonstrated by a typical water contact angle of 109°. However, more studies have not been carried out there since the primary objective was to look at the kinetics. Similarly the stability of OTS molecule was addressed in the previous chapter although the results of those studies clearly indicated the potential to tune hydrophobic behavior of surfaces by tailoring the functional organosilane molecules used for SAM formation. In this chapter, accordingly, we report the enhancement in the hydrophobicity of the SAM on the curved surfaces (silica particles). Our strategy is to optimize the hydrophobicity of silica particles (~100 nm) using different organosilane molecules (as the chemical compositions determine the surface free energy) and thus have a greater influence on the wettability and then to achieve hierarchical micro-nano roughness by their coating on a smooth silica surface. The molecules employed are: octadecyltrichlorosilane- OTS, octyltrichlorosilane-OTCS, 3-aminopropyltrimethoxysilane-APTMS, 3-[tris (trimethylsilyloxy) silyl] propyl methacrylate- MSMA, poly (MSMA), dodecyltrichlorosilane (DTS), and decyltrichlorosilane (DTCS). Characterization data obtained using CA measurements, FTIR spectroscopy and SEM have been discussed to illustrate the reasons for this superhydrophobic behaviour.

5. 2 Experimental Aspects

5.2.1 Materials

n-Octadecyltrichlorosilane,(C_{18}, OTS) (95%), octyltrichlorosilane (C_8, OTCS), dodecyltrichlorosilane(C_{12}, DDS), decyltrichlorosilane (C_{10}, DCS), 4-Aminopropyltrimethoxysilane (APTMS), 4-[tris (trimethylsilyloxy) silyl] propyl methacrylate (MSMA) and Tetraethyl orthosilcate (TEOS) were obtained from Aldrich, while toluene (99.5 %), ethanol (99.5 %) and ammonia were purchased from Qualigens. Commercially available n-type, one-side polished, silicon wafers of (100) orientation with 0.001-0.007 Ω-cm resistivity were used as substrates. These silicon wafers (1x1 cm^2) were rinsed with deionized water (18 MΩ cm), sonicated in ethanol and dried under

a flow of nitrogen. These wafers were soaked in 1:10 deionized HF: H_2O solution for 40 s to remove a native SiO_2 layer and further immersed in a *piranha* solution (7:3 concentration H_2SO_4: H_2O_2) for 30 min at 80 ^oC to grow a fresh oxide layer, followed by rinsing with deionized water and drying in a stream of nitrogen before their use for experiments. Silica particles were prepared by using the well-known Stober's method as reported elsewhere [25].

5.2.2 Silanization

Prior to silanization, silica particles were dried for 10 hrs at 150 ^oC under nitrogen atmosphere and were used immediately. In a typical synthesis procedure, 25 mg silica particles (100-150 nm) were dispersed in dry toluene and stirried for 30 min. To the above mixture 10 ml, 1 % OTS (w/w) in toluene was added drop wise, and in order to ensure a complete monolayer formation of OTS on silica, the mixture was refluxed for 24 hrs under nitrogen atmosphere. This solution was then allowed to stand for few hours, filtered and washed several times with toluene and ethanol in order to remove unreacted OTS. This (OTS-silica) was subsequently dried in a vacuum oven at 60-70 ^oC for 4 hrs and used for further characterization. Similarly, the silanization was carried out by changing the % of OTS (w/w) in toluene (i.e. 5, 10, 15, 20, and 25) and also by using different silane reagents such as APTMS, MSMA, OTS, OTCS, DTS, and DTCS. In each case, 10% silane (w/w) in toluene was used for surface modification. Figure 5.1 shows a schematic of typical terminal groups and their arrangements, in which the silane molecules are linked to silica surface through Si-O-Si linkage with different terminal functional group, which determines its wettability.

5.2.2.1 Mixed Mono/ Multilayer Formation

Mixed mono/multilayer of APTMS: OTS (1:1) and OTS:OTCS (1:1) To form a mixed mono/multilayer, silane reagents were mixed in toluene (APTMS and OTS (1:1) (w/w)) and then added drop wise on to the silica particles dispersed in toluene.

5.2.2.2 Polymerization of MSMA Monomer

Polymerization of MSMA monomer (*in situ*): 25 mg silica particles were dispersed in dry toluene and stirred for 30 min. To this a solution 2.5 mg 5-(Trimethoxysilyl) propyl

methacrylate monomer, 1 ml triethyl amine (as a catalysts) and azobis isobutyronitrile (AIBN, as an initiator) were added and the mixture was refluxed for 24 hrs under nitrogen atmosphere. Subsequently this mixture was cooled, allowed to stand for few hours, filtered and washed several times with toluene and ethanol in order to remove excess of monomer and the resultant poly- (MSMA) silica was used for further characterization.

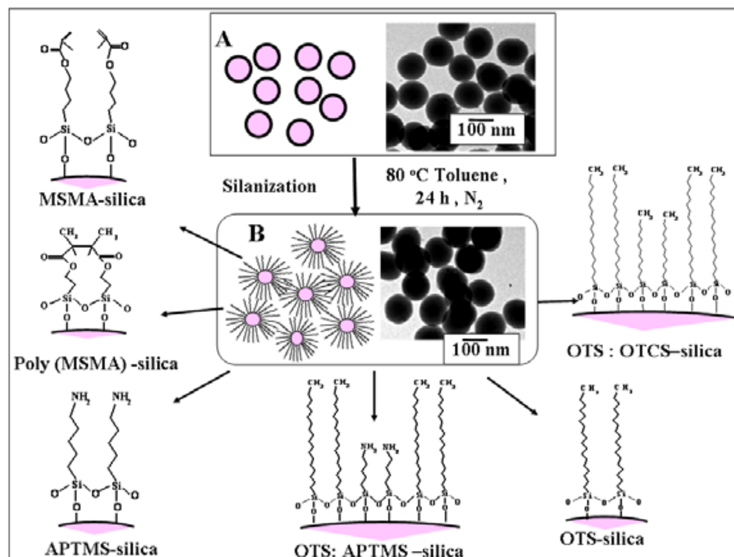

Figure 5.1: Schematic representation of surface modification of silica particles using different organosilane reagents, (A) bare silica particles and the corresponding TEM indicating a particle size of ~ 100-150 nm; and (B) modified silica particles using organosilane molecule viz., OTS, OTCS, APTMS, MSMA and poly-(MSMA) and mixed mono/multilayers of OTS:APTMS and OTS:OTCS; the corresponding TEM of silica particles after silanization, as the thickness of silane molecules is in range 2-10 nm no significant change is observed after silanization

5.3 Characterization

Scanning electron microscopic (SEM) measurements were carried out on a Leico stereoscan model 450 instrument equipped with Phoenix energy dispersive analysis of x-ray (EDX) attachment. Transmission electron microscopic (TEM) measurements were carried out a JEOL 1200 EX TEM operated at an accelerating voltage of 120 kV. The bare silica and modified-silica particles were dispersed in the appropriate (e.g., toluene) solvent and drop/spin casted to form a film on Si substrate, which was dried at 100 ^{o}C for an hour. The water sessile drop contact angle (CA) measurements were carried out on GBX–model 'Digidrop' CA meter. CA was calculated by measuring the average angle at three different locations. The modified-silica particles were made in the form of a pellet

after mixing with spectroscopic grade KBr and the FTIR spectra were recorded using a Perkin Elmer 1615 spectrometer in a diffuse reflectance mode (DRIFT). Thermogravimetric analysis was carried out on a Seiko thermal analyzer model No: TCA/DIA–32. Thermal stability of OTS-silica was studied by CA measurements after annealing Si substrate in nitrogen for 5 mins at different temperatures.

5.4 Results and Discussion

5.4.1 FTIR Spectroscopy

Superimposed FTIR-DRIFT spectra of both pristine and modified silica samples using different silane molecules are shown in Figure 5.2, which gives clear evidence for surface modification. In the low frequency region, 700-1400 cm^{-1}, fundamental Si-O bands (bending vibrations at ~ 800 cm^{-1} and stretching vibrations at 1000-1300 cm^{-1} respectively) are invariant with surface modification, while in the high frequency region (2800-4000 cm^{-1}) certain distinct changes could be seen. Nevertheless, both samples show bands at 804, 1040 and 1220 cm^{-1} which could be attributed to fundamental Si-O vibrations [25-26]. The band at 980 cm^{-1} is related to the stretching modes of isolated silanols and is visible only in case of bare silica, which interestingly disappears after the thermal treatment at 300 ^{o}C. Further the absence of this band in OTS-silica sample indirectly suggests OTS bonding on the silica surface. In case of SiO_2, the bands at 1672, 1872, and 1987 cm^{-1} could be due to physically adsorbed water [25-27]. Interestingly, these bands disappear after a thermal treatment at 700-800 ^{o}C, although these bands are also absent in case of OTS-silica, perhaps due to hydrophobic nature of surface. More significantly, disappearance of a broad peak corresponding to the –OH stretching normally observed on any SiO_2 surface indicates the transition from a hydrophilic to hydrophobic surface, presumably due to the presence of a monolayer. New bands at 2850 and 2919 cm^{-1} of $–CH_2$ due to C-H symmetric and antisymmetric stretching respectively indicate the presence of organosilane mono/multilayers after functionalization of the silica surface [25]. The asymmetric C-H stretching mode due to terminal CH_3 at 2958 cm^{-1} is a sign of a densely assembled monolayer [1]. A comparison of this spectrum with that of long chain alkane hydrocarbon clearly suggests the presence of ordered and close packed molecular assembly. These bands are more pronounced in case of OTS-silica,

APTMS:OTS–silica, and OTS:OTCS–silica samples due to the presence of a long hydrocarbon chain, while in case of other samples MSMA-silica, Poly (MSMA)-silica and APTMS-silica, these bands are slightly shifted and less intense in comparison with that of OTS-silica.

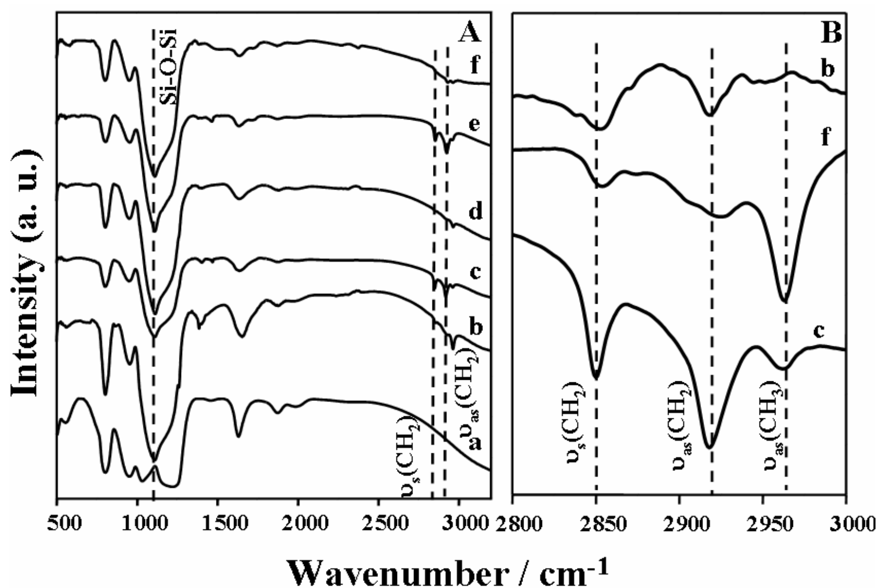

Figure 5.2: A) Superimposed FTIR-DRIFT spectra of (a) bare and modified silica particles, (b) APTMS–silica, (c) OTS-silica, (d) MSMA-silica, (e) OTS: APTMS–silica and (f) poly-MSMA), and B) the superimposed FTIR spectra of OTS-silica, poly (MSMA) and APTMS-silica are shown in the different spectral window (2800-3000 cm^{-1}).

The superimposed FTIR-spectra are shown in a different spectral window (2800-3000 cm^{-1}, Figure 5.2B) for the ease of comparison. Shift in the peak positions is perhaps attributed to the entanglements of hydrocarbon chains after polymerization and also perhaps to the effect of neighboring electron withdrawing carbonyl group.

5. 4. 2 Thermogravimetric Analysis

Figure 5.3 shows superimposed TG curves of silica and modified-silica samples. In case of pristine silica, a sharp decrease in weight in the temperature range 50-150 ^oC, could be attributed to the loss of physisorbed water. On the contrary, the TG profile of modified-silica shows two steps of weight loss, one below 150 ^oC and other in the region 200-600 ^oC. A former weight loss is either due to the desorption of water or due to solvents used for monolayer formation, although the weight loss in this region is less as compared to that of silica, due to its hydrophobic nature. Further, the more pronounced

weight loss is attributed to the loss of silane mono/multilayer, which is not at a particular temperature since the organic layer decomposes slowly from the silica surface up to 600 ^{o}C, after which the weight loss is similar to that of silica.

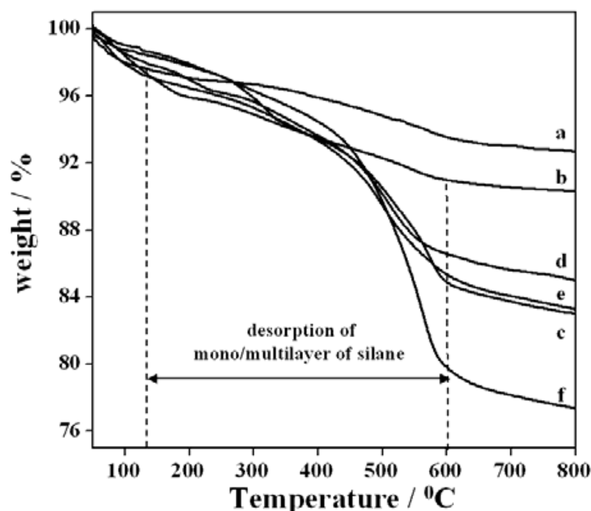

Figure 5. 3: Superimposed thermogravimetric profiles of (a) bare silica, (b) APTMS–silica, (c) OTS-silica, (d) MSMA-silica, (e) OTS:APTMS-silica, and (f) poly (MSMA)-silica samples in nitrogen atmosphere at a heating rate 10 ^{o}C /min.

The pronounced weight loss for each silane-modified silica as compared to that for pristine silica is due to the decomposition of organic moiety present in form of mono/multilayer [25, 28]. In each of the samples, the weight loss is varied according to the composition of the silane reagent. For example, TG analysis reveals more pronounced weight loss for poly (MSMA)-silica sample of 15 % (may be due to the surface polymerization), while APTMS-silica shows only 2 % as compared to that of pristine due to the decomposition of organic moiety present in the mono/multilayer. Thus a combined analysis of FTIR and TGA gives a clear evidence of surface modification.

5.4.3 Contact Angle (CA) Measurements

CA measurements have been carried out on these surface modified silica samples to observe the change in wetability. Bare silica particles are hydrophilic in nature as demonstrated by CA less than 10° (Figure 5.4A) while, in case of APTMS-silica and MSMA-silica the observed CAs are 60° and 80° respectively due to the presence of $–NH_2$ and $-CH=CH_2$ terminal functionality.

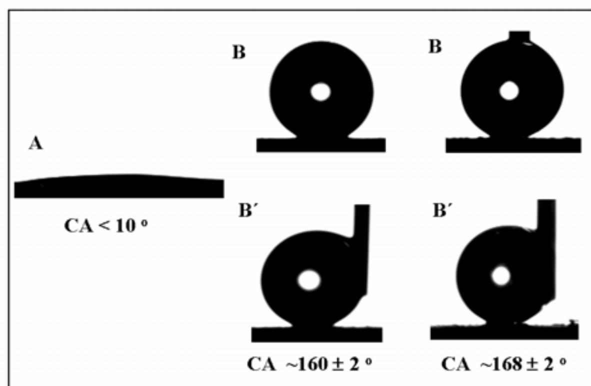

Figure 5.4: A comparison of shape of water droplets on A) bare silica, B) OTS-silica, and C) poly (MSMA)–silica particles, coated on Si substrate; B) and C) positions could rarely be realized since the water droplet rolls off towards the side as shown in B') and C').

Interestingly, for OTS : APTMS–silica and OTS : OTCS-silica, the observed CAs are 135° and 162° respectively suggesting the possibility of domain formation of mixed monolayers especially in the latter case, where the molecular level corrugation is very high since both manolayers have a terminal methyl group. Although the presence of mixed mono/multilayers of silane creates a hierarchical micro/nano structure (surface rougness), the difference in a CA is mainly due to the different chemical functionality present on the surface. In addition, a high CA hysteresis (in the latter case a low CA hystersis) is observed to suggest that it follows the Wenzel state, while latter follows a Cassie state [28]. All results summarized in Table 5.1 indicate the variation of CA with respect to the terminal functional group.

Table 5.1: Variation of the average water contact angle with respect to the surface modification of the silica particles coated on Si substrate

Nature of Surface	Terminal Surface functional groups	Water Contact angle (^{o}) ± 2
Bare silica	-OH	< 10
APTMS- silica	$-NH_2$	60
MSMA- silica	$-CH=CH_2$	80
APTMS : OTS-silica	$-NH_2$, $-CH_3$	135
OTCS -silica	$-CH_3$	158
OTS: OTCS- silica	$-CH_3$	160
OTS- silica	$-CH_3$	162
Poly (MSMA)-silica	$-CH_3$	168

In all these cases the variations in the CA can be attributed to the presence of a hydrocarbon chain of OTS and the formation Si-O-Si network due to the polymerization of OTS and MSMA. The fact that a water droplet can easily roll off the surface (as seen in Figure 5.4 B' and 5.4 C' respectively) shows a self-cleaning or dirt repellant property.

In both cases, a sessile water drop CA is almost stable up to 30 min on the surface although the volume of the water decreases i.e., evaporation of a water droplet takes place through constant CA mode as shown in Figure 5.5A [17]. In addition, CA measurments are also carried out to study the thermal stability of OTS-silica as a function of annealing temperature as shown in Figure 5.5B. CA (155 $^{o} \pm 1$) remains almost constant up to the annealing temperature of 500 ^{o}C, although it then starts to decline slowly from 520 ^{o}C.

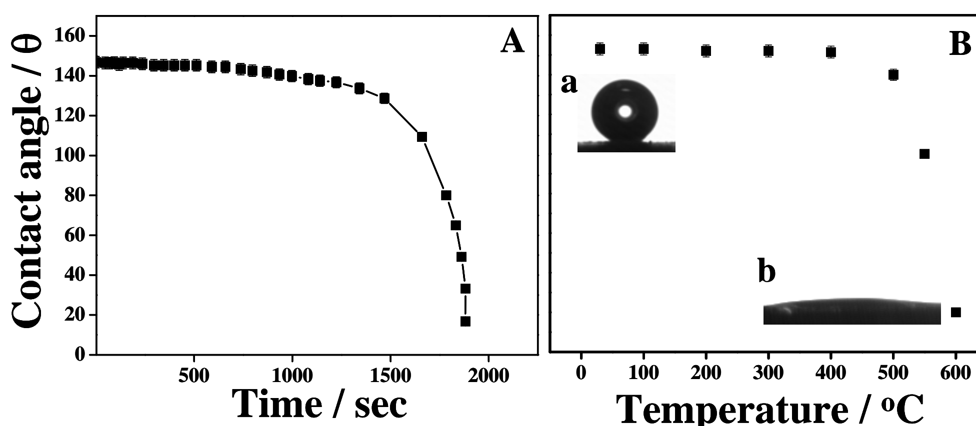

Figure 5.5: A) Time dependent and B) temperature dependent CA measurements for 15 % OTS (w/w) (in toluene) silica particles spin coated on Si substrate; CA measurements were carried out after annealing the substrate in nitrogen for 5 minutes after heating at different temperatures and subsequently cooling to room temperature; inset of (B) shows the shape of the water droplet on OTS-silica particles on Si substrate at (a) room temperature and (b) after annealing and subsequently cooling the same substrate at 500^{0} C in nitrogen.

After annealing at a temperature of 600 ^{o}C, CA of OTS-silica particles coated on Si substrate rapidly decreases up to 30°, which is usually reported for bare silica particles, indicating a complete degradation of OTS mono/ multilayer. Inset of Figure 5.5B shows the shape of the water droplet on the OTS-silica particles on Si substrate at room temperature (Figure 5.5B.a) and after annealing the same film at 500 ^{o}C in nitrogen atmosphere (Figure 5.5B.b). The results imply excellent surface stability. For all the samples the observed CA variation is due to the surface silanization, which creates both the surface roughness and the required chemical functionality [29]. Indeed, these results

conclusively indicate that CA could be carefully manipulated to a desired value by tuning the surface functional group.

5.4.4 Scanning Electron Microscopy (SEM)

Figure 5.6 shows SEM images (representative) of bare silica and OTS-silica films formed on Si substrates indicating a sharp contrast in the morphology. The OTS-functionalized case leads to a very smooth and fairly ordered arrangement of silica particles and also a good dispersion, while bare silica exhibits considerable non-uniformity. The highly improved morphology obtained from OTS-functionalized silica particles can be attributed to configurational interactions between molecular end groups possibly enabling sliding of the landed nanoparticle in the film formation process towards the step edges on the growth front. In case of bare silica nanoparticles once local closed packed units are formed upon landing, it may be difficult for such units to unfold and planarize, causing rough 3D growth. On the other hand the OTS-functionalized particles will intrinsically lead to soft landing and flexible morphology that can evolve towards planarization. These speculations may have to be substantiated by further work.

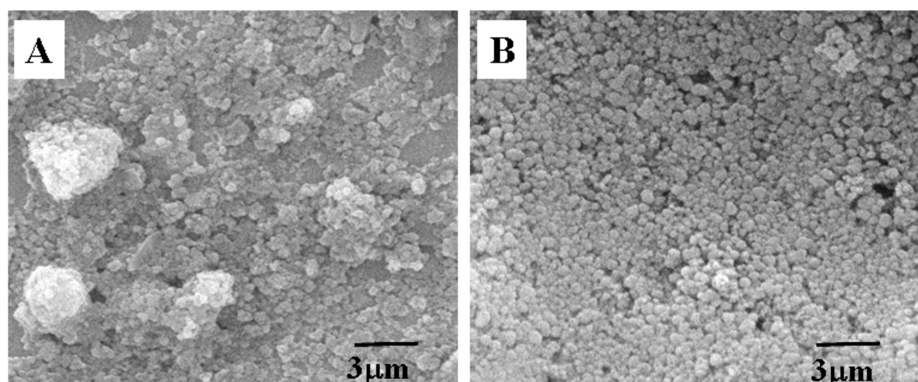

Figure 5. 6: The SEM images of A) bare silica and B) OTS-silica particles coated on Si substrate

Figure 5.7 shows a schematic representation of the bare and surface modified silica particles drop coated on Si substrate. On bare silica particles CA angle is less than 10° (as mentioned earlier) giving the evidence of the –OH groups. While in case of the modified silica particle, CA depends on the interaction between water droplet and the functional groups present on the surface, which are responsible for the hydrophobicity

along with the surface roughness. In all cases silica particles do act as micro domains on which silane mono / multilayers create nano roughness, which together with the presence of functional group is responsible for the enhancement in CA.

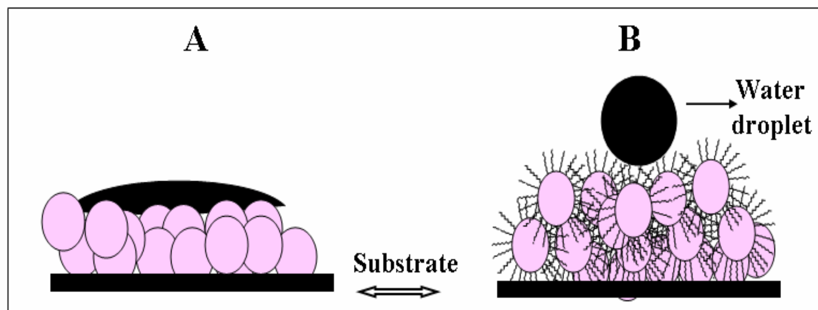

Figure 5.7: Schematic representation of water CA on bare and surface modified silica particles drop coated on Si substrate.

In order to understand the possible link between the amount of SAMs on silica particles and ensuing hydrophobic properties, the variation of CA has been examined by changing the concentration of OTS systematically in toluene for surface modification; corresponding changes on silica surfaces are shown in Figure 5.8.

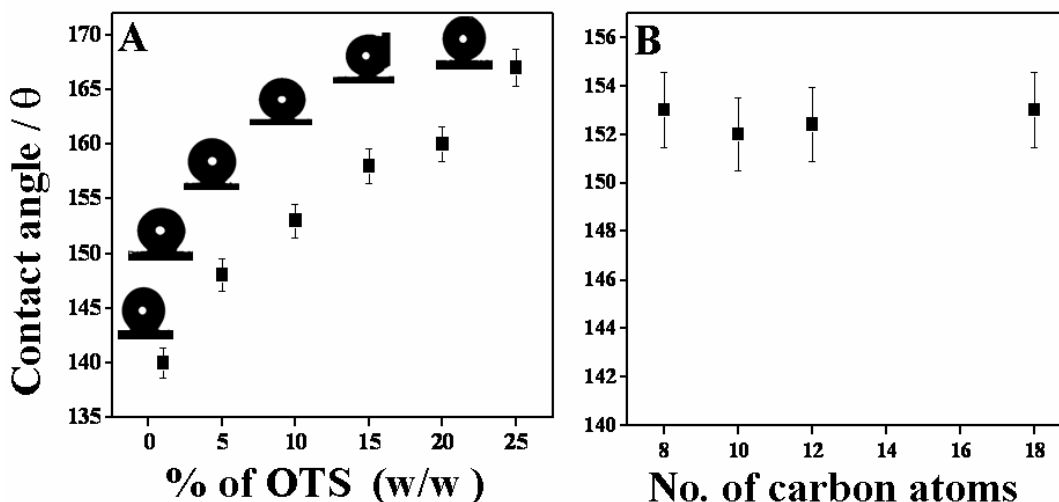

Figure 5. 8: Water sessile drop contact angle variation on silica particles modified by A) changing the % of OTS (w/w) in toluene, and B) varying the chain length of the silane molecules.

In the case of silica particles modified using 1 % OTS (w/w) in toluene the CA is 144°, which is as expected although this increases further with a corresponding increase in the % of OTS (w/w) in toluene. For, silica particles modified using 25 % OTS (w/w) in toluene, the CA increases up to 168°, and then get saturated. As the extent of silanization

is increased, multilayer formation through Si-O-Si network due to the polymerization of OTS molecule occurs on the surface of silica particles, thus creating the hierarchical microstructure and nanoscale surface roughness. This makes the surface of the silica particles essentially superhydrophobic in nature. Compositional change on nanoscale also gets crucial evidence from FTIR spectra of silica particles as indicated in Figure 5.9A at different % of OTS (w/w) in toluene over the 2800-3000 cm^{-1} spectral window. A slight shift to higher wavenumbers in the peak positions at 2850 and 2919 cm^{-1} due to C-H stretching (symmetric and antisymmetric) vibrational modes of $-CH_2$ in OTS-silica with respect to % OTS (w/w) in toluene, as expected for alkane chains with gauche conformational isomers of OTS due to the multilayer formation [30].

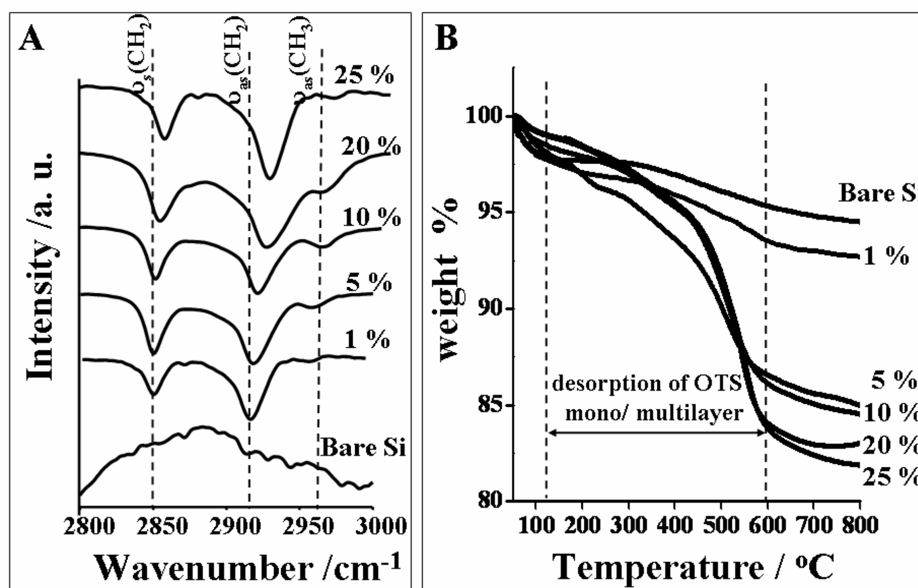

Figure 5.9: Superimposed A) DRIFT-FTIR spectra (over the 2800-3000 cm^{-1}), and B) thermogravimetric curves (in nitrogen atmosphere, at a heating rate 10 ^oC/ min.) of OTS-silica particles at different % of OTS (w/w) in toluene

In addition, thermogravimetric analysis of OTS-silica at different % of OTS (w/w) in toluene (Figure 5.9B) shows the enhancement in the weight that also supports the multilayer formation. As suggested in many earlier studies by Stevens et al., there is a possibility of multilayer structure which consists of alternating cross polymerized monomers with highly oriented trans -$C_{18}H_{37}$ chains, in which the half of the hexagonal sites have the chain pointing upwards while other half pointing downwards [30]. CA is found to be almost constant with respect to the chain length of the molecule as shown in

Figure 5.8B. This is in excellent agreement with the CA as a function of nanoscale roughness, since increase in chain length can increase the roughness in nanometre range due to interdigitation between chains. However, after a critical value of chain length, molecular level corrugation may not vary drastically which could explain the trends in Figure 5.8B where the formation of multilayer occurs when the same chemical group i.e. $–CH_3$ is present at the terminal position. These results are in good agreement with the conclusions of similar studies on 2D SAMs [31].

5.4.5 Comparison in CA between SAM on Planar and Curved Surfaces

CA value on the surface modified silica film is indeed much greater than that of OTS-SAM on planar Si substrate (109 ^{o}), which can be attributed to the presence of curvature in the former case (contributing to the hierarchical morphological changes) due to silica particles as shown in Figure 5.10. It is well known that roughness of the hydrophobic surface amplifies its hydrophobicity significantly and the wetting properties of such rough surface can be described by two theoretical models namely Wenzel (Homogeneous wetting) and Cassie-Baxter (CB) (Heterogeneos wetting).

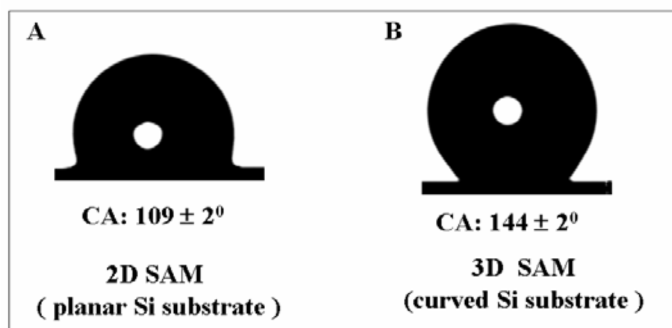

Figure 5. 10: A comparison of sessile drop water contact angle measurements of OTS-SAM on planar (Si (100) substrate) and curved Si (silica particles) surface.

In the Wenzel model the liquid wets the troughs of roughness completely while in the CB model there are cavities captured therein. The corresponding relevant modifications of the basic Young's equation, γ_{SV}-γ_{SL}= γ_{LV} cosθ provide Wenzel equation, $\cos \theta_w = r \cos \theta_y$ and Cassie and Baxter equation, $\cos \theta_{CB} = f_1 \cos \theta_1 + f_2 \cos\theta_2$, $f_1 + f_2 = 1$. Here, γ_{SV}, γ_{SL}, and γ_{LV}, are the interfacial tensions occurring at the solid-vapor, solid-liquid, and liquid-vapor interfaces respectively and θ is the equilibrium CA. θ_w is an

equilibrium CA on a rough surface, given by Wenzel's equation and r is roughness factor (the surface free energy of the solid part of a rough surface is *r* times higher than that of a flat surface). θ_{CB} is the CA at a heterogeneous surface composed of two different materials proposed by Cassie and Baxter, f_1 and f_2 with CA of θ_1 and θ_2 respectively. The Wenzel model describes the homogenous wetting of the surface with large CA hystersis. In contrast, the CB model describes the heterogeneous wetting of the surface with low angle of hystersis. Both the models, however suggest that the superhydrophobicity of the surface is determined by both the surface chemistry and the surface roughness i.e., how a droplet of a liquid sits and rolls on a surface [1].

The enhancement in the CA for a simple surface is often discussed by using the Cassie-Baxter equation: $\cos \theta_r = f_1 \cos \theta - f_2$. In our case, θr (144°) and θ (109°) are CAs of OTS SAM on silica particles (curved) and on a smooth Si (planar) substrate surface, respectively (Figure 5.10). In case of, n-layers (multilayer), θr and θ could change to 168 ^{o} and 120 ^{o} respectively and it is easy to deduce that increasing the fraction of air (f_2) increases CA of the rough surface (θr). According to this equation, the f_2 value for the OTS-silica sample (on curved surface) is estimated to be 0.71.This means that air occupies about 71 % of contact area due to the radius of curvature of the silica particles. As the percentage of OTS (w/w) increases on the silica particles, due to the multilayer formation, this could contain even 95 % of air between the alkane chains, thus facilitating a higher contact angle and even the self-cleaning property of the surface [24]. Interestingly, this could also be compared with the recent report by Xi et.al, in which the decrease in refractive index arising from air entrapment in silica particles has been exploited for application in antireflective coatings [32].

5. 5 Conclusions

Our unique silica nanoparticle films obtained by surface modification using selected self-assembled mono/multilayers of organosilane molecules demonstrate the tuning of the hydrophobic/hydrophilic properties of a surface by controlling the chain length, nature of molecule as well as by the use of a simultaneous mixture of two or more SAMs. For example, some tailor made films show superhydrophilicity with a CA of 10° while others are superhydrophobic with a CA of 168° after surface modification with

alkyltrichlorosilane. More interestingly, the water CA can be increased up to 168° by forming multilayers of OTS. These results suggest that creating the micro/nano scale surface roughness through surface silanization could mimic structure of lotus leaf. Since both, chemical functionality and the surface roughness are responsible for superhydrophobicity, this could be tuned to make different types of such silica particles useful for many potential applications including selective adsorbents and catalysts, chromatographic supports and in microfluidic devices.

5.6 References

[1] (a) A. Ulman, '*An introduction to ultra thin organic films from Langmuir-Blodgett to Self-assembly*, Academic Press, London **1991**. (b) J. Sagiv, *J. Am. Chem. Soc.* **1980**, 102, 92. (c) R. Maboudian, *Mater. Res. Soc. Bull.* **1998**, 24, 47. (d) M. J. Hostetler, J. J. Stokes, R. W. Murray, *Langmuir*, **1996**, 12, 4604.

[2] (a) W. Barthlott, C. Neinhuis, *Planta*, **1997**, 202, 1. (b) H.C. Von Baeyer, *Science* New York, **2000**, 40, 12. (c) R. Bossey, *Nat. Mater*, **2004**, 2, 401.

[3] (a) D. H. Jung, I. J. Park, Y. K. Choi, S. B. Lee, H. S. Park, J. Ru¨he, *Langmuir*, **2002**, 18, 6144. (b) K. Tadanaga, J. Morinaga, A. Matsuda, T. Minami, *Chem. Mater*. **2000**, 12, 590. (c) A. Nakajima, K. Hashimoto, T. Watanabe, *Langmuir,* **2000**, 16, 7044.

[4] (a) S. R. Coulson, L. Woodward, J. P. S. Badyal, S. A. Brewer, C. Willis, *J. Phys. Chem. B* **2000**, 104, 8846. (b) H.Y. Erbil, A. L. Demirel, Y. Avci, O. Mert, *Science* **2004**, 299, 1477. (c) S. Shibuichi, T. Onda, N. Satoh, K. Tsujii, *J. Phys. Chem.* **1996**, *100*, 19512. (d) W. Chen, Y. Fadeev, M. C. Heieh, D. Oner, J. Youngblood, McCarthy. (e) T. J. *Langmuir* **1999**, *15*, 3395. (f) D. O¬ ner, J. McCarthy, *Langmuir* **2000**, *16*, 7777. (g) A. Nakajima, K.Hashimoto, T. Watanabe, *Monatsh. Chem.* **2001**, *132*, 31.

[5] (a) K. K. S. Lau, J. Bico, K. B. K. Teo, M.Chhowalla, G. A. J. Amaratunga, W. I. Milne, G. H. McKinley, K. K. Gleason, *Nano Lett.* **2003**, 3, 1701. (b) L. Feng, S.Li, Y.Li, H. Li, L. Zhang, J. Zhai, Y. Song, B. Liu, L.Jiang, D.Zhu, *Adv. Mater*. **2002**, 14, 1857. (c) L. Feng, S.Li, H. Li, J.Zhai, Y. Song, L. Jiang, D.Zhu, *Angew. Chem. Int. Ed.* **2002**, 41, 1221. (d) L. Feng, Y. Song, J. Zhai, B. Liu, J. Xu, L. Jiang, D. Zhu, *Angew. Chem., Int. Ed.* **2003**, 42, 800.

[6] (a) H. Li, X. Wang, Y. Song, Y. Liu, Q. Li, L. Jiang, D.Zhu, *Angew.Chem., Int. Ed.* **2001**, 40, 1743. (b) M. Cao, X. Song, J. Zhai, J. Wang, Y.Wang, *J. Phys. Chem. B* **2006**, 110, 13072. (c) Y. C. Hong, H. S.Uhm, *Appl. Phys. Lett.* **2006**, 88, 244101. (d) K. Tadanaga, N. Katata, T.Minami, *J. Am. Ceram. Soc.* **1997**, 80, 1040.

[7] (a) E. Balaur, J. M. Macak, H. Tsuchiya, P. J. Schmuki, *Mater. Chem.* **2005**, 15,

4488. (b) H. Y. Erbil, A. L. Demirel, Y. Avci, O. Mert, *Science* **2003**, 299, 1377. (c) W. Chen, A. Y. Fadeev, M. C. Hsieh, D. Oner, J. Youngblood, T. J. McCarthy, *Langmuir* **1999,** 15, 3395. *Mod. Phys.* **1985**, 57, 827.

[8] (a) S. R. Coulson, I. Woodward, J. P. S. Badyal, S. A. Brewer, C. Willis, *J. Phys. Chem. B* **2000**, 104, 8836. (b) R. Fu¨rstner, W. Barthlott, *Langmuir* **2005**, 21, 956. (c) J. Zhang, J. Li, Y. Han, *Macromol. Rapid Commun.* **2004**, 25, 1105. (d) J. T. Han, D. H. Lee, C. Y. Ryu, K. Cho, *J. Am. Chem. Soc.* **2004**, 126, 4796.

[9] (a) J.-Y. Shiu, C.-W. Kuo, P. Chen, C.-Y. Mou, *Chem. Mater.* **2004**, 16, 561. (b) J. P. Youngblood, T. J. McCarthy, *Macromolecules* **1999**, 32, 6800. (c) W. Chen, A. Y. Fadeev, M. C. Hsieh, D. O¨ ner, J. Youngblood, T. J. McCarthy, *Langmuir* **1999**, 15, 3395. (d) S. Shibuichi, T. Onda, N. Satoh, K. Tsujii, *J. Phys. Chem.* **1996**, 100, 19512.

[10] T. J. McCarthy, D. Oner, *Langmuir* **2000**, 16, 7777.

[11] (a) N. Zhao, F. Shi, Z. Wang, X. Zhang, *Langmuir*, **2005**, 21, 4714. (b) N. Zhao, F. Shi, Z. Wang, X. Zhang, *Langmuir* **2005**, 21, 4714. (c) Y. Jiang, Z. Wang, X. Yu, F. Shi, H. Xu, X. Zhang, *Langmuir* **2005**, *21*, 1986. (d) X. Zhang, F. Shi, X. Yu, H. Liu, Y. Fu, Z. Wang, L. Jiang, X. Li, *J. Am. Chem. Soc.* **2004**, *126*, 3064. (e) X. Yu, Z. Wang, Y. Jiang, F. Shi, X. Zhang, *Adv. Mater.* **2005**, *17*, 1289.

[12] (a) H. Chien-Te, F. Wen-Syuan, *Appl. Phys. Lett.*, **2006**, 88, 244120. (b) S. Li, H. Li, X. Wang, Y. Song, Y. Liu, L. Jiang, D.Zhu, *J. Phys. Chem. B* **2002**, *106*, 9274.

[13] (a) I. Woodward, W. C. E. Schofield, V. Roucoules, J. P. S. Badyal, *Langmuir* **2004**, 19, 4442. (b) M. Ma, R. M. Hill, J. L. Lowery, S. V. Fridrikh, G. C. Rutledge, *Langmuir* **2005**, *21*, 5549.

[14] (a) D. H. Jung, I. J. Park, Y. K. Choi, S. B. Lee, H. S. Park, J. Ru¨he, *Langmuir,* **2002**, 18, 6144. (b) J.-Y. Shiu, C.-W. Kuo, P. Chen, C.-Y. Mou, *Chem. Mater.* **2004**, *16*, 4,561. (c) J. Fresnais, L. Benyahia, J. P. Chapel, F. Poncin-Epaillard, *Eur. Phys. J.: Appl. Phys.* **2004**, 26, 209.

[15] (a) K. Tadanaga, J. Morinaga, A. Matsuda, T. Minami, *Chem .Mater.* **2000**, 12,

590. (b) T. Kawai, T. Sakata, *Nature* **1980**, *286*, 474. (c) J. Schwitzgebel, J. G. Ekerdt, H. Gericher, A. Heller, *J. Phys. Chem.* **1995**, 99, 5633. (d) R. Wang, K. Hashimoto, A. Fujishima, M. Chikuni, R. Kojima, A. Kitamura, M. Shimohigoshi, T. Watanabe, *Nature* **1997**, 388, 431. (e) R. Wang, K. Hashimoto, A. Fujishima, M. *Spectrosc*. **1989**, 1145, 300.

[16] (a) L. Zhai, F. C. Cebeci, R. E. Cohen, M. F. Rubner, *Nano Lett.* **2004**, 4, 7. (b) J.-Y. Shiu, C.-W. Kuo, P. Chen, C.-Y. Mou, *Chem. Mater.* **2004**, *16*, 4,561.

[17] (a) A. Nakajima, K. Hashimoto, T. Watanabe, *Langmuir*, **2000**, 16 , 7044. (b) L. Zhai, F. C. Cebeci, R. E. Cohen, M. F. Rubner, *Nano Lett.* **2004,** 4, 7. (c) M. Sun, C. Luo, L. Xu, H. Ji, Qi. Ouyang, D. Yu, Y. Chen, *Langmuir*, **2005**, 21, 8978 and reference therein. (d) Erbil, H. Y.; Demirel, A. L.; Avci, Y.; Mert, O. *Science* **2003**, *299*, 1377. (e) X. Y. Lu, C. C. Zhang, Y. C. Han, *Macromol. Rapid Commun.* **2004**, *25*, 1606. (f) X. Y. Lu, J. L. Zhang, C. C. Zhang, Y. C. Han, *Macromol. Rapid Commun.* **2005**, *26*, 637.

[18] T. Soeno, K. Inokuchi, S. Shiratori, *Trans. Mater. Res. Soc. Jpn.* **2003**, *28*, 1207.

[19] Ping-Szu Tsai, Yu-Min Yang, Yuh-Lang Lee *Langmuir* **2006,** *22,* 5660.

[20] F. Shi, X. Chen, L. W. Jia Niu, J. Yu, Z. Wang, Xi Zhang, *Chem. Mater.* **2005,** *17,* 6177.

[21] (a) S. Herminghaus, *Europhys. Lett.* **2000**, *52*, 165. (b) N. L. Abbott, J. P. Folkers, G. M. Whitesides, *Science,* **1992**, *257*, 1380. (c) J. Bico, C. Tordeux, D. Que´re´, *Europhys. Lett.* **2001**, *55*, 214.

[22] (a) M. Callies, D. Que´re´, *Soft Mater*. **2005**, *1*, 55. (b) P. Lenz, *Adv. Mater.* **1999**, *11*, 1531.

[23] (a) K. R. Shull, T. E. Karis, *Langmuir* **1994**, *10*, 334. (b) M. Hui, M. J. Blunt, *J. Phys. Chem. B* **2000**, *104*, 3833. (c) D. Yoo, S. S. Shiratori, M. F. Rubner, *Macromolecules* **1998**, *31*, 4309.

[24] (a) T. Onda, S. Shibuichi, N. Satoh, K. Tsujii, *Langmuir* **1996**, *12*, 2125. (b) S. Shibuichi, T. Onda, N. Satoh, K.Tsujii, *J. Phys. Chem.* **1996**, *100*, 19512.

[25] S. A. Kulkarni, S. A. Mirji, A. B. Mandale, K. P. Vijayamohanan, *Thin Solid*

Films, **2006**, 496, 420 and references therein.

[26] J. Zhang, W. Huang, Y. Han, *Langmuir*, **2006**, 22, 2946 and reference therein.

[27] R. Wang, G. Baran, Stephanie L. Wunder, *Langmuir* **2000**, 16, 6298

[28] (a) R. Wang, S. L. Wunder, *J. Phys. Chem. B* **2001**, *105,* 173. (b) a) N. R. Wenzel, Ind. Eng. Chem, 1936, 938. (c) N. R. Wenzel, Ind. Eng. Chem. 1936, 28, 988. (d) Cassie, Baxter, *Trans. Faraday Soc*, **1944**, 40, 546. (e) Baxter and Cassie. J. Text. Inst., **1945**, 36, T67.

[29] C. Yang, U. Tartaglino, B. N. J. Persson, *PRL* **2006**, 97, 116104.

[30] M. J. Stevens, *Langmuir* **1999**, 15, 2274.

[31] A.Y. Fadeev, T. J. McCarthy, *Langmuir* **2000,** 16**,** 7268.

[32] J. –Q. Xi, M. F. Schubert, J. K. Kim, E. F. Schubert, M. Chen, S. Lin, W. Liu, J. A. Smart, *Nature Photonics*, **2007**, 1, 176.

CHAPTER 6

Selected Applications of The Self Assembled Monolayers in Microelectromechanical Systems

CHAPTER 6A

Tuning of Anisotropic Etching Rates of Silicon Using Surface Functionalization

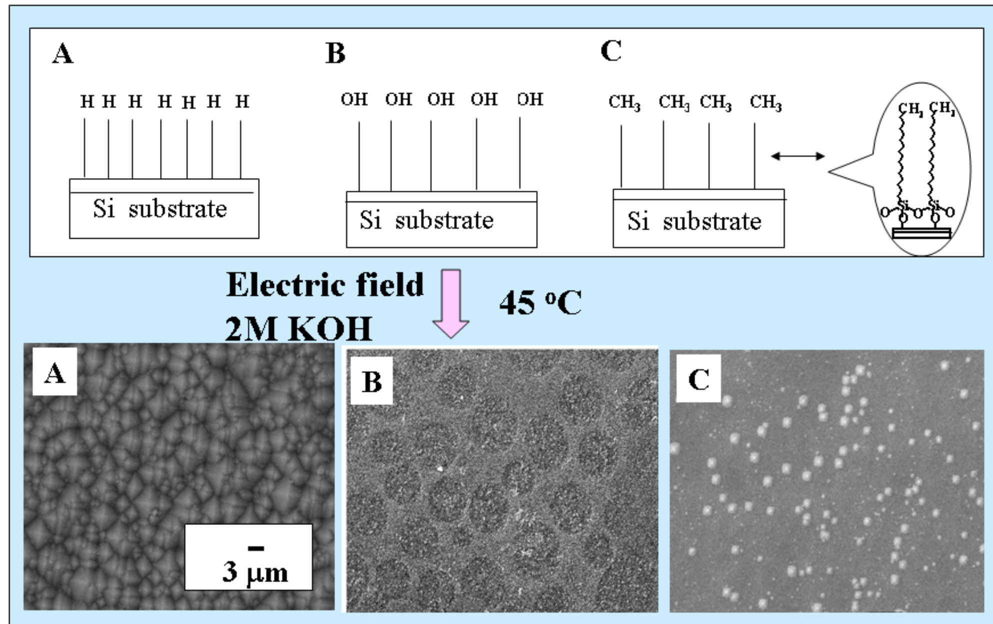

This chapter deals with electrochemical measurements on both bare (treated with HF and piranha) and octadecyltrichlorosilane (OTS) functionalized Si electrodes in 2 M KOH aqueous solution at 45 °C, to demonstrate a correlation between the kinetics of silicon dissolution and optimum surface morphology. The study reveals that the etching rate and morphology of the Si can be profitably controlled by surface functionalization using self-assembled monolayers.

6A.1 Introduction

Anisotropic etching of Si in alkaline solution has been widely used for controlling the surface morphology during the fabrication of diverse micromechanical structures for many years [1-5]. For example, anisotropic etching of semiconductors is used for making simple structures such as diaphragms, cantilevers for pressure and acceleration sensors and also for fabrication of three-dimensional structures, required in micro-electromechanical systems (MEMS) [1-7]. Usually, aqueous alkaline solutions, including KOH, NaOH, NH_4OH or LiOH, aqueous solutions of tetramethyl ammonium hydroxide (TMAH) [5,6], ethylenediamine-pyrocatechol (EDP), or hydrazine-pyrocatechol are used as etchants [7]. Among these, the most popular one is the KOH-based solution and further control is also possible by tuning various factors such as crystallographic planes, doping concentration, etching bath composition, temperature, and stirring rate [8-10]. However, in order to fabricate these ultra-small structures such as grooves, diaphragms, beams and membranes for mechanical sensors and actuators, selective etching of Si with high precision is absolutely essential. Therefore further modulation of the anisotropic etching (and understanding of etch-stop mechanisms) is very important in micromachining technology. Although it is well known that the formation of pyramidal hillocks during etching can be suppressed by the addition of oxidizers to consume hydrogen [6], or by etching under anodic bias [7], the exact mechanism is not clear. It is believed that these functions are achieved either by P^+ doping or by an electrochemical etch-stop mechanism [11]. The etching rate also depends on the hydrophobicity/ hydrophilicity of the substrate and hence an increase in the hydrophilicity is very important because the formation of Si-OH or $Si-O^-$ bonds leads to the polarization of the Si-Si backbone, which enhances the rate of etching reactions. These reactions indeed, proceed via a potential-independent mechanism although the surface morphology is remarkably sensitive to the potential applied to the semiconductor.

The formation of self assembled monolayers (SAMs) of trichloro or trimethoxy silanes containing a long alkane chain on Si surface is used as an anti-stiction agent during MEMS fabrication that would offer several advantages due to its hydrophobic nature [12-15]. Apart from providing precise control over surface properties in the patterning of materials by soft lithography, SAMs act as direct etch resists on Si by

controlling the generation of features in the underlying substrate via wet etching. The long-chained alkyltrichlorosilanes deposited by printing have proven capable of withstanding wet chemical etching conditions for any length of time [16-21].

In earlier chapters (II-V), we have illustrated the usefulness of alkyltrichlorosilane molecules to tune the hydrophobicity of Si substrates by tailoring the functional group of the silane molecules. Although thermal stability of these monolayers has been discussed in details, questions related their chemical and electrochemical stability have not been considered despite its importance in semiconductor processing. In the first part of this chapter (6A) we address such concerns with special reference to etching of Si in aqueous KOH solution. We demonstrate the role of OTS monolayer for controlling the etching rate and morphology of the Si substrate after various pretreatments, such as HF (A), *piranha* (B) and OTS (C) monolayer formation. These treatments generate a, hydrogen (-H), hydroxyl (-OH) and methyl ($-CH_3$) terminal functional groups respectively on the Si substrates, which assists the kinetics of silicon dissolution along with modulating the surface morphology. These results are also relevant for many other areas since the electrochemistry of Si in alkaline medium has many important industrial applications.

6A. 2 Experimental

6A. 2. 1 Chemicals

n-Octadecyltrichlorosilane ($CH_3(CH_2)_{17}SiCl_3$), was obtained from Aldrich, while all other chemicals were purchased from Qualigens. Commercially available n-type, one-side polished, silicon wafers of (100) orientation with 0.001-0.007 Ω-cm resistivity were used as substrates. The silicon wafers (1 x 1 cm^2) rinsed by deionised water (18 MΩ cm), sonicated in ethanol and dried under a flow of nitrogen were subsequently oxidized in a freshly prepared *piranha* solution (7:3 $H_2SO_4 : H_2O_2$) for 30 min at 80 ^oC to grow a fresh oxide layer. These cleaned wafers were further rinsed with deionized water, dried in a stream of nitrogen and used for all experiments.

6A. 2. 2 Substrate Preparation

Freshly cleaned Si wafers were treated with HF for few seconds to make its surface hydrophobic, while *piranha* treatment (30 min) created hydrophilic (-OH) group

on the surface [12, 22, 23]. Another batch of freshly cleaned Si wafers was immersed in 0.5 mM OTS solution in toluene for 30 min and was subsequently removed from OTS solution, followed by extensive rinsing with toluene and drying before further characterization. All these experiments were carried out in nitrogen atmosphere [12].

6A. 2. 3 Electrode Preparation

In order to obtain good ohmic contacts with copper wire, Si wafer was cleaned with HF solution for 30 s and was scratched on the rear side, cleaned from the detached particles of silicon and then rubbed with In-Ga eutectic. A copper wire was subsequently fixed for contact using silver epoxy and finally sealed with standard epoxy adhesive.

6A. 3 Characterization

The contact angle on Si (100) substrate was measured by using water sessile drop on GBX model 'Digidrop' contact angle meter. The OTS monolayer was also characterized by grazing angle FTIR spectroscopy on a Perkin Elmer 1615 spectrometer. Scanning electron microscopy (SEM) measurements were carried out on a Leico stereoscan model 440 instrument equipped with a Phoenix energy dispersive analysis of X-ray (EDX) attachment. Cyclic voltammetry and Impedance measurements were carried out with a conventional three-electrode system at 45 ^{o}C in alkaline medium (2M KOH) under nitrogen atmosphere, using a cell comprising of surface modified Si as the working electrode, a large area Pt flag as a counter electrode and Pt wire as a quasi reference electrode in dark conditions. All the voltmmograms were recorded at scan rates of 5 and 100 mV/s. After etching, the silicon electrode was dipped in 1 M H_2SO_4 for 2 min to stop the etching reactions, and was then rinsed with ultra-pure water and dried by N_2. All the electrochemical measurements were carried out at open circuit potential, at which the etching and water reduction processes occurred simultaneously. Cyclic voltammetry experiments were performed on an Autolab PGSTAT 30 (ECO CHEMIE) instrument, whereas electrochemical impedance measurements were carried out with a Solartron 1255B frequency response analyzer (FRA) interfaced to 1287 potentiostat /galvanostat. The measurements were performed over a wide frequency range of 100 kHz-10 Hz with

10 mV rms amplitude at regular time intervals for 45 min. The optimum time for etching was determined from few preliminary experiments using the same system.

6A. 4 Results and Discussion

Theory

The reaction mechanism of the anisotropic etching of silicon is discussed in brief as follows [11, 24].

Hydrogenation of Si substrate normally occurs by the HF treatment,

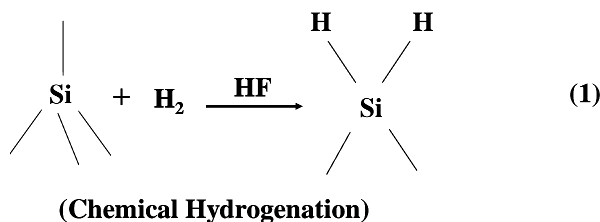

(Chemical Hydrogenation)

In the second step a Si-H surface bond is converted to a Si-OH bond. This reaction is catalyzed by OH - ions (equation 2).

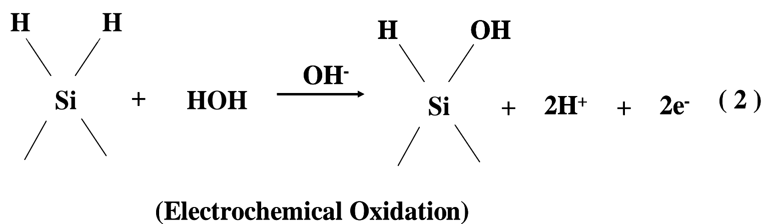

(Electrochemical Oxidation)

The presence of OH^- on the surface atom polarizes and destabilizes the Si-Si back-bond. In the next step, OH^- ions from water add to the "positively" charged surface atom to which an OH is already bonded. This further destabilizes the remaining back-bonds and the surface atom is dissolved, leaving behind a Si-OH or Si-H site at the surface (equations 3-5).

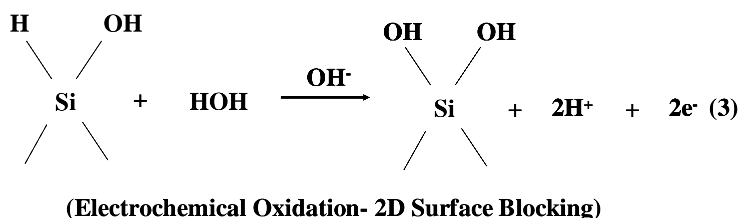

(Electrochemical Oxidation- 2D Surface Blocking)

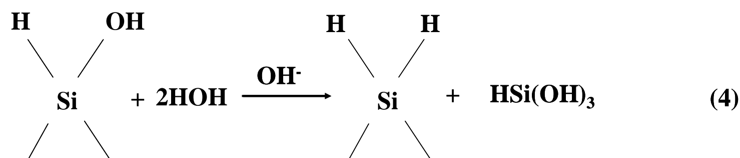

(Chemical Etching)

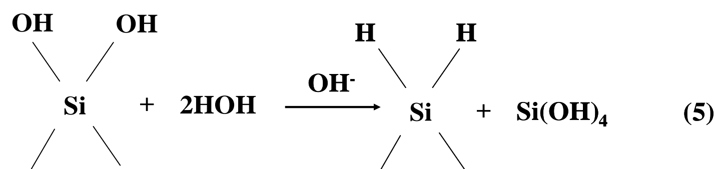

(Chemical Etching)

The overall process involves the $4e^-$, which moves into the silicon crystal, where they stay in the conduction band for a while without recombining.

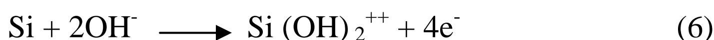

$$Si + 2OH^- \longrightarrow Si\,(OH)_2^{++} + 4e^- \qquad (6)$$

In the next process, these electrons leave the crystal and react with the water in the solution as shown below.

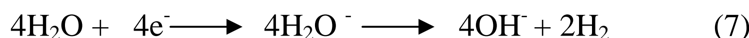

$$4H_2O + 4e^- \longrightarrow 4H_2O^- \longrightarrow 4OH^- + 2H_2 \qquad (7)$$

Thus silicon remains electrically neutral and the new OH^- ions are generated which are further recycled in the etching process. From the above equation, it is clear that the dissolution of silicon is an electrochemical process, although no net current flows. Hence, change in the electric behavior at the interface may strongly influence the etching.

After first step, hydrolysis of the Si $(OH)_2^{++}$ ions takes (place as shown below), negatively charged $SiO_2\,(OH)_2^{--}$ species are repelled by the interface, which are soluble in the etchant.

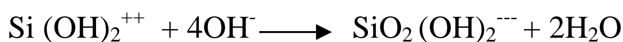

$$Si\,(OH)_2^{++} + 4OH^- \longrightarrow SiO_2\,(OH)_2^{---} + 2H_2O$$

The net chemical reaction is

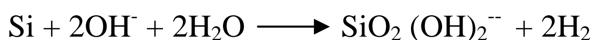

$$Si + 2OH^- + 2H_2O \longrightarrow SiO_2\,(OH)_2^{--} + 2H_2$$

6A. 4. 1 Contact Angle Measurements

It is well known that the surface treatment of Si with *piranha* and HF leaves its surface hydrophilic and hydrophobic respectively, since in the former case hydroxyl groups, and in the latter case, hydrogen atoms are bonded to the surface silicon [22-23].

In comparison, a freshly cleaned Si substrate dipped in OTS solution (mM) in toluene forms a compact monolayer of OTS through Si-O-Si linkage on Si substrates, which maks the surface more hydrophobic.

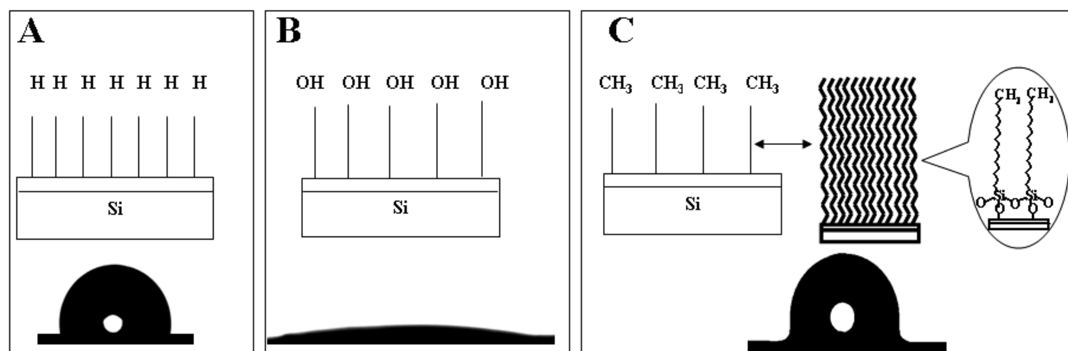

Figure 6A. 1: Schematic representation of the surface functional groups present on the Si substrate after treatment with the A) HF, B) *Piranha* and C) OTS solution, and corresponding images show a shape of the sessile water droplet there upon.

Accordingly, Figure 6A.1 shows a comparison of the shape of a water droplet on the Si treated with (A) HF, (B) *piranha*, and (C) OTS solution, along with their observed contact angles (CAs) (A ~ 90°, B ~< 15° and C ~110 ± 1° respectively). This variation gives indirect evidence for the presence of -H, -OH and -CH_3 terminal surface functionalities. In addition, the characterization of the OTS-SAM formation using FTIR, XPS, CV, Impedance and AFM as discussed in chapter II and III in details supports for the presence of a compact, oriented and fully covered (~99 % with thickness ~ 2.14 nm) monolayer on the Si substrate [25].

6A. 4. 2 Cyclic Voltammetry

Figure 6A.2 shows a comparison of the cyclic voltammetric behavior of various modified Si electrodes in 2 M KOH at 45 ^oC. The open circuit potential (OCP) for both (A) HF and (B) *Piranha* treated Si electrode amounts to about –1.2 V. However, the surface passivation peak (PP) for HF treated Si electrode is observed at –0.68 V, where the peak current increases to a maximum followed by a low value in the passivation range. The current in the return sweep to negative potential is low since the surface is passivated while the low intensity peak at cathodic region (-1 V) is attributed to the re-activation of the dissolution process [24].

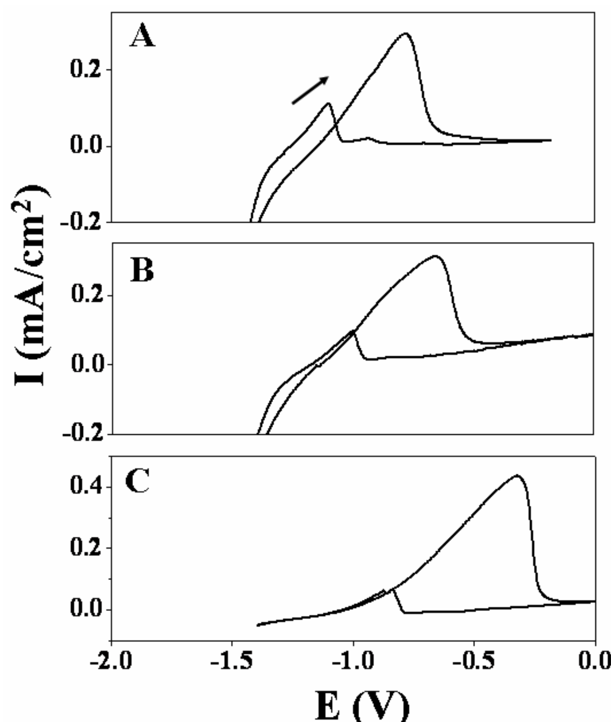

Figure 6A.2: Cyclic voltammograms of bare Si (100) [A) HF and B) *piranha* treated] and C) OTS-Si electrode in 2 M KOH solution at 45 ^{o}C at a scan rate of 5 mV/s; arrow indicates the scan direction.

In comparison, the PP after *piranha* treatment (Figure 6A.2B) is rather broad than that obtained after of the HF treatment, perhaps due to the slow etching rate. Usually the anodic current is due to the oxidation of silicon is fast below the peak potential as more and more Si dissolves, while its passivation occurs at a higher potential, inhibiting the further faradic processes of Si dissolution. Interestingly, the PP for OTS monolayer derivatized Si electrode is observed at -0.31 V (OCP is -0.8 V), along with a broadening of the PP, indicating a kinetically sluggish etching. This could be explained due to the enhanced chemical stability of the surface because of the monolayer or may be many stable intermediates are formed during the chemical etching. The slower rate of passivation due to oxide formation could also be one of the contributing factors.

In addition, in all the three cases, it is observed that at 100 mV/s scan rate, the peak current increases with respect to successive cycles although the peak position is invariant. Further, for 5 mV/s scan rate, there is a slight shift of 0.1 V in the anodic as well as in cathodic peak position for each successive cycles. This could be explained since it has been reported that in the initial stage, the surface of silicon is smooth although it becomes rough subsequently due to the formation of the pyramids. Hence, as

the cathodic current increases, on the rough silicon surface, the hydrogen evolution reaction is more favoured. Futher, the increase in the surface roughness with time leads to etching and repassivation at lower potential [26].

6A. 4. 3 Impedance and SEM analysis

In order to explore this further in relation to the change in surface morphology, we have carried out impedance measurements in 2 M KOH at 45 ^{o}C and accordingly, such a plot for bare Si electrode after HF treatment at sequential time interval is shown in Figure 6A. 3A.

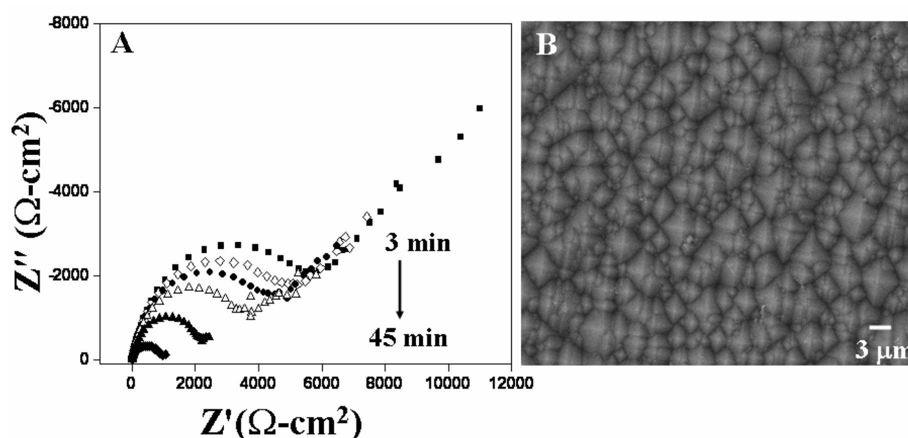

Figure 6A. 3: A) Impedance plot for bare Si electode treated with HF in 2M KOH at 45 ^{o}C at a potential close to OCP = -1.3 V; B) SEM image of Si electrode after impedance measurements; frequency swept is from 100 kHz-10 Hz with 10 mV rms amplitude at sequential time interval for 45 min.

For the convenience of analysis, this plot is divided into high and low frequency regions respectively. In the high frequency region, a well–defined semicircle is observed due to the space charge and the Helmholtz layer at the semiconductor/solution interface, which is perhaps indistinguishable whereas the lower frequency region is attributed to the diffusion related phenomena. Two main possibilities of the diffusive species are the OH^- ion diffusion through a thin layer of silicate at the electrode surface, and the silicate product diffusion outwards from the surface respectively. The charge transfer resistance (R_{ct}) is high in the initial stages as Si is covered with Si-H bonds that have an energy level inside the valence band of the semiconductor which could not act as surface states, although could act as mediators in the charge transfer process. However, etching produces a high density of surface states, causing R_{ct} to decrease facilitating the charge transfer at the electode /electrolyte interface [26].

Scanning electron micrograph (Figure 6A.3B) after electrochemical impedance measurements (for about 45 min) reveal interesting surface morphology comprising of high density pyramids of variable size (from ~3 to 0.5 μm), formed during the etching process and many small pyramids are formed in the close proximity of large ones. As reported earlier, it could be possible that the large sized pyramids are formed during the initial stages of etching, while intermediate species like silicates and hydrogen bubbles generated during the reaction could remain in close proximity to the surface preventing further etching reactions to generate rough surface with many small pyramids. Many evidences suggest that the pyramid formation is mainly due to hydrogen bubbles masking the silicon surface as influenced by the surface hydrophilicity [28]. As the hydrophilicity of the surface increases, adhesion of hydrogen bubbles to the surface decreases, generating a better surface finish. Thus an increase in hydrophilicity is very important since the formation of Si-OH or Si-O^- bonds could lead to the polarization of the Si-Si backbone.

Similar impedance plot of a bare Si electrode after *piranha* treatment in 2M KOH at 45 ^oC is shown in Figure 6A. 4A. Since the surface is hydrophilic right from the initial stage of dipping, more Si-OH bonds could contribute as surface states facilitating charge transfer at the electrode/electrolyte interface. As a result, low R_{ct} value is obtained in comparison with earlier results. In addition, R_{ct} does not change significantly with respect to time. Interestingly, the formation of round marks due to different etching depth is observed after impedance measurements as shown in Figure 6A.4B. In this case, the dissolution of the native oxide is obtained directly in KOH. Since dissolution and re-deposition of the oxide layer is not uniform in this anisotropic etchant, the silicates and the hydrogen bubbles generated during etching get physically trapped in the depressed areas leading non-uniform domains. This is consistent with the explanation of Sakaino et. al., for similar kind of features, in terms of the non-uniformity of the native oxide layer or lateral variation of the oxide stoichiometry (SiO_x) [28]. In comparison with bare Si, OTS-Si electode (Figure 6A.5A) shows higher R_{ct} value indicating enhanced barrier for the electron transfer process at the electrode/electrolyte interface. Further, the figure does not show any significant change with time due to its hydrophobic nature.

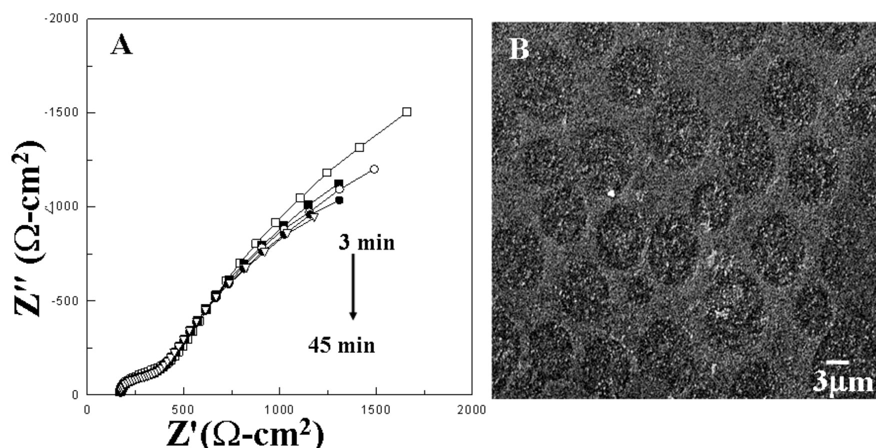

Figure 6A. 4: A) Impedance measurements at different time interval of bare Si electrode after *piranha* cleaning in 2M KOH at 45 ^{o}C at a potential close to OCP = -1.3 V; (B) SEM image of Si electrode after impedance measurements; frequency swept is from 100 KHz-10 Hz with 10 mV rms amplitude at sequential time interval for 45 min.

Figure 6A.5A shows the SEM image of the OTS-monolayer derivatized Si electrode after ~ 3 min in KOH solution, where fractal shaped islands or dendrites of silicon oxide are formed, perhaps form the hydrolysis of the alkyl silane chain. In addition, the OCP for bare and OTS- Si electrodes are about –1.2 V and -0.8 V respectively suggesting variation in the surface passivation of Si. Xia's group has recently shown a similar coupling of chemical and electrochemical reactions accounting for the unusual features [11]. Since monolayer derivatized Si electode bears a long hydrocarbon chain with a hydrophobic (–CH_3) terminal group on the surface, it could easily repel hydroxyl groups (OH^-), which are responsible for the etching process, thus preventing the dissolution of the Si at least during the initial stages. The OH^- ions first adsorb onto the monolayer surface followed by a slow penetration through the monolayer to react with the siloxane moieties breaking up Si-O-Si bond. The OH^- ions are more likely to break up the Si-O-Si bonds, although the repulsive interaction between them can in principle, decrease the rate significantly. As a result, suppression of pyramid formation (i.e. very low density pyramids) is observed after electrochemical measurements (Figure 6A.5C). Further, evidence for the stability of monolayer in the alkaline medium comes from the time dependent CA measurements, where an average value of 109° (in the initial stage) indicates that the monolayer is intact although its subsequent abrupt decrease signals partial destruction.

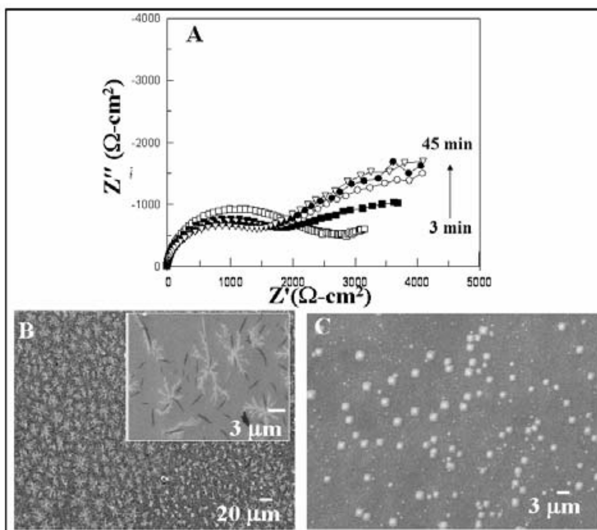

Figure 6A. 5: A) Impedance plot for OTS-monolayer derivatized Si (100)) in 2M KOH at 45 ^{o} C at a potential close to OCP = -0.8 V. SEM image of OTS-Si electrode after impedance measurements for B) 3 min at different magnifications C) and 45 min; frequency swept is from 100 kHz-10 Hz with 10 mV rms amplitude at sequential time interval for 45 min.

6A.4 Conclusions

The present study reveals the importance of groups like –H, -OH and $-CH_3$ on the Si surface to control the surface morphology. Cyclic voltammograms for OTS monolayer derivatized Si electrode in alkaline medium is rather broad in comparison with that for the bare (HF as well as *piranha* treated) Si electrode indicating the sluggish etching process, perhaps due to the hydrophobic-hydrophilic interaction or enhanced chemical stability of the surface. In addition, impedance measurements of OTS-Si electode shows higher R_{ct} value indicating an enhanced barrier for electron transfer process at the electrode/electrolyte interface. Different morphological features are particularly observed on controlling the etching rate of the silicon surface with different terminal functionalities (-H, -OH and $-CH_3$). For example, with HF pretreatment, the formation of pyramidal hillocks is seen, while silicon surface with piranha treatment shows round marks due to different etching depths. In addition, the formation of low density pyramids in case of OTS-monolayer derivatized silicon demonstrates its use as a good etch resist. The study reveals that the etching rate and morphology of the Si can be controlled by surface functionalization.

6A. 5 References

[1] D. L. Kendall, *Appl. Phys. Lett.* **1975,** 26 ,195.

[2] H. Seidel, L. Csepregi, A.Heuberger, H. Baumga¨rtel,. *J. Electrochem. Soc.* **1990,** 137, 3612.

[3] M. J. Vellenkoop, A. J. van Rhijn, G. W. Lubking, A. Venema, *Sensors Actuators* A, **1991,** 25-27, 699.

[4] N. Tirole, D. Hauden, P. Blind, M. Froelicher, L.Gaudriot, *Sensors Actuators A* **1995,** 48, 45.

[5] M. Elwenspoek, H. Jansen, '*Silicon Micromachining*' Cambridge University Press: Cambridge, UK, **1998,** 7.

[6] C. M. A. Ashruf, P. J. French, P. M. M. C. Bressers, J. J. Kelly, P. M. Sarro, *Sensors Actuators A* **1998,** 66, 284.

[7] S. D. Collins, *J. Electrochem. Soc.* **1997,** 144, 2242.

[8] I. Zubel, M. S. Karmkowska, *Sensors Actuators A* **2001,** 93, 138, and references therein.

[9] O. J. Glembocki, E. D. Palik, G. R. de Guel, O.L. Kendall, *J. Electrochem. Soc.***1991,** 138, 1055.

[10] K. Sato, M. Shikida, Y. Matsushima, T. Yamashiro, K. Asaumi, Y. Iriye, M. Yamamoto, *Sensors and Actuators A* **1998,** 64, 87.

[11] X. Xia, Colin M. A. Ashruf, P. J. French, J. Rappich, J. J. Kelly, *J. Phys. Chem. B* **2001,** 105, 5722 and references therein.

[12] A. Ulman, '*An introduction to ultra thin organic films from Langmuir- Blodgett to Self-assembly*' Academic Press, London **1991**.

[13] U. Srinivasan, M. R. Houston, R. T. Howe, R. Maboudian, *J. Microelectromech. Syst.* **1998,** 2, 252.

[14] Y. Xia, M. Mrksich, E. Kim, G. M. Whitesides, *J. Am. Chem. Soc.* **1995,** 117, 9576.

[15] P. Galambos, *Encyclopedia of materials: Science and Technology* **2001**, 5598.

[16] A. Kumar, H. A. Biebuyck, N. L. Abbott, G. M. Whitesides, *J. Am. Chem. Soc.* **1992,** 114, 9188.

[17] E. Kim, A. Kumar, G. M. Whitesides, *J. Electrochem. Soc.* **1995,** 142, 628.

[18] N. L. Abbott, A. Kumar, G. M. Whitesides, *Chem. Mater.* **1994,** 6, 596.

[19] J. L. Wilbur, E. Kim, Y. Xia, G. M. Whitesides, *Adv. Mater.* **1995,** 7, 649.

[20] K. R. Finnie, R. Haasch, R.G. Nuzzo, *Langmuir* **2001,** 17, 6968.

[21] K. R. Finnie, R.G. Nuzzo, *Langmuir*, **2001,** 17, 1250.

[22] Y. J. Chabal, G. S. Higashi, K. Raghavachari, V. A. Burrows, J. *of Vacuum Science & Technology A: Vacuum, Surfaces, and Films* **1989,** 7, 2104.

[23] H. Angermann, Th. Dittrich, H. Flietner, *Applied Physics A: Materials Science & Processing* **1994,** 59, 193.

[24] S. Cattarin, M. M. Musiani, *J.Phys. Chem.B* **1999,** 103, 3162.

[25] S. A. Kulkarni, S. A. Mirji, A. B. Mandale, K. Vijayamohanan, *Thin Solid Films* **2006,** 496, 420.

[26] S. Cattarin, M. M. Musiani, *J. Phys. Chem. B*. **1999,**103, 3612.

[27] S. A. Campbell, K. Cooper, L. Dixon, R. Earwaker, S.N. Port, D. J. Schiffrin, *J. Micromech. Microeng.,* **1995,** 5, 209.

[28] K. Sakaino, Y. Kawabata, S. Adachi, *J. Electrochem. Soc*. **2000,** 147, 153.

CHAPTER 6B

Application Of Self-Assembled Mono/Multilayers As Molecular (Polymeric) Glues For Low Temperature Wafer Bonding

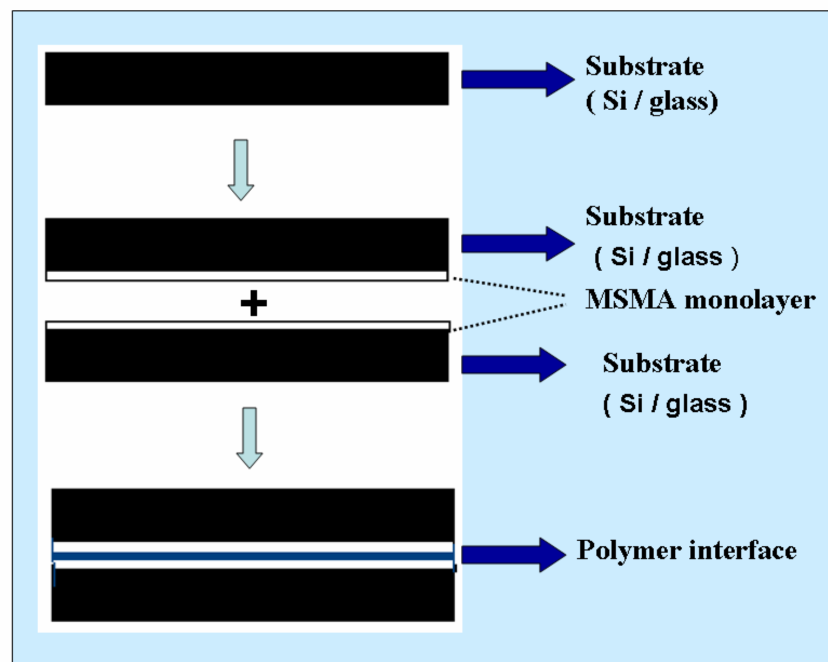

In this chapter we report an improved process of wafer bonding at a low temperature (less than 80 ^{o}C) with the help of a molecular (polymeric) glue using self assembled mono / multilayers of acrylate / methacrylate alkoxy silyl monomer. By using this type of a glue, substrate pairs like silicon-silicon, silicon-glass, and glass-glass systems can be strongly bonded by the polymerization of the terminal vinyl unsaturation of mono / multilayers using a thermal / photo initiator. This type of glues will be very useful for the bonding and integration of microstructures involved in MEMS and VLSI packaging processes.

6B.1 Introduction

Wafer substrate bonding has become a key technology for materials integration in various areas of microelectromechanical systems (MEMS), micro optoelectromechanical systems (MOEMS), microelectronics, optoelectronics and substrate fabrication [1-5]. It is also widely used for vacuum packaging, hermetic sealing and for encapsulation. For example, silicon wafer bonding technology is applicable in various MEMS fabrication and also for the manufacturing of various devices for sensing and actuation. Thus there is an increasing need to develop new easy techniques for wafer to wafer bonding and also to understand the mechanism of wafer bonding to achieve the objectives of micro processing compatibility and device reliability.

Commonly employed types of wafer bonding in microstructure fabrication include direct bonding, anodic bonding and intermediate-layer bonding. In the direct bonding method wafers are directly contacted without assistance of any significant pressure or any intermediate layers or fields [6-9]. The bonding in this case mainly depends on the smoothness of the surface, and requires some form of thermal cycling (in the temperature range 500-1100 ^{o}C) soon after the contact to increase the bond strength. The anodic bonding is typically performed between a glass substrate and silicon wafer, where wafers are contacted after applying an electric field at a temperature in the range of 300–500 ^{o}C [10-13]. In the intermediate-layer bonding technique an intermediate layer promotes the wafer bond, which includes the use of eutectic bond, with polymers adhesive, solders, or thermo compression bonds [14-23]. Adhesive wafer bonding uses polymers or inorganic adhesives as intermediate bonding materials [17-23]. This bonding technique is very suitable for non-uniform surfaces, and can be carried out at very low temperatures, and is simple to use. In all the above mentioned methods, the wafer bonding is carried out at high temperature (500-1100 ^{o}C), and also in few cases adhesive layers or intermediates used for wafer bonding. Since most of the MEMS packaging processes involve steps at elevated temperatures, a small variation in the processing temperature might cause the device failure and therefore, it is an important prerequisite to carry out the wafer bonding at moderate temperatures.

One of the important methods of bonding between a glass wafer / substrate and a silicon wafer/substrate at relatively low bonding temperatures is using an intermediate layer of alkaline ion barrier between the two wafers at a temperature between 300 ^{o}C and 500 ^{o}C using photosensitive benzocyclobutene (BCB) [14-16]. However, the bonding quality obtained through this is relatively poor at the lower limit of temperature. Although an anodic process between silicon and a glass substrate at 200 ^{o}C by irradiating a light beam to relax the network structure of glass to promote the diffusion of modifier ions in the glass is known. It is difficult to irradiate the entire bonding area of the substrates, especially for wafer level bonding, since the electrode might shield the light beam. In one of the approaches, direct bonding using polymeric materials like polymethylmethacrylate (PMMA), polyacrylate, polyimide and polycarbonate have been reported [24]. However these polymers are bonded to low-thermal-expansion materials such as Si and fused silica and hence thermal stresses can induce fractures during annealing treatments of the inorganic part of the bonded wafer pair. Similarly, photosensitive materials like SU-8 (negative photoresist), AZ-4620 (positive photoresist), SP341 (polyimide), JSR (negative photoresist) and BCB are used as adhesive intermediate bonding layers between the silicon wafers at low bonding temperature. These photosensitive materials act as the intermediate layer and will not form any covalent bond on the silicon surface.

In the previous part of chapter 6 (i.e., chapter 6A), we have established the possibility that the etching rate and morphology of the Si substrate could be profitably controlled by surface functionalization using SAMs, a result important for semiconductor processing. In the similar lines of application of SAMs to microelectronics technology, we here (chapter 6B) demonstrate the functioning of low temperature wafer bonding at 80 ^{o}C by forming the mono/ multilayer of acrylate/methacrylate alkoxy silyl monomer on the silicon wafer, having the terminal vinyl group, which is polymerized using thermal/ photo initiator. Chemical interactions occurring at molecular level between two surfaces seem to promote the wafer bonding at low temperature (scheme 6B. 1). The use of SAM (monomer having terminal unsaturation) has many merits as it forms a strong Si-O-Si covalent bond on silicon, which is polymerized at the termini using the thermal/photo initiator at a moderate temperature.

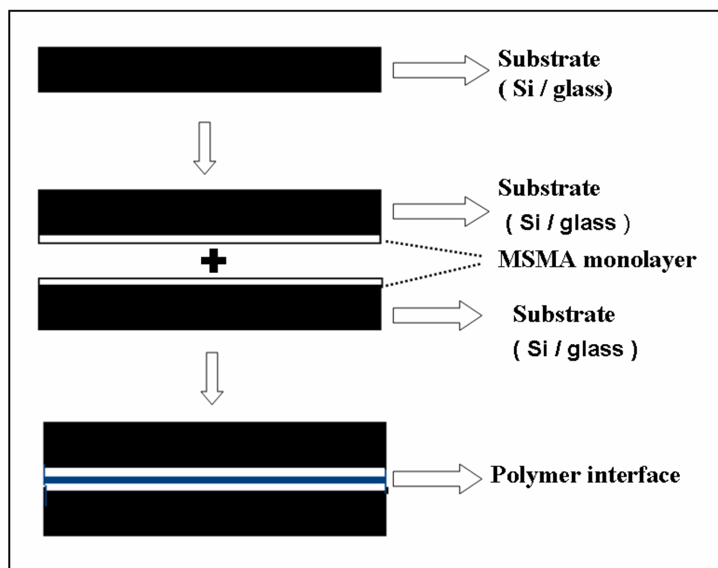

Scheme 6B. 1: Schematic representation of molecular (polymeric) glue formation, in which a monolayer of MSMA monomer is formed on both the Si substrate, the thermal initiator (Azobis isobutyronitrile) solution (less than 1 %) in chloroform is drop casted on these two substrates and subsequently adhered on each other and baked at 80 ^{o}C for 24 h, a polymer interface binds wafers.

6B. 2 Experimental

6B. 2.1 Chemicals

3-[tris (trimethylsilyloxy) silyl] propyl methacrylate (MSMA) was obtained from Aldrich, while all other chemicals were purchased from Qualigens. Commercially available Si (n-type, one-side polished, of (100) orientation with 0.001-0.007 Ω-cm resistivity) and glass wafers were used as a substrate. These silicon or glass wafers were rinsed by milli-Q reagent water (18 MΩ-cm), sonicated in ethanol and dried under a flow of nitrogen. These wafers were subsequently soaked in 1:10 HF:H_2O solution for 30 s to remove the native SiO_2 layer. After soaking in a *piranha* solution (7:3 H_2SO_4: H_2O_2) for 30 min at 80 ^{o}C to grow a fresh oxide layer, these substrates were subsequently rinsed with deionized water, dried in a stream of nitrogen and used for experiments.

6B. 2. 2 Monolayer Formation and Wafer Bonding Process

Silicon/glass wafers cleaned by the above procedure were dipped in 1 mM 3-(trimethoxysilyl) propyl methacrylate (MSMA) solution in toluene at 65 ^{o}C for 24 h, followed by extensive washing with toluene till free from of the monomer (to be designated as MSMA-Si/glass). All the experiments were carried out in nitrogen

atmosphere. In a typical bonding process, thermal initiator (like Azobis isobutyronitrile) solution (less than 1 %) in chloroform was drop casted on MSMA–Si/glass wafers and these two substrates were adhered on each other and baked at 80 ^{o}C for 24 h. All experiments were carried out in a dust free atmosphere.

6B. 2. 3 Characterization

All samples prepared by the above procedure were tested for flexural strength measurement (three point bending test) on an Instron universal testing machine using a 100 N load cell to monitor load changes using a sample size of 45 mm. After placing the specimen on the test fixture with careful alignment, it was compressed to fracture under a constant loading speed (displacement rate) of 0.75 mm/min. Scanning electron microscopy (SEM) was carried out on a Leico stereo scan model 440 instrument equipped with Phoenix energy dispersive analysis of x-ray (EDX) attachment.

6B. 3 Results and Discussion

6B. 3. 1 Monolayer Formation

MSMA is an interesting compound with unique terminal functionality, in which, alkoxy group of monomer (alkoxy silyl monomer) binds to the silicon wafer surface through Si-O-Si linkage, while the vinyl group of the monomer is available for polymerization (Figure 6B.1).

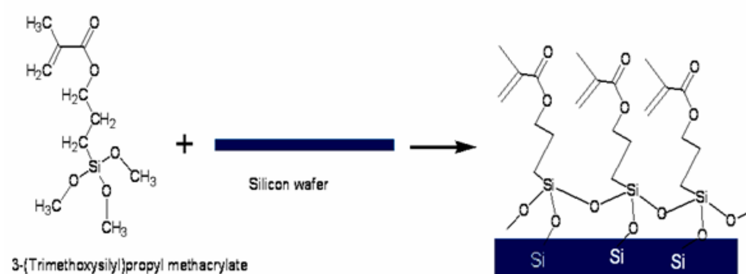

Figure 6B. 1: Schematic representation of the MSMA (monomer) monolayer formation on the Si substrate.

For the bare Si, water contact angle is less than 10 ^{o}, which slightly increases up to 50 ^{o} after the monolayer formation. The thickness of this monolayer is ~0.7 nm. The unsaturated vinyl terminal groups are active and can easily be polymerized by using either a thermal or photo initiator (Figure 6B.2A). The bonding process comprises

polymerization of vinyl groups (present on silicon wafer), which acts as a molecular (polymer) glue to bind silicon wafers chemically.

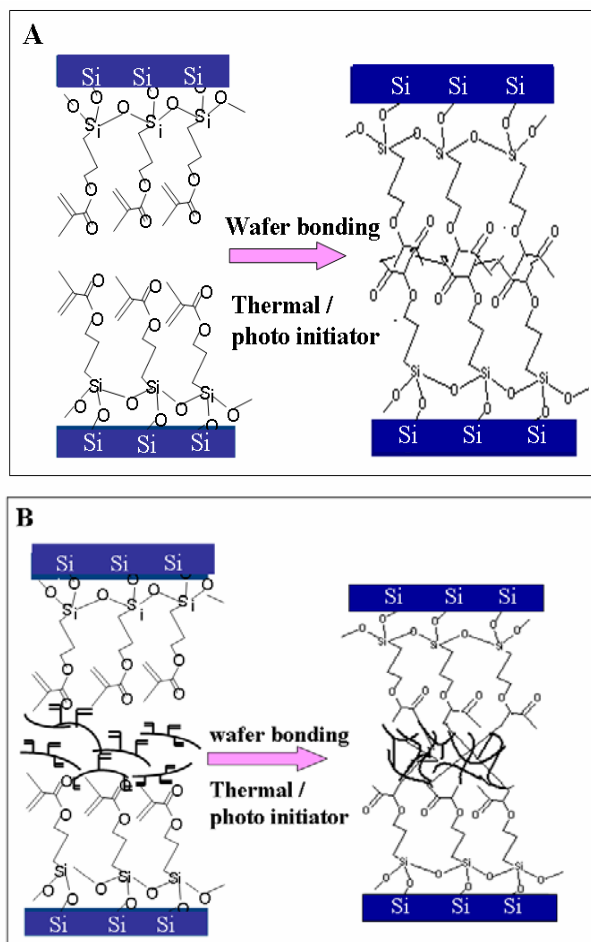

Figure 6B.2: Schematic representation of wafer bonding process by forming MSMA (monomer) monolayer on each wafer with terminal vinyl group, A) thermal initiator (Azobis isobutyronitrile) B) thermal initiator mixed with EGDMA copolymer solution (less than 1 %) in chloroform drop casted on each substrate, these two substrates adhere on each other and subsequently baked at 80 ^{o}C for 24 h to form molecular (polymeric) glue.

In one of the important approaches for wafer bonding, ethylene glycol dimethacrylate (EGDMA) homoploymer solution is also added externally along with the thermal initiator, to form polymeric glue as shown in Figure 6B.2. This method is particularly useful for silicon-glass and glass-glass bonding at 200-300 ^{o}C, which will be beneficial in packing or assembling at ambience. Some of these bonded wafers soaked in the various organic solvent (such as chloroform, toluene, etc.) for several hours ensuring good solvent stability.

6B.3.2 SEM Analysis

Figure 6B.3 shows the SEM image of the cross sectional view of one of these bonded wafers. The thickness of the polymeric glue is less than 5 μm and there is no sharp discrepancy. The absence of any crack or fracture is specially noteworthy suggesting the effectiveness of interfacial bonding

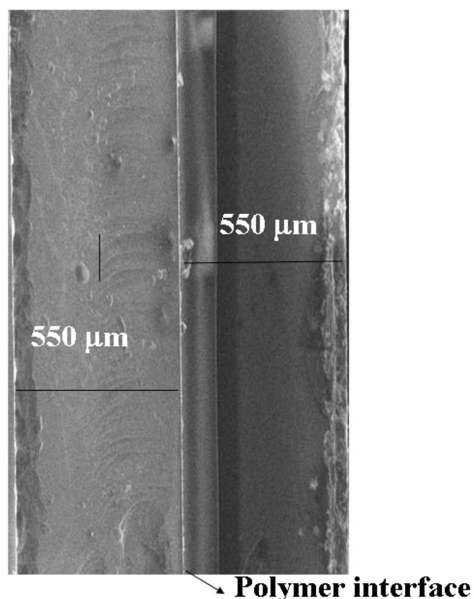

Figure 6B. 3: Scanning electron micrograph of the cross sectional region of bonded Si wafers using the molecular (polymeric) glue by forming the monolayer of MSMA monomer.

6B.3.3 List of Control Experiments of Wafer Bonding

Similarly a series of control experiments (without forming the monolayer of MSMA) carried out for the silicon-silicon, silicon-glass, and glass-glass bonding pairs are given in Table 6B.1 along with their most important results. There are several methods to quantify bond strength, including pressure burst tests, tensile shear tests and knife–edge tests that are sensitive to the loading configuration and the accuracy while measuring the length of the induced cracks. Some of these have been carried out to reach these conclusions as illustrated in Table 6B.1.

Table 6B.1: A list of control experiments carried out for wafer –wafer, wafer-glass and glass-glass bonding using SAMs along with their observations

No.	Experiment	Observations	Conclusion
1	Bare Si- Si substrate bonding using thermal initiator (AIBN) at 80 ^{o}C for 24 h.	Silicon wafers are easily separated out.	There is no specific reaction between two silicon wafer surfaces in presence only AIBN.
2	Bonding between two substrate having MSMA monolayer on both the Si substrate, using AIBN at 80 ^{o}C for 24 h.	Silicon wafers are easily separated.	The concentration of monomer on silicon wafer may be too low to polymerize with other monomer of monolayer present on the Si wafer.
3	Bonding between two substrate having MSMA monomer monolayer, by using EGDMA homopolymer along with thermal initiator and subsequent heating at 80 ^{o}C for 24 h.	Si wafers are not separated.	EGDMA polymer acts as a bonding interface between two Si wafers.
4	Wafer Monomer monolayer-TMPTMA homopolymer, AIBN drop, 80 ^{o}C	Si wafers are separated by application of force.	Modification in reaction condition is required
5	Copolymer of monolayer with EGDMA- copolymer of monolayer with EGDMA, AIBN drop, 80 ^{0}C	No reaction	-
6	Bare silicon–MSMA drop- EGDMA homopolymer, AIBN drop, 80 ^{o}C	Si wafers are not separated.	MSMA can attach to Si wafer the homopolymer of EGDMA can act as a crosslinking agent. The pendant double bonds of EGDMA homopolymer react with double bond of MSMA monolayer.

MSMA: 3-[tris (trimethylsilyloxy) silyl] propyl methacrylate
AIBN: Azobis isobutyronitrile
EGDMA: Ethylene glycol dimethacrylate

6B.3.4 Bond Strength Measurements

Bond strength measured using the flexural strength method (three point bending test), where load (KN) vs displacement (mm) curves for bonding between two silicon wafer with (A) MSMA and (B) MSMA + EGDMA homopolymer are shown in Figure 6B.4. When a tensile force is applied as a function of time with a constant increase in load, the material shows complianance until a force of approximately 9 N and becomes rigid beyond this value. At approximately 55 N, the super glue adhesive holds the substrate but the silicon wafers break. Although we could not determine the exact force to separate these substrates, the shearing strain at 55 N is about 0.087 MPa, which is calculated from the load displacement curve. Further, the load displacement curve also gives a good indication of the force with which the adhesive can safely withstand.

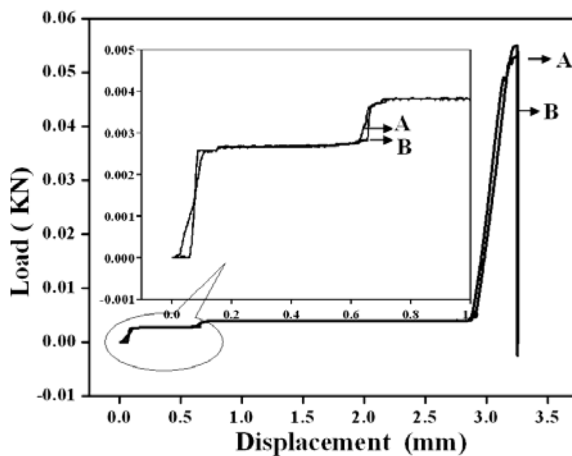

Figure 6B.4: Flexure test measurements on the bonded wafers A) between two silicon wafer with MSMA monomer, and B) between two silicon wafers with MSMA + EGDMA homopolymer.

6B. 4 Conclusions

A low temperature wafer bonding procedure (less than 80 ^{o}C) by using a molecular (polymeric) glue prepared with self assembled mono/multilayer of acrylate / methacrylate alkoxy silyl monomer (on Si and glass substrate) has been successfully demonstrated in this chapter. Many surfaces of silicon-silicon, silicon-glass, and glass-glass systems can be strongly bonded by using this type of glue after the polymerization of the terminal vinyl unsaturation of mono/ multilayers using either a thermal or a photosensitive initiator. This type of glue will be very useful for the integration of microstructures and microelectronics involved in MEMS and VLSI packaging processes

since the simple and low temperature wafer bonding (less than 100 ^{o}C) method does not require critical reaction conditions and possess good solvent stability.

6B. 5 References

[1] M. A. Schmidt, *Proceedings of the IEEE*, **1998**, 86, 1575.

[2] A, Berthold, P. M. Sarro, P. J. French, M. N. Vellekoop, *Sensors and Actuators A* **1991**, 21, 919.

[3] A.V. Chavan, K. D. Wise, *A IEEE Trans. Electron devices* **2002**, 49 (1), 164.

[4] D.-J. Lee, B.-K. Ju, Y.-H. Lee, J. Jang, M.-H. Oh, *Proc. Micro Electro Mechanical Systems,* **2000**, 253.

[5] M. A. Huff, A. D. Nikolich, M.A. Schmidt, *J. Microelectromech. Syst.* **1993**, 2 (2), 74.

[6] Q.-Y. Tong, U. Gösele, *"Semiconductor wafer bonding: Science and technology"*, John Wiley & Sons, Inc., New York, USA, **1999**.

[7] C.T. Pan, P. J. Cheng, M.F. Chen, C.K. Yen, *Microelectronics Reliability* **2005**, 45, 657.

[8] U. Go¨ sele, A. Schumacher, G. Kra¨uter, *Sensors and Actuators A* **1998**, 70, 271.

[9] D. E. Booth, C. E. Hunt, *Proceedings of the 3rd International Symposium on Semiconductor Wafer Bonding,* **1995**, 201.

[10] E. Obermeier, *Proc. of Third International Symposium on Semiconductor Wafer Bonding: Science, Technology and Applications Pennington, USA.* **1995**, 95, 212.

[11] G. Wallis, D. I. Pomerantz, *J. Appl. Phys.*, **1969**, 40(10), 3946.

[12] T. Corman, "Vacuum-sealed and gas-filled micromachined devices", *Ph.D. Thesis*, Micro System Technlogy, Department of Signals, Sensors and Systems, Royal Institute of Technology (KTH), Stockholm, Sweden, **1999**.

[13] T. T. Veenstra, J. W. Berenschot, J. G. E. Gardeniers, R. G. P. Sanders, M. Elwenspoek, A. van den Berg, *J. of the Electrochemical Soc.* **2001**, 148 (2) 68.

[14] F. Niklaus, *Sensors and Actuators A* **2001**, 92, 235.

[15] W. P. Eaton, S.H. Risbud, R .L. Smith, *Appl. Phys. Lett.* **1994**, 65 (4), 439.

[16] S. K. Malik, R. Srinath, R. A. Pearson, R. Kodnani, J. Dzwilefsky, A. Call, "*Proc. SPIE Los Angeles, USA,* **1995**, 26, 130.

[17] Q. –Y Tong, U. Gosele, '*Semiconductor Wafer bonding'* , *Wiely, New York,* **1999**.

[18] J. M. Noworolski, E. Klaassen, J. Logan, K. Petersen, N. I. Maluf, *Sensors and Actuators A* **1996**, 54, 709.

[19] L. A. Field, R.S. Muller, *Sensors and Actuators A*, **1990**, 23, 935.

[20] S. A. Audet, K. M. Edenfeld, *Proc. Transducers Chicago, USA* **1997**, 287.

[21] J. M. McNamara, J. S. Raby, *Proc. IEEE SOS/SOI Technology Workshop* **1988**, St. Simons Island, USA 14.

[22] J. Oberhammer, F. Niklaus, G. Stemme, *Sensors and Actuators A* **2003**, 105 (3), 297.

[23] J. Oberhammer, Sensors *and Actuators A* ***2004**,* 110, 407.

[24] G.A.C.M. Spierings, J. Haisma, F.J.H.M. van der Kruis, *Philips Journal of Research*, **1995**, 49 (1), 139.

CHAPTER 7

Conclusions and Future Prospects

This last chapter provides a summary of the major outcomes of the present study with respect to the preparation, characterization and various properties of SAM on Si/SiO_2 interface along with its possible applications. The chapter also outlines some of the limitations of present investigations along with possible methods to overcome them in future; plausible precautions and safety hazards during the preparation and processing of SAM also have been suggested. Lastly, many exciting opportunities to carry out further work in this interdisciplinary area is indicated which predict major advances likely to be realized soon.

7.1 Introduction

All the previous chapters have clearly demonstrated the usefulness of self assembled monolayers (SAMs) for MEMS due to their fundamental importance in surface modification and also for their potential applications in nanotechnology [1–4]. More specifically, alkyltrichlorosilane SAM on Si/SiO_2 interface has been extensively studied as a representative system using diverse techniques, since their mere presence provides a suitable low energy surface coating. Consequently, many important issues related to their preparation, characterization, stability and electrochemical properties of alkane silane SAMs on both planar and spherical Si/SiO_2 interface have been addressed along with their important applications in microfabrication. During the course of these investigations, several valuable insights have been obtained to ensure reproducible properties by controlling preparation conditions of SAMs such as concentration of silane (in mM range), selection of solvent (containing optimum amount of water), temperature (room temperature preferred) and environment. Further, several important new information regarding the kinetics, mechanisms and electron transfer behavior have been gained by the combined evidence collected from different type of experimental techniques, which would be extremely valuable to design suitable SAMs not only for microfabrication of MEMS but as active or functional monolayers for molecular electronics applications also [1-9].

7. 2 Major Accomplishments

Major outcomes of the present investigations using various SAMs of alkyl trichloro/trimethoxy silanes on Si/SiO_2 interface during the last five years are as follows:

- A better understanding of the growth kinetics and thermodynamic stability of octadecyltrichlorosilane (OTS) SAM on Si/SiO_2 interface has been obtained using contact angle measurements in conjunction with a diverse type of other surface characterization techniques.
- Chain length dependent electrochemical properties of alkyltrichlorosilane monolayer on Si/SiO_2 interface in the presence and absence of external redox

probe like ferrocene have been illustrated which indeed help in tuning the properties of SAMs for specific applications.

- A positive shift (200 mV) in the flat band potential after monolayer formation has been observed indicating a subtle variation in the surface state distribution due to the covalent coupling of the silane monolayers, along with concomitant changes in the charge carrier concentration and space charge layer width.
- A comparison of the quality of OTS monolayer on both planar as well as on spherical Si/SiO_2 interfaces has been achieved to highlight the role of curvature on monolayer behavior.
- An enhancement in thermal stability of OTS SAM on curved silica surface (350 ^{o}C) in comparison with that on planar (250 ^{o}C) Si substrate in air has been observed.
- A novel method of preparation of hydrophobic silica particles (100-150 nm) by surface functionalization using different alkyltrichlorosilanes has been illustrated, where, the solubility (dispersion) of these silica particles in non polar solvent will have far reaching implications in composite coating.
- Role of OTS-monolayer in controlling the etching rate and morphology of the Si in alkaline solution has been elucidated.
- An improved process of Si wafer bonding at a low temperature (less than 80 ^{0}C) by making molecular (polymeric) glues using self assembled mono/ multilayer of acrylate / methacrylate alkoxy silyl monomer has been established.

However, since SAMs in principle can isolate any semiconducting substrate from its ambience by virtue of its passivation behavior, there are some obvious limitations and these are discussed in the following section.

7.3 Possible Limitations

- During SAM formation, the silicon surface must be freshly cleaned and oxidized, which is accomplished by either growing a thin oxide (~ 20 Å) film with the help of *piranha* solution *or* by a suitable thermal treatment to ensure enough density of –OH groups for covalent bond formation. Both the process are complicated, as

piranha solution reacts violently with organic contaminants (one must be careful while handling) and thermal process requires high temperature treatment with accurate control.

- For all SAM formation steps, alkyltrichlorosilane must be freshly prepared, as it is sensitive to ambient humidity and it is extremely important to prevent the lateral polymerization of SAM precursors. Therefore, it is necessary to control many environmental parameters like humidity, temperature, amount of sunlight etc., along with the amount of water present in the solvent to obtain high-quality SAMs with conformal coverage.
- A finite number of defects (pinholes) present in fully covered SAMs (~ 99.9 % coverage) can affect all macroscopic phenomena such as wettability since most of these properties are highly sensitive to the distribution of these defects.
- Many of our findings are on Si wafers and hence these studies have to be supplemented by results obtained using actual test structures. The lack of microfabrication facility is, undoubtedly, responsible for this type of a limitation. Neverthless, we believe that these results are useful for device applications since the surface chemistry aspects are invariant to the external geometry.

Despite these limitations, our studies clearly show that SAMs can effectively be used in MEMS/NEMS fabrication as well as in device applications due to their good thermal and chemical stability, ease of preparation, low surface energy and adhesion, hydrophobic nature, and insulating properties. In addition, these SAMs would be of interest to many researchers engaged in molecular electronics since many SAM molecules can be designed specially for applications like biosensors, resonant tunneling diodes and several optoelectronic devices.

7. 4 Future Scope

Self assembly is ubiquitous in many natural systems as it plays a prominent role in making objects, patterns, and complex functional systems for various applications in nanotechnology. For example, several approaches for using SAMs for nanofabrication are already under investigations ranging from molecular manipulation, through

supramolecular chemistry, to organization of much larger systems made by the controlled self-assembly of colloids. Thus SAMs can be used either directly in a device (for example, a SAM in a molecular electronics device), or indirectly to assist conventional microfabrication processes (for example, transfer of a pattern made in phase-separated block copolymers to a substrate with reactive ion etching). In the near future, we anticipate a hybrid approach, combining micro/nanofabrication, through SAM, which is supposed to be the dominant method in nature for making devices and systems [10-14].

Application of SAMs in the area of micro/nanofabrication provides several attractive features because of its flexibility in controlling various molecular interactions (electrostatic, covalent and van der Waals type) and simple methodology leading to a control of some inherent properties such as lubrication and anti-stiction behavior. For example, it can generate a structure with subnanometer precision, offering unprecedented opportunities to simplify and develop new processes. More significantly, this could involve many components, which are too small to be manipulated robotically, thus integrating incompatible technologies, which is not, otherwise normally possible. Hence the creation of hierarchical structures in three dimensions and on curved surfaces (which is helpful in building MEMS devices with more complicated architectures), is possible to target specific applications of SAMs as per our demand by applying even external driving forces.

Following are the possible areas, where SAMs are likely to make substantial impact in the near future.

- Since controlling surface forces is one of the key challenges in the design, fabrication, and operation of MEMS, molecularly tailored SAM will be increasingly used during microfabrication to avoid release stiction.
- During the operation of MEMS devices some of the problems due to wear will be minimized by using suitable SAMs which could also offer better lubrications. In the next few years use of selective SAMs to tackle “in-use stiction” will become a standard practice.
- In nano and micro device fabrication, isolation of the individual components while assembling step at nano level is a critical challenge, which will be

overcome by using SAM as an interfacial layer (as a barrier) to inhibit undesirable diffusion.

- Shrinking device dimensions and increasing aspect ratios in integrated circuits (IC) require the introduction of new materials and thin-film deposition techniques at atomic level. Atomic layer deposition (ALD) will certainly provide great potential for producing very thin (sub nanolayer), conformal barrier films with precise control of the thickness and composition at the atomic level precision needed in microelectronics. Similarly, electro migration, which is one of the major factors affecting Cu interconnect reliability at higher operating temperature can be prevented by the application of SAMs [15].

- Molecular recognition is a key step in the development of biosensors and other sensing devices. However, the sensitivity and reliability of these devices depends extensively on the interfacial properties, which could be or tuned at molecular level simply by tailoring the tail group of SAM molecules. In addition, this strategy would be of further aid to develop devices for the applications in molecular electronics [1, 2, 10].

- Emerging technological revolution towards the fabrication of functional devices on chip (such as 'lab-on-a- chip') requires effective micro patterning. It is difficult to achieve high precision with conventional lithography and SAM offers a versatile way for selective etching. Techniques like dip-pin lithography are expected to play a key role in this regard.

- Efficiency of photonic materials depends on their surface area, which can be enhanced by organizing ordered arrays of nanoclusters on semiconducting substrates. Towards this application, SAM offers a reliable way of assembling ordered arrays of 100-1000 nm diameter microspheres of photonic band crystals.

- The sensitivity of SAM to an applied external field (electric/magnetic/electromagnetic) could be exploited to position the final assembly at device location for specific applications. For example, electric field

assisted self-assembly is used to position nanowires on a pad or to control the orientation of self-assembled patterns in a block copolymer blend.

Although, SAMs are insensitive to small variations in processing, limitations in fabricating small, complex functional components for various future applications demand the necessity for the development of new methodologies. Proof-of concept experiments in mesoscale self–assembly demonstrate that this technique poses fascinating scientific and technical challenges and offers the potential to provide access to hard–to–fabricate structures.

Although, SAMs have been employed to make molecular electronic devices, for the most part of it still remains as a research tool. The engineering and scientific enthusiasm for challenges and utility driven research related to self-assembly continues to grow and we anticipate important developments toward the integration of self-assembled structures in existing microfabricated systems in the immediate future. An increased interest in mimicking biological functions to produce complex structures (BIOMEMS), is expected along with the broad participation of multiple disciplines in addressing some of the challenges currently limiting self-assembly. Self-assembly, we believe, will be a central approach to nanofabrication in future. It is expected that self-assembly process will be a cost effective and efficient method for manufacturing nano-scale devices, although a few systems will remain difficult for commercial exploitation due to aforementioned limitations.

7. 5 References

[1] A Ulman. *An introduction to ultra thin organic films from Langmuir-Blodgett to Self-assembly*, Academic Press, London **1991**.

[2] A. Ulman, *Chem. Rev*. **1996,** 96, 1533.

[3] R. Maboudian, *Mater. Res. Soc. Bull.* **1998,** 23, 47 and references therein.

[4] J. Sagiv, *J. Am. Chem. Soc.* **1980,** 102, 92.

[5] S. E. Lyshevski, '*MEMS and NEMS: Systems, Devices, and Structure*s',CRC Press **2002**.

[6] J. Bryzek, *Sensors and Actuators A* **1996**, 56, 1.

[7] M. J. Madou, '*Fundamentals of Microfabrication'* (Boca Raton, FL: CRC press company) **1997.**

[8] R. S. Muller, R.T. Howe, S. D. Senturia, R. L. Smith, R. M. White, *Microsensors* New York: IEEE Press **1990**.

[9] S. M. Sze, *Semiconductor Sensors*. New York: Wiley, **1994**.

[10] B. A. Parviz, D. Ryan, G. M Whitesides, *IEEE Transactions on Advanced Packaging*, **2003,** 26, 233.

[11] R. D. Piner, J. Zhu, F. Xu, S. H. Hong, C. A. Mirkin, *Science* **1999**, *283*, 661.

[12] H. Zhang, Z. Li, C. A. Mirkin, *Adv. Mater.* **2002**, *14*, 1472.

[13] P. A. Smith, C. D. Nordquist, T. N. Jackson, T. S. Mayer, B. R. Martin, J. Mbindyo, T. E. Mallouk, *Appl. Phys. Lett.* **2000,** 77, 1399.

[14] Y. D. Yin, Y. N. Xia, *J. Am. Chem. Soc.* **2003, 1**25, 2048.

[15] M. Leskel, M. Ritala, *Angew. Chem. Int. Ed.* **2003,** 42, 5548.

List of Publications

1. *"Thermal Stability of Self-Assembled Octadecyltrichlorosilane Monolayers on Planar and Curved Silica Surfaces"* **S. A. Kulkarni**, S. A. Mirji, A. B. Mandale, K. Vijayamohanan, *Thin Solid Films* **2006**, 496, 420.

2. "*Suppression of electron transfer characteristics of ferrocene by OTS monolayers on a Silicon/electrolyte Interface*" **S. A. Kulkarni**, B. A. Kakade, I. S. Mulla, K. Vijayamohanan, *J. Colloid and Interface Sci.* **2006**, 299, 777.

3. "*Electrochemical characterization of self-assembled monolayers on semiconducting substrates for MEMS applications"* **S. A. Kulkarni**, I. S. Mulla, K. Vijayamohanan, *J. Physics: Conference Series* **2006**, 34, 322.

4. **"***Growth Kinetics and Thermodynamic Stability of Octadecyltrichlorosilane Self Assembled Monolayer on Si (100) substrate*" **S. A. Kulkarni**, S. A. Mirji, A. B. Mandale, R. P. Gupta, K. Vijayamohanan, *Materials Letters* **2005,** 59, 3890.

5. "*Synthesis and characterization of polyimides and co-polyimides having pendant benzoic acid moiety*" by M. Kulkarni, S. Kothawade, G. Arabale, **D. Wagh,** K. Vijayamohanan, R. A. Kulkarni, S. P. Vernekar, *Polymer* **2005,** 46, 3669.

6. "*Enhanced supercapacitance of multiwalled carbon nanotubes functionalized with ruthenium oxide***"** G. Arabale, **D. Wagh**, M. Kulkarni, I. S. Mulla, S. P. Vernekar, K. Vijayamohanan, A. M. Rao, *Chem. Phys. Lett.* **2003,** 376, 207.

7. "*Metal Ion Reactivity with 1, 4-Benzenedimethanethiol Monolayers on Gold*" by M. Venkataramanan, K. V. G. K Murty, T. Pradeep, **D. Wagh** and K. Vijayamohanan *Langmuir* **2000,**16,7673.

8. "*Tuning the hydrophobic properties of silica particles"* S. A. Kulkarni, S. B. Ogale, K. Vijayamohanan, and Communicated to *Langmuir* **2007.**

9. "*Interfacial Behavior of Alkyltrichlorosilane Monolayers on Silicon: Control of Flat-Band Potential and Surface State Distribution Using Chain Length Variation"* **S. A. Kulkarni**, K. Vijayamohanan, Communicated to *Surface Science* **2007.**

10. "*Tuning of the anisotropic etching rates of Si using surface functionalization*" **S. A. Kulkarni,** K. Vijayamohanan Communicated to *J. Colloid and Interface Science* **2007**.

11. "*Fungal Processing of Glass: Morpho-Chemical Surface Modifications and Nanosysnthesis*" **S. A. Kulkarni**, A. Syed, S. Singh, A. Gaikwad, K. Vijayamohanan, A. Ahmad, S. B. Ogale. Communicated to *J. Mater. Chem.* **2007**

Patents

1. "*An improved process for the preparation of high surface area carbon useful for fuel cell and ultracapacitor*" **D. Wagh**, G. Arabale, M. Kulkarni, S.P. Vernekar, I. S. Mulla and K. Vijayamohanan, *US Patent*, (20050221981) **2005.**
2. **"***An improved process of wafer bonding at a low temperature by making a molecular, polymeric glue using self assembled monolayer / multilayers for MEMS applications"* **S. A. Kulkarni**, S.S. Satav, M.G. Kulkarni, K. Vijayamohanan, filed as *India Patent* **2007**.
3. "*Method of processing of glass materials*" **S. A. Kulkarni,** S.B. Ogale, A. Ahmad, K. Vijayamohanan, filed as *Indian Patent* **2007.**